BENJAMIN EVEREST

DISSIPATION AS A RESOURCE FOR CONSTRAINED DYNAMICS IN OPEN MANY-BODY QUANTUM SYSTEMS

DISSIPATION AS A RESOURCE FOR CONSTRAINED DYNAMICS IN OPEN MANY-BODY QUANTUM SYSTEMS

BENJAMIN EVEREST

Non-equilibrium physics in open many-body quantum systems

September 2013 - March 2017

Benjamin Everest: *Dissipation as a resource for constrained dynamics in open many-body quantum systems,* Non-equilibrium physics in open many-body quantum systems, © September 2013 - March 2017

and i keep on thinking
it's time to move on
move out to the city so huge
meet me some people

— *Liars*, Gregory Alan Isakov

ABSTRACT

This thesis studies non-equilibrium open quantum systems where the dissipation is crucial to the achievement of novel physical regimes. We focus on atomic systems which allow for the coupling of a ground state to a Rydberg state, relying on the strong interactions between Rydberg atoms to produce the collective behaviour that we aim to investigate. For atoms in an optical lattice undergoing standard dissipation forms, e.g. loss and dephasing, we find these simple settings allow for the production of models contained in the non-equilibrium realm.

We start by looking at a system with engineered pair dissipation on a one-dimensional lattice. When the dissipation is strong relative to a tunnelling process it creates a quantum Zeno effect which projects the system onto a Zeno-subspace. This subspace is found to contain complexes which experience a binding due to the dissipation. The properties of these complexes are found to feature spin-orbit coupling and, in certain instances, a flat band.

We then study what kinetically constrained models (KCMs) can be reproduced in a lattice system. KCMs are models which typically feature trivial steady states, but a complex relaxation dynamics. These models appear in the fields of glasses and soft matter physics. We find a general framework for the consideration of a quantum Hamiltonian and a classical potential with strong dephasing noise. We then focus on a model mimicking volume excluded KCMs and find characteristic constrained behaviour, such as ergodicity breaking.

We apply this framework to the decay of a many-body localised state in an open system with interactions in which we find the decay to be classical in the two interaction limits. For weak interactions, it follows a stretched exponential form due to pair relaxation, while for strong interactions the decay follows a compressed exponential, now being modelled as an Avrami process due to the correlated relaxation. We also find that on-site loss only affects the strong interacting limit.

We then move on to the study of universal non-equilibrium behaviour in the directed percolation (DP) class. We consider on-site atomic loss and gain as a substitute for the standard decay channel. We show that this replaces the absorbing state with an enlarged absorbing space, leading to a loss of the DP transition at lower average densities. This class of DP-like systems has received little study, and we present a method of experimentally realising it in current set-ups.

We finish with a look at a quantum DP model, where we consider its quantum and classical limits. We find that the transition changes from first to second order as the system becomes more classical, fea-

turing a bi-critical point. We then numerically demonstrate that the same transitions are visible in idealised and Rydberg models.

PUBLICATIONS

[1] B. Everest, M. R. Hush, and I. Lesanovsky. "Many-body out-of-equilibrium dynamics of hard-core lattice bosons with non-local loss." In: *Phys. Rev. B* 90.134306 (2014). DOI: 10.1103/PhysRevB.90.134306.

[2] B. Everest, M. Marcuzzi, and I. Lesanovsky. "Atomic loss and gain as a resource for nonequilibrium phase transitions in optical lattices." In: *Phys. Rev. A* 93.023409 (Editor's Suggestion) (2016). DOI: 10.1103/PhysRevA.93.023409.

[3] B. Everest, M. Marcuzzi, J. P. Garrahan, and I. Lesanovsky. "Emergent kinetic constraints, ergodicity breaking, and cooperative dynamics in noisy quantum systems." In: *Phys. Rev. E* 94.052108 (2016). DOI: 10.1103/PhysRevE.94.052108.

[4] B. Everest, I. Lesanovsky, J. P. Garrahan, and E. Levi. "Role of interactions in a dissipative many-body localized system." In: *Phys. Rev. B* 95.024310 (2017). DOI: 10.1103/PhysRevB.95.024310.

[5] M. Buchhold, B. Everest, M. Marcuzzi, I. Lesanovsky, and S. Diehl. "Nonequilibrium effective field theory for absorbing state phase transitions in driven open quantum spin systems." In: *Phys. Rev. B* 95.014308 (Editor's Suggestion) (2017). DOI: 10.1103/PhysRevB.95.014308.

ACKNOWLEDGMENTS

During my three-and-a-half years of post-graduate study I have had the pleasure to know and learn from a fantastic group of people. The lessons and the relationships formed are most valuable part of my time here. Here I give my thanks to them in no particular order.

I would like to thank Prof. Igor Lesanovsky for his fine supervision. Igor has always offered an ear when asked and provided more opportunities than the time available. He gave direction and goals to my PhD and shaped its form, teaching me how one approaches scientific research. He consistently supported my ideas and provided useful nudging to keep me working hard and reach my own goals. It has been a great journey with him and, as I hope this thesis attests, a successful one.

As the pair so often appear in author lists together, it seems only fitting to thank Prof. Juan P. Garrahan next. I took Juan's classical mechanics course as an undergraduate and it remains a fond memory. He has consistently provided advice on pursuing a career and been a joy to collaborate with on various projects.

Throughout my PhD I have had two post-doc mentors. The first was Dr. Michael Hush. When I first started I was nervous and unsure of my place in the group and in science. Michael taught me all the essentials to survive, both through demonstration and direct teaching. He maintained a constant professional and friendly attitude that I try to emulate still.

I then worked with Dr. Matteo Marcuzzi. Matteo is a brilliant scientist and man. His depth of knowledge on a vast array of topics, including outside of science, is inspiring. Through discussions with him I have learned more than with anyone else for he takes the time to explain even the smallest detail should you ask. With him, I have done the work I am most proud of, and attribute the greatest part of it to his efforts. Matteo has been an excellent mentor and friend.

I wish to also thank other post-docs and staff I have had the pleasure of getting to know and work with: Emanuele Levi a great colleague and friend, Sam Genway, Weibin Li, Beatriz Olmos, and Daniel Viscor.

My fellow PhDs have been a great source of discussion, teaching, and friendship. James Hickey and Suzie Abbs introduced me to PhD life, Rob Turner showed me the ropes of C++, Claire Davis-Tilley was always happy to chat, and Tom Oakes, my good friend, always open to discuss all the crazy ideas that come to us both.

I also wish to thank everyone who participated in my organised Theory Meetings. They gave me a great chance to learn and become

more in-tune with those I worked with. I owe much of this to Igor and Juan.

I thank my parents, Deborah and Timothy Everest. They have supported me through all my studies and helped in whatever way they could during these years. I owe a great deal to their teachings in my early life and their continued wisdom.

I wish to thank my wife and partner Katarzyna Macieszczak. She inspires me everyday to be my best-self and is the most brilliant person I have ever met. We went through PhD-life together, and her endless support has gotten me through the hardest parts of these years. She is an amazing scientist and an inspiration both in my work and my life.

CONTENTS

LIST OF FIGURES

ACRONYMS

BEC Bose-Einstein Condensate

KMC Kinetic Monte Carlo

QJMC Quantum Jump Monte Carlo

KCM Kinetically Constrained Model

FA Fredrickson-Andersen

NN Nearest-Neighbour

MBL Many-Body Localisation

CDW Charge Density Wave

DP Directed Percolation

1 INTRODUCTION

Traditionally, physicists have asked questions focussed on the microscopic laws, those which govern a single or pair of particles. The belief being that such laws could scale upwards, extending to describing systems comprised of many-bodies and leading to a full description of the universe. This is known as the constructionist hypothesis, and it has brought about great advancement and is of course a continuing line of reasoning within physical study, particularly in particle physics. In this pursuit however, severe roadblocks are encountered, the most obvious being the N-body problem. When it came to understanding beyond two interacting particles, the laws which were discovered for pairs could not be analytically solved. Instead it was pertinent to reconsider these problems as many-body from the start.

Many-body physics is the study of emergent collective phenomena, the resultant effect of the individual interactions of large ensembles of particles. In the essay "More is different" by P.W. Anderson [1] it is elegantly put:

> *"...the whole becomes not only more than but very different from the sum of its parts."*

This comment is primarily on the topic of symmetries. Physics at its core is a study of the symmetries of nature. Crucially, the microscopic symmetries can be wholly different to an ensemble's symmetries. This means that when approaching the solution of a many-body problem the details of the microscopic become irrelevant, and one can simply focus on the symmetries of the system as a whole.

On a fundamental level, many-body physics is of interest for the simple fact that all that surrounds us is many-body. Isolated, single "particle" systems are in-fact rare, and even in situations where the free-particle approximation works well in order to understand its final or equilibrium state its many-body nature must be invoked. Beyond that, many of the most fascinating phenomena in physics are many-body, including superconductivity [2], Bose-Einstein condensation [3] and the glass transition [4, 5], to name but a few.

New types of phenomena, that cannot be predicted from the particle level, emerge on the many-body scale, a prototypical example being that of a phase transition. A phase is a description of the state of matter, characterised by the value taken by a specific macroscopic observable, usually referred to as the order parameter. We can illustrate this idea with the Ising model. The Ising model consists of a spin$-1/2$ square-lattice system, with each site featuring states $\uparrow \equiv 1$ and $\downarrow \equiv -1$. These sites experience two effects: a nearest neighbour

interaction, $V > 0$, and a magnetic field, h. This gives a function for its energy, a Hamiltonian, for L sites as

$$H = -\sum_{\langle k,j\rangle}^{L} V\sigma_k\sigma_j - \sum_{k}^{L} h\sigma_k \tag{1.1}$$

where $\sigma_k \in \{-1, 1\}$ and $\langle k, j\rangle$ runs over all nearest neighbours of each site k. For the case of $h = 0$, depending on the temperature, this system will either exhibit a ferromagnetic or paramagnetic phase. At low temperatures, the thermal fluctuations are small, i.e. $k_B T \ll V$, meaning that the interactions dominate. This means that the lowest energy state is all the states either aligned all up or down, known as the ferromagnetic phase. In the other limit, $k_B T \gg V$, the fluctuations will be such that the interaction is sub-leading resulting in neither state being preferred for any given site. This results in the paramagnetic phase which is a statistically-independent mixture of up and down states. For the Ising model the associated order parameter is magnetisation, $M = \sum_k \sigma_k/L$, where $M = 0$ is paramagnetic and $M = \pm 1$ is ferromagnetic at zero temperature.

Between phases lies a phase transition, at which point the system undergoes a non-analytic change in its properties. In the Ising model example, in dimensions of two or greater, as the temperature is increased the system changes from the magnetisation having a finite value to being zero i.e. ferromagnetic to paramagnetic. This transition is continuous as the "sharp" change occurs in second-order derivative of the order parameter. At phase transitions the continuity of the microscopic description appears to be violated as extreme critical phenomena takes place, leading to singularities. This is in-part due to the fact that phase transitions, and their non-analytic nature, formally only exist in the thermodynamic limit, i.e. for infinite sized systems.

Systems can be split into either open or closed. A closed system is one which only interacts in amongst itself, while an open system has an interaction with a bath or environment which lies outside the description of the system of interest. An open system's interaction with its environment can be, for example, characterised by an exchange of particles or energy. Environments are typically considered to be large in comparison to the system, such that the exchange between the two influences the system state but does not significantly affect the environment. An open system is far more common in physical settings, and as such will be the main focus of this thesis.

When understanding phases and phase transitions one must also talk about thermodynamic equilibrium. Systems which can feature a thermodynamic equilibrium state are composed of large ensembles of particles and, when closed, are able to explore all configurations at a specified energy. When open, the energy is not fixed so rather the system explores the configurations at different energies with probabilities following a Gibbsian distribution [6]. This exploration of the

state space causes, on average, the systems to display stable macroscopic quantities, such as energy and magnetisation. These states are also referred to as *steady states*, however not all systems in a steady state are at equilibrium. The determination through statistics of a system's state at equilibrium gives the framework of statistical mechanics, which has been a vital tool in the understanding and characterisation of equilibrium systems.

All those systems which cannot be categorised as equilibrium are in the field of non-equilibrium physics. Such systems can either be transient, as they approach an equilibrium state, or not feature an equilibrium state at all. These systems have received extensive study in recent decades as they continue to elude full characterisation. Often, non-equilibrium systems have to be addressed by tailored approaches as we still lack an overarching framework, such as statistical mechanics provides for equilibrium. A prototypical example of the field lies in glasses. Glasses, although appearing stable when in a solid state, in-fact feature a "frozen" liquid structure. Rather than being in an equilibrium state, they instead have a very long, temperature dependant, relaxation time causing them to be non-equilibrium systems [5, 7–10].

Non-equilibrium systems can feature so-called dynamical phase transitions. There are multiple definitions of these phase transitions that have yet to be agreed upon, particularly in quantum settings [11, 12]. Generally they are a transition that alters the form of the dynamics, featuring a non-analytic change in the properties. They can be related to changes in the form of the relaxation, or a more fundamental changes in the dynamics.

A possible explanation for glassy dynamics is found in kinetically constrained models (KCM). A kinetic constraint is where rules are placed on a system governed by a simple microscopic dynamics. This is generally through the suppression or restriction of connections between certain configurations or states. For example, in a dense fluid of hard spheres the diffusion of a sphere is limited by its neighbourhood, i.e. there must be no other spheres in its way for it to progress. Typically these systems feature trivial steady states, meaning their long-time dynamics samples a simple equilibrium distribution. Their relaxation to the steady state however can be complex and highly structured at sufficiently high densities and low temperatures due to the constraint. Key examples of KCMs are the Fredrickson-Anderson model, the east model and triangular lattice gas models [8, 13–16].

Constrained systems and non-equilibrium physics have been found in the active field of ultracold atoms. The field of atomic physics has sky-rocketed since the late 1990's and become a staple experimental platform in the exploration of quantum systems and many-body physics. Ultracold systems provide a highly tunable and accessible experimental platform for advanced studies of physical systems. The

field began in the 1920's when the theory of Bose-Einstein condensation (BEC) was developed [17], predicting a new state of matter. A BEC is a dilute bosonic gas cooled to very low temperatures such that a large proportion of the bosons occupy the ground state of the system, causing it to act as a macroscopic quantum gas, being described by a single wavefunction. The transition to a bosonic BEC occurs below a critical temperature, which for a three-dimensional system is approximately

$$T_c \approx \left(\frac{n}{\zeta(3/2)}\right)^{2/3} \frac{2\pi\hbar^2}{m k_B} \tag{1.2}$$

where n is the particle density, m is mass of each boson and ζ is the Riemann zeta function. At the time of its discovery, the technology requirements made a BEC's realisation impossible and it was not until the 1970's when the idea of the laser cooling of atoms [3, 18] was proposed that such low temperatures became possible. Finally the BEC was achieved [19–21], and this new phase of matter was observed for the first time earning those involved the Nobel prize. In contrast, at low temperatures fermions show a state known as Fermi degeneracy where due to the exclusion of the occupation of the same state they instead occupy the full set of the lowest energy eigenstates. Fermi degeneracy in dilute fermionic gases was also achieved shortly after the BEC [22–24]. These systems have been shown to exhibit such properties as superfluidity [3], Feshbach resonances [3], and the BEC-BCS crossover [25].

Ultracold atoms offer an excellent setting for quantum simulation [26, 27]. Quantum simulation is the idea of using a highly tunable quantum system to simulate specific quantum models of theoretical interest, including those which are fundamental to condensed matter theory, as classical computers are limited in their degree to simulate complex quantum systems. Typically atomic gases are produced in environments which are highly tunable; by use of potentials from lasers or magnetic fields the shape of the atomic gas and its dimensionality may be tuned. The shapes possible range from quasi-one-dimensional cigar shaped gases to exotic lattices. Optical lattices are briefly reviewed in App. A. Different atomic or molecular species may also be used which feature unique properties such as different cooling wavelengths, different ratios of the elastic to inelastic collisions, fermionic vs bosonic behaviour, magnetic properties and much more. Furthermore, the interactions between the atoms and molecules can be tuned using Feshbach resonances [28]. Typically the set-ups also allow for state population and density measurements of the atomic cloud. With these tools the geometry, density, and interactions of the gas can be set at the desired parameters. This allows for the simulation of many-body systems devised in fields from soft-condensed matter to cosmology. Some examples

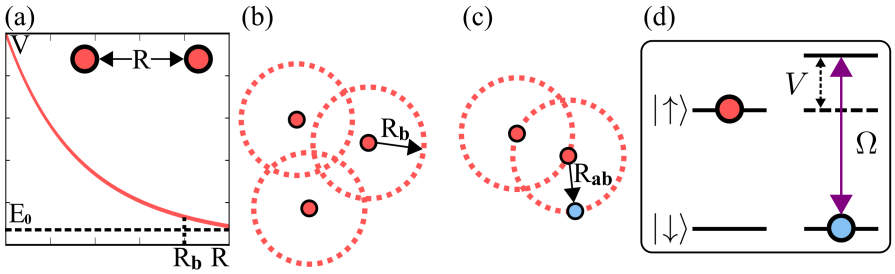

Figure 1.1: Illustration of blockade and anti-blockade effects. (a) shows a sketch of the form of the interaction between Rydberg atoms following a $\sim 1/R^6$ shape, and has labelled on it an approximation of the blockade radius, R_b, as a result of this interaction. E_0 represents the energy of the Rydberg state without any interaction dressing. (b) is a cartoon of the blockade effect with the blockade radius shown around Rydberg atoms (red), where none of the Rydberg atoms exist inside one another radii. (c) is the anti-blockade effect, where now the unexcited atom (blue) is coupled to the Rydberg state as it lies on the radius of another. (d) shows the energy level diagram of the anti-blockade set-up, with the ground state ($|\downarrow\rangle$) being coupled to the Rydberg state ($|\uparrow\rangle$) by a laser with Rabi frequency Ω, represented by the purple arrow, at detuning Δ which is equal to the experienced interaction V, shown as a dashed black arrow, from the neighbouring Rydberg atom.

include, the Bose-Hubbard model and observation of the superfluid-Mott-insulator transition [3, 29–33]. Furthermore, atomic ensembles have applications in detection and metrology with atomic clocks [34], the observation of gravitational effects [35, 36], and in quantum information [37].

A field from atomic physics that is employed frequently in this thesis is that of Rydberg atoms [38, 39]. A Rydberg atom features a single valance electron excited to a high principle quantum number, typically $n > 50$. Notably, Rydberg atoms were crucial in the 2012 Nobel prize for non-destructive quantum measurement, making use of their long lifetimes [40]. Due to the high principle quantum number spontaneous radiative decay is greatly suppressed instead being dominated by black body radiation [41]. This results in lifetimes on the order of μs's, being well within the length of experimental studies. The most striking feature of Rydberg atoms is their strong interactions. High-lying orbitals are very much stretched outwards from the nucleus, their radius scaling as

$$r = \frac{n^2\hbar^2}{ke^2m_e} \tag{1.3}$$

where m_e is the mass of the electron and $k = 1/4\pi\epsilon_0$. Due to the n^2 dependence this radius will be large. This allows them to be modelled

as oversized hydrogen atoms, with the nucleus being the combination of the atomic nucleus and the non-excited electrons. Their dipole moment depends only on the outer electron leading to a heavily exaggerated polarisability. In turn, very strong van der Waals interactions occur between Rydberg atoms as

$$V \approx C_6/R^6, \tag{1.4}$$

with the van der Waals coefficient scaling as $C_6 \propto n^{11}$ [39], and where R is the distance between Rydberg atoms. The shape of this interaction is shown in Fig. 1.1(a). The strong interactions lead to two interesting phenomena: the blockade and anti-blockade effects.

The Rydberg blockade effect [42] stems naturally from experimental systems and is the result of strong Rydberg-Rydberg interactions. We consider a system of atoms which is coupled resonantly to a Rydberg state by a laser with Rabi frequency Ω, as shown in Fig. 1.1(d). When a single atom is excited to its Rydberg state, it causes atoms within the so-called "Blockade radius" to have their Rydberg state moved off-resonance as there is now the extra energy from the interaction. The blockade radius is defined as

$$R_b = \sqrt[6]{\Omega/C_6}, \tag{1.5}$$

being the distance beyond which the energy shift, due to the interaction, becomes smaller than the line broadening from the laser coupling, which is of the order of Ω. For Rydberg atoms Ω lies in the MHz range meaning the blockade radius is typically on the order of μm's. Such distances are large in a quantum gas, meaning that "macroscopic" objects can be formed using the blockade effect with one such being "super-atoms", regions of atoms contained within a single Rydberg blockade radii. These occur as there can be only be a single Rydberg atom, but it can be any of them, creating a superposition of all one-excitation (Fock) states with equal amplitudes. For systems larger than a single radii, super-atoms can form interesting geometries of blockade radii [43–48], an example of a single state of which is shown in Fig. 1.1(b). It has also been shown to be a useful tool in quantum information problems [37, 49], and has applications in the production of single photon sources [50, 51].

The anti-blockade effect [52, 53] follows directly from the blockade, using it to precisely control Rydberg excitations in the system. If the coupling laser, instead of being resonant with the Rydberg state, is blue detuned, then at the anti-blockade radius the atoms will in-fact, through the interaction, be resonant with the excitation laser. As this detuning can be accurately controlled it allows for this radius to be adjusted to some extent to fit the needs of the problem. The possibility of tuning the blockade distance is particularly important when employing this effect in a lattice system as it can be set to certain neighbouring positions. The key phenomena from this effect, that will be

employed in this thesis, is once there is a single Rydberg atom it can start a cascade of excitations at approximately fixed distances from one another, an example of which is shown in Fig. 1.1(c). It has been found that the anti-blockade effect has applications in quantum simulation and is useful in the production of non-equilibrium constrained systems [10, 54–57]. It is this intersection between Rydberg atomic systems and constrained systems that will be primarily investigated in this thesis as rich non-equilibrium physics often stems from the presence of competing dynamical processes and strong interactions.

Within atomic physics there are several alternatives to Rydberg atoms for the achievement of similar phenomena, namely ions and polar molecules. Trapped ions are crucial in the field of quantum computation [58, 59], with the first controlled-NOT quantum gate proposal being specifically for ions [60]. Trapped ions allow for the clean production of interacting particles, via the coulomb force, which can be trapped for long times, in the range of ms-s, and controlled coherently with minimal interaction with the environment. They are however produced in low numbers, with systems typically composed of < 20 ions. Polar molecules [61] feature strong interactions through their dipole-dipole forces, as with Rydberg atoms. Polar molecule gases can feature much higher densities than trapped ions and are a relevant competitor to Rydberg atoms for interacting many body physics simulation. In both cases however their interactions can not be switched on and off like a Rydberg atom, which usually features a non-interacting ground state, a feature used throughout this thesis.

Atomic systems tend to be open on longer time-scales, experiencing, for example, such processes as atomic loss from traps and the emission and absorption of photons. As such there has recently been considerable effort in the study of open quantum systems. The extra noise from the interaction with the environment in quantum systems is often viewed as a destructive process. Decoherence in some instances removes all the quantum nature, a major opponent to the achievement of the quantum computer [62]. Decoherence of a quantum gas in a lattice can be controlled by the properties of the lattice as commented on App.A. New studies have shown that it in fact dissipation can be a resource for the achievement of systems with intriguingly rich dynamics. In particular, a competition between coherent and incoherent processes can give rise to seemingly counter-intuitive phenomena. Examples include the occurrence of slow or glassy dynamics [10, 55, 57, 63], the relaxation into stationary states with spatial correlations [64–66], the observation of intermittency and bistabilities [66–69], the creation of entanglement by dissipation [70–78], the production of effective interparticle interactions [79, 80], and the emergence of equilibrium [69, 81–84] and out-of-equilibrium universal behaviour [56].

1.1 THESIS OVERVIEW

This thesis focusses on the study of open non-equilibrium many-body quantum systems that can be realised in atomic Rydberg systems, or equivalent settings, and explores the dynamics present in each model. We present a particular focus on the utilisation of noise as a resource for the production of constrained models. In Ch. 2, we review essential theory and the techniques used to study the models.

Ch. 3 focusses on a binding resulting from strong dissipation. The dissipation takes the form of a distance-selective pair loss, engineered using the anti-blockade effect and natural decay channels. When this dissipation is strong in comparison to other processes, the quantum Zeno effect [85] restricts the system to a reduced subspace. Within this subspace structures form that show interesting properties.

In Ch. 4 we study a general method for understanding what kinetically constrained models [8, 10, 15] can be realised in quantum many-body lattice systems under strong dephasing noise. We provide a general framework for calculating the connectivity of the model, and comment on the realisability of certain models. We choose to focus on an example of a excluded volume model.

We apply the findings of Ch. 4 in Ch. 5 to the problem of many-body localisation (MBL) [86], a field garnering greater attention recently due to the phenomena preventing the thermalisation of a closed quantum system. We show the influence of interactions on the decay form of open MBL systems, presenting the models which govern both the weak and strong interactions limits. We go on to predict further results that could be experimentally tested in current set-ups.

We then move on to study systems which belong to the directed percolation (DP) universality class [87], a key non-equilibrium class of phase transitions. Ch. 6 focusses on the production of a DP-like model utilising on-site atom loss and gain as a resource. We find that it produces a model which has received minimal study and offers a potential experimental platform for the realisation of DP-like systems in all dimensions, a currently outstanding problem. In Ch. 7 we look at a quantum version of a DP model and look at the result of a crossover from the "quantum" to the "classical" limit.

2

BACKGROUND

We start with a review of the essential tools and concepts employed in this thesis. Each chapter focuses on open quantum systems, so a review of their description and the techniques used here to study them is given.

2.1 OPEN QUANTUM SYSTEMS

The original efforts in quantum mechanics focussed on closed quantum systems, singularly contained settings with no interactions with the outside world. As progress was made with quantum theory many new fundamental questions arose, the most outstanding of which is probably the measurement problem. When a quantum system is measured, no matter what the state is at the time of measurement, it will always be observed in an eigenstate of the measurement, or observable, operator. This is known as the *collapse* of a wavefunction. For example, considering a two level system with state $|\psi\rangle = a|0\rangle + b|1\rangle$ where $|a|^2 + |b|^2 = 1$. Measurements are performed on observables defined by operators, $\hat{O}$. Observables must meet the condition of being hermitian, i.e. $\hat{O} = \hat{O}^\dagger$, and occur outside of the system's Hamiltonian. Crucially, whenever a measurement is made, the system is found in an eigenstate, $|\phi\rangle$, of the observable, i.e. $\hat{O}|\phi\rangle = \lambda|\phi\rangle$ where λ is the associated eigenvalue. Considering a general observable defined as $\hat{O} = \lambda_0|0\rangle\langle 0| + \lambda_1|1\rangle\langle 1|$, the two associated eigenstates are $|0\rangle$ and $|1\rangle$ with eigenvalues λ_0 and λ_1 respectively. This means that when measured by $\hat{O}$ the outcome is $|0\rangle$ with probability $|a|^2$ giving measurement result λ_0 and $|1\rangle$ with probability $|b|^2$ giving measurement result λ_1. Once measured, in either state, further instantaneous measurements by $\hat{O}$ will yield the same result meaning the system has collapsed into the measured eigenstate. This represents a non-unitary loss of information in the system, as the state prior to the measurement can only be "recovered" by building up sufficient statistics by preparing and measuring under the same protocol many copies of the state.

This action of individual measurement is still ad hoc in quantum theory and has yet to be resolved exactly how this collapse occurs. This example points out the important role that an external action plays in the evolution of a quantum system and has led to a growing effort towards understanding *open* quantum systems [88] i.e. those which interact with their environment with non-unitary actions. Here I will discuss the theoretical description of open quantum systems

and the methods that are used to analyse them throughout this thesis. For simplicity we set $\hbar = 1$.

2.1.1 *The density matrix and the Lindblad master equation*

The state of a quantum system is described by a wavefunction, $|\psi(t)\rangle$, which is time dependant. The evolution of this state is governed by the Schroedinger equation

$$H|\psi(t)\rangle = i\frac{\partial|\psi(t)\rangle}{\partial t}. \tag{2.1}$$

Throughout this thesis we will study open quantum systems. An open system is one which interacts with an environment or bath. This means that we assume that we can separate the total Hamiltonian as

$$H = H_S + H_B + H_I \tag{2.2}$$

where H_S, H_B, H_I represent the Hamiltonians of the system, the bath and their interaction respectively. In order to only extract the dynamics of the system we require a different formalism than the simple Schroedinger equation.

We focus primarily on many-body systems in this thesis such that we will mostly use second quantisation to represent states of a system i.e. rather than describe each particle individually, assigning each an amplitude at every point in the state space, we instead assign particles to states. Considering a two-level system, a single particle state of the system would be defined as a superposition of these two states $|\psi(t)\rangle = a(t)|0\rangle + b(t)|1\rangle$, where $a(t)$ and $b(t)$ define the probabilities that the system is found in either state, meaning they must satisfy $|a(t)|^2 + |b(t)|^2 = 1\ \forall\, t$. For a two particle system in second quantisation, the state of the system is now defined as how many particles are in either state, written as

$$|\psi(t)\rangle = a(t)|2,0\rangle + b(t)|1,1\rangle + c(t)|0,2\rangle \tag{2.3}$$

where for each state, $|n_0, n_1\rangle$, n_0 and n_1 are the number of particles in states $|0\rangle$ and $|1\rangle$ respectively. This is extended to many-body systems with N particles and $\mathcal{N}$ states by assigning amplitudes to the states $|n_0, n_1, ..., n_\alpha, ..., n_{\mathcal{N}-1}\rangle$ requiring that $\sum_\alpha n_\alpha = N$. Each of these states are referred to as Fock states or number states. If the particles are bosonic then the number of particles able to occupy a single state is unlimited, while for fermions $n_\alpha \leqslant 1\ \forall\, \alpha$.

To represent the state of the system we introduce the most general description, the density matrix, ρ. For a system with a Hilbert space of states $|\psi_j\rangle$, the density matrix is defined as

$$\rho = \sum_{i,j} p_{i,j}\,|\psi_i\rangle\langle\psi_j|\,. \tag{2.4}$$

where a density matrix must satisfy the properties of positivity i.e. all of its eigenvalues are positive, hermiticity i.e. $\rho = \rho^\dagger$, and it must be normalised such that $\mathrm{Tr}[\rho] = 1$. The expectation value of an operator, $\hat{O}$, is found by $\langle \hat{O} \rangle = \mathrm{Tr}\left[\hat{O}\rho\right]$.

Density matrices encompass two unique cases of states. Pure states can always be written as $\rho = |\psi\rangle\langle\psi|$ and easily identified as when $\rho^2 = \rho$. A mixed state allows for a broader interpretation of the state, in which part of the uncertainty on its nature is due to classical statistics. For example if you are aware that with probability p you have initiated a system in state $|\psi\rangle$ and with probability $1-p$ you have state $|\phi\rangle$ then it cannot be written as pure state, instead it is represented by $\rho = p|\psi\rangle\langle\psi| + (1-p)|\phi\rangle\langle\phi|$. Mixed states are identified as when $\rho^2 \neq \rho$.

The interaction with an environment, as with a measurement, enters as a non-unitary action on the system. The operations from the interaction with the environment are typically called *jump operators*, $\hat{L}$, as they represent a sudden change in the state of the system. Note, jump operators do not have to be hermitian. Taking our previous example of a two-level system with the jump operator being $\hat{L} = \hat{n}$ with the initial density matrix being pure with the state of the above example i.e.

$$\rho_i = |\psi\rangle\langle\psi| = |a|^2|0\rangle\langle 0| + |b|^2|1\rangle\langle 1| + ab^*|0\rangle\langle 1| + a^*b|1\rangle\langle 0|. \tag{2.5}$$

After the action of $\hat{n}$, we know it is either in $|0\rangle$ or $|1\rangle$ with probabilities $|a|^2$ and $|b|^2$ respectively and this can no longer be written as a pure state as there are now two classically weighted states of the system i.e.

$$\rho_i \to \rho_f = |a|^2|0\rangle\langle 0| + |b|^2|1\rangle\langle 1|. \tag{2.6}$$

We see that the system loses the off-diagonal parts of the density matrix, also known as the coherences. This more clearly shows the loss of information through of a non-unitary operation. This formalism of the state allows us to continue the study of an open quantum system's dynamics after a collapse due to the presence of mixed states.

For all parts of this thesis we will study the evolution of open quantum systems under the Born-Markov approximation [89]. This approximation requires the following conditions to be satisfied:

- Born approximation - the system and bath are coupled weakly in comparison to the other relevant couplings in the system. This ensures that the density matrix of the system can always be considered to factorise out of the total density matrix i.e. system-bath correlations are negligible with respect to system-system and bath-bath ones.

- Markov approximation - the evolution of the system at the current time has no dependance upon its history. In an open quantum system this is equivalent to assuming that the bath is large and the relaxation time short. This would mean that any information that enters the bath from the system, e.g. a photon emitted into the bath, has a very low probability of returning, or at least the timescale of the return is longer than the period-of-interest.

Provided these assumptions are satisfied then the system's dynamics may be modelled using the Lindblad master equation [89],

$$\dot{\rho} = -i[H, \rho] + \sum_j (L_j \rho L_j^\dagger - \frac{1}{2}\{L_j^\dagger L_j, \rho\}), \tag{2.7}$$

where ρ is the density matrix of the system, H is the Hamiltonian of the system, and the L_j operators are jump operators which define the interaction of the system with the bath. These jump operators may also be referred to as incoherent processes, while the evolution by H is coherent.

The evolution of an expectation value of operator, A, may also be calculated using

$$\langle \dot{A} \rangle = i \langle [H, A] \rangle + \sum_j \left\langle (L_j^\dagger A L_j - \frac{1}{2}\{L_j^\dagger L_j, A\}) \right\rangle. \tag{2.8}$$

2.1.2 *Second-order perturbation of the master equation*

A common tool that is used in each section of this thesis is Kato perturbation theory or the resolvant method [88, 90]. The method allows for a perturbative approach to systems where a process, or rate, is dominant in the system allowing the projection of the Lindblad master equation onto the physically relevant space specified by this dominant action. This specific method is also referred to as the adiabatic elimination of the fast degrees of freedom.

We consider the instance where the master equation Liouvillian, $\mathcal{L}$, can be split into dominant, $\mathcal{L}_d$, and perturbative, $\mathcal{L}_p$, parts

$$\dot{\rho} = (\mathcal{L}_d + \mathcal{L}_p)\rho. \tag{2.9}$$

$\mathcal{L}_d$ is considered dominant when the timescale of its action is much lower than the perturbative term. We express the the dominant term in its diagonal basis with eigenvalues, k_i, and eigenspaces or pseudo-projectors, P_i:

$$\mathcal{L}_d = \sum_i k_i P_i. \tag{2.10}$$

These projectors form a complete orthogonal set,

$$P_i P_j = \delta_{i,j} P_i, \tag{2.11}$$

$$\sum_i P_i = 1. \tag{2.12}$$

Provided $\mathcal{L}_d$ is physical, i.e. preserves positivity of the density matrix, then it will feature at least a single 0 eigenvalue, $k_0 = 0$, while the rest have a negative real part. P_0 is then a projector onto the steady state space of the Liouvillian. This then leaves the master equation as

$$\dot{\rho} = \mathcal{L}_p \rho + \sum_\lambda k_\lambda \rho_\lambda, \tag{2.13}$$

where $\rho_\lambda = P_\lambda \rho$ and the index λ omits the steady state space. The system will rapidly evolve via $\mathcal{L}_d$, meaning that on a short timescale for $\mathcal{L}_p$ the system will reach the steady state space $\mu = P_0 \rho$. We define the projector on the irrelevant space as $Q = \sum_\lambda P_\lambda$. We then split Eq. (2.13) into the evolution in the relevant and irrelevant spaces

$$\dot{\mu} = P_0 \mathcal{L}_p \mu + P_0 \mathcal{L}_p Q \rho, \tag{2.14}$$

$$Q\dot{\rho} = Q\mathcal{L}Q\rho + Q\mathcal{L}\mu. \tag{2.15}$$

Formal integration of Eq. (2.15) gives

$$Q\rho(t) = e^{tQ\mathcal{L}} Q\rho(0) + \int_0^t d\tau e^{(t-\tau)Q\mathcal{L}} Q\mathcal{L}\mu(\tau). \tag{2.16}$$

We assume that we start entirely in the steady state space i.e. $Q\rho(0) = 0$ which gives

$$Q\rho(t) = \int_0^t d\tau e^{(t-\tau)Q\mathcal{L}} Q\mathcal{L}_p \mu(\tau), \tag{2.17}$$

which is substituted into Eq. (2.14) to give

$$\dot{\mu} = P_0 \mathcal{L}_p \mu + P_0 \mathcal{L}_p \int_0^t d\tau e^{(t-\tau)Q\mathcal{L}} Q\mathcal{L}_p \mu(\tau). \tag{2.18}$$

We then take a Laplace transform of Eq. (2.14) to find

$$\mathbb{L}[\dot{\mu}](s) = P_0 \mathcal{L}_p \mathbb{L}[\mu] + P_0 \mathcal{L}_p \frac{1}{s - Q\mathcal{L}} Q\mathcal{L}_p \mathbb{L}[\mu] \tag{2.19}$$

where s is the transformed frequency. Applying the assumption that the amplitude of $\mathcal{L}_d$ is dominant, Eq. (2.19) is then expanded to second order in $\mathcal{L}_p$ as

$$\mathbb{L}[\dot{\mu}] \approx P_0 \mathcal{L}_p \mathbb{L}[\mu] + P_0 \mathcal{L}_p \frac{1}{s - Q\mathcal{L}_d} Q\mathcal{L}_p \mathbb{L}[\mu]. \tag{2.20}$$

We then perform an inverse Laplace transform

$$\dot{\mu} \approx P_0 \mathcal{L}_p \mu(t) + P_0 \mathcal{L}_p \int_0^t d\tau e^{(t-\tau)\mathcal{L}_d} Q\mathcal{L}_p \mu(\tau). \tag{2.21}$$

Expanding $\mathcal{L}_d$ in terms of its projectors and expanding the exponential, we find

$$\dot{\mu} \approx P_0\mathcal{L}_p\mu(t) + \sum_\lambda P_0\mathcal{L}_p \int_0^t d\tau e^{(t-\tau)k_\lambda} P_\lambda \mathcal{L}_p \mu(\tau). \tag{2.22}$$

Using integration by parts, this remaining integral is re-expressed as

$$\begin{aligned}\dot{\mu} \approx & P_0\mathcal{L}_p\mu(t) + \sum_\lambda P_0\mathcal{L}_p[(\frac{-1}{k_\lambda} P_\lambda \mathcal{L}_p(\mu(t) + \mu(0)e^{tk_\lambda})) \\ & - \frac{e^{tk_\lambda}}{k_\lambda}\int_0^t d\tau e^{-\tau k_\lambda} P_\lambda \mathcal{L}_p \frac{d\mu(\tau)}{d\tau}].\end{aligned} \tag{2.23}$$

As we are interested in the long time dynamics, i.e. long with respect to the timescasle of $\mathcal{L}_p$, it allows for the remaining integral term and the term $\mu(0)e^{tk_\lambda}$ to be set to zero, leaving an effective master equation of the form

$$\dot{\mu} \approx P_0\mathcal{L}_p\mu(t) - \sum_\lambda \frac{1}{k_\lambda} P_0\mathcal{L}_p P_\lambda \mathcal{L}_p \mu(t). \tag{2.24}$$

For problems considered in this thesis higher orders do not affect the dynamics provided you are sufficiently in the required perturbation limit.

2.2 KINETIC MONTE CARLO

Used throughout this thesis is the numerical method, kinetic Monte Carlo (KMC). This technique may be used to simulate the dynamics of a transition-rate defined classical system. It works by randomly selecting a transition or jump between two states weighted by the rate of transition between them and advancing the time based upon the idea that these events occur following a Poisson distribution. In all cases we will use the rejection-free, or Bortz-Kalos-Lebowitz algorithm [91].

Considering a system with states indexed as k, with the transition rate between states k and k' defined as $r_{k\to k'}$. For a state with a total transition rate, $R_k = \sum_{k'} r_{k\to k'}$, it will have a "survival" probability in time as

$$P = e^{-R_k t}. \tag{2.25}$$

This defines the probability that no jump has occurred from state k up to time t. After initialising the system at time $t = 0$, the algorithm to simulate a single trajectory follows as:

1. Generate from a uniform distribution a random number $u \in (0, 1]$.

2. Calculate the total rate, R_k, for the current state, k.

3. Calculate the change in time, $\Delta t = R_k^{-1} \ln(1/u)$, until the next jump.
4. Update the time, $t \to t + \Delta t$
5. Calculate the cumulative rate function $C_{k,k'} = \sum_{j=0}^{k'} r_{k \to j}$.
6. Generate a uniform random number $u' \in (0, 1]$.
7. Select the transition to occur by which k' satisfies the condition $C_{k,k'-1} < u' R_k \leqslant C_{k,k'}$
8. Perform the transition to the selected state k'.
9. Repeat until a specified condition is met.

This technique may be continued to generate a trajectory until the total rate of the current state is 0, such states are known as absorbing states, or a condition is satisfied such as a fixed number of jumps or a maximal time. In all instances in this thesis the condition of max-time is used. Trajectories may then be averaged to study the behaviour of the mean value of observables in the system.

2.3 QUANTUM JUMP MONTE CARLO

To numerically simulate open-quantum system dynamics a primary technique is quantum jump Monte Carlo (QJMC) [92, 93]. The incoherent processes shown as the jump operators in Eq. (2.7) are the transitions that will be randomly selected by the Monte Carlo algorithm. Unlike with KMC, a quantum system continues to evolve between jumps, which in turn influences the probability of certain jumps occurring in time, leading to a more complex algorithm.

A key component of this approach is the effective Hamiltonian. Eq. (2.7) is rewritten as

$$\dot{\rho} = -i \left(H_{\text{eff}} \rho - \rho H_{\text{eff}}^{\dagger} \right) + \sum_j L_j \rho L_j^{\dagger}, \tag{2.26}$$

where

$$H_{\text{eff}} = H - \frac{i}{2} \sum_j L_j^{\dagger} L_j. \tag{2.27}$$

H_{eff} is a non-hermitian operator meaning it does not preserve the normalisation of the state. It can be shown that to first order [92, 93], for a single trajectory of the state, in between jumps the system is evolved by H_{eff}. The decay of the normalisation then translates to an increasing probability of a jump giving a definition of the survival probability as

$$P_{|\psi\rangle}(\Delta t) = |e^{-i \Delta t H_{\text{eff}}} |\psi\rangle|^2. \tag{2.28}$$

The form of H_{eff} is best calculated at the start of the simulation and stored.

After initialising the system in a pure state $|\psi\rangle$, the algorithm to produce a single quantum trajectory follows as:

1. Generate a uniform random number $u \in (0, 1]$.
2. Calculate the survival probability using Eq. (2.28).
3. Calculate the time, Δt, at which $P_{|\psi\rangle}(\Delta t) = u$.
4. Update the time, $t = t + \Delta t$.
5. Evolve the state, $|\psi\rangle \to e^{-i\Delta t H_{\text{eff}}} |\psi\rangle$.
6. Calculate the cumulative rate function $C_{j,j'} = \sum_{j=0}^{j'} P_j$ where $P_{j'} = \langle\psi| L_{j'}^\dagger L_{j'} |\psi\rangle \,/\, \sum_j \langle\psi| L_j^\dagger L_j |\psi\rangle$.
7. Generate a uniform random number $u' \in (0, 1]$.
8. Select the transition to occur by which j' satisfies the condition $C_{j,j'-1} < u' \leqslant C_{j,j'}$
9. Perform the selected jump on the state as, $|\psi\rangle \to L_{j'} |\psi\rangle$.
10. Normalise $|\psi\rangle$.
11. Repeat until a specified condition is met.

This produces a single quantum trajectory for that initial condition. This algorithm is then repeated and the resulting trajectories averaged to produce the dynamics of the density matrix, which is equivalent to the dynamics produced by the Lindblad master equation [92].

IMPLEMENTATION — The implementation of the QJMC algorithm is more complex than that of KMC which can largely be input exactly as shown above. With a KMC trajectory, the only large dataset that needs to be stored is the state of the system, which if we consider the system to be composed of L sites each with x states then at most this is an L-size array of integers. Large system sizes ($L \approx 10000$) can be reached with KMC before any considerations for efficiency need to be made.

With QJMC this is not the case. Already the state is much larger as we are dealing with a quantum state rather than a classical state, meaning that for each trajectory the state that needs to be stored is x^L doubles. H_{eff} and each L_j must also be stored, which are all of size x^{2L}. There is a frequent tendency for these items to be sparse, i.e. the majority of their entries are zero, in which case it is much more efficient to store them as sparse arrays. Ultimately, this means that the size of the stored items grows much faster with L than in classical systems, putting a limit on the system sizes possible in this

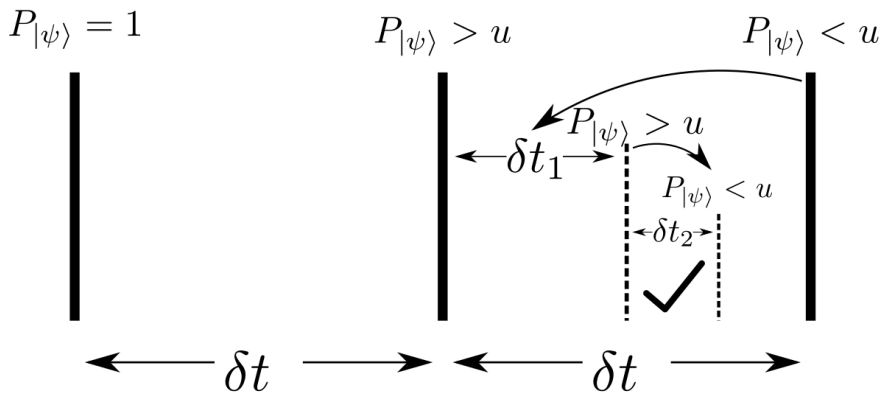

Figure 2.1: Illustration of the binary search algorithm for only three time step values. This is the true binary search algorithm for this problem rather than the order of magnitude time step change described in the text. It shows a single search starting at $P_{|\psi\rangle}(\Delta t = 0) = 1$ and progressing by the time step, δt. The $P_{|\psi\rangle}(\Delta t)$ is found to go below the random number, u, at the second time step, meaning the jump lies between the $\Delta t = \delta t \rightarrow 2\delta t$. The time step is then reduced to $\delta t_1 = \delta t/2$, where $P_{|\psi\rangle}(\Delta t)$ is found above u at the time step. Again the time step is reduced to δt_2 and at which point $P_{|\psi\rangle}(\Delta t)$ is found below u meaning the jump occurs at time $\Delta t = \delta t + \delta_1 + \delta_2$. If the algorithm was to continue it would search the area indicated by the "tick" mark.

algorithm, typically $L = 15$ is a maximum. During the algorithm there is also the expensive, according to how much processing time it takes, calculation of $e^{-i\Delta t H_{\text{eff}}}$ as it involves the evaluation of the exponential of a matrix. Furthermore, when trying to find the value of Δt at which $P_{|\psi\rangle}(\Delta t) - u = 0$, it can rarely be solved for analytically. As such, for example, a bisection method [94] needs to be used, or an equivalent algorithm, which requires many calculations of the exponential.

There are many solutions to these problems, most of which are system dependent. Employed in Sec. 7, I use a technique that puts a greater emphasis on memory to put all calculations of the exponentials to the start of the program borrowing from the discrete QJMC algorithm [92, 93]. It works as follows: From each trajectory you aim for read-out of the state at specified times, for example if you are running each trajectory for time T then you may take n readouts of the state leading to a readout at each time $t_k = kT/n$ which are separated by time $\delta t_0 = T/n$. If we consider a no-jump trajectory it means that all we would require to get a readout of the state at each of these times is $e^{-i\delta t_0 H_{\text{eff}}}$ to evolve between them.

For a trajectory which features jumps, the same action is performed. The state is first evolved by $e^{-i\delta t_0 H_{\text{eff}}}$ to progress to the next t_i and then the value of $P_{|\psi\rangle}(\delta t_0) - u$ is checked. If it is negative then a jump has occurred in this last time step. The exact time could then be found

using the bisection method using the two time values as bounds but I found it more efficient to pre-set an accuracy in time. This is done by evaluating and storing at the start of the algorithm $e^{-i\delta t_1 H_{\text{eff}}}$ where $\delta t_1 = \delta t_0/10$. Then when a jump is detected, it returns to the previous time-step and instead evolves by $e^{-i\delta t_1 H_{\text{eff}}}$. Again the jump is tested for after each evaluation. When it is detected it returns to the previous time-step and then evolves by $e^{-i\delta t_2 H_{\text{eff}}}$ where $\delta t_2 = \delta t_0/100$. This continues, evolving the state by $e^{-i\delta t_j H_{\text{eff}}}$ where $\delta t_j = \delta t_0/10^j$ until a good accuracy in time is acquired, and the earlier time is selected. The power of this method comes in that each of these exponentials is calculated at the start, and the number of them required can be determined by the system properties i.e. the time T and the maximal possible rate of the jumps. The action of then applying these matrices to the state is fast and allows for the algorithm to be much quicker. It does however put more in the memory, controlled by the degree to which each of these exponentials are sparse. This method is based upon the binary search algorithm, its direct implementation, shown in Fig.2.1, would lead to faster computation but more memory usage as it would require a halving of the time step rather than a change by an order of magnitude. For the systems discussed in Sec. 7 I found a limit of $L = 13$ on high performance computer systems. An open source implementation of this algorithm can be found at Ref. [95].

3

MANY-BODY OUT-OF-EQUILIBRIUM DYNAMICS OF HARD-CORE LATTICE BOSONS WITH NON-LOCAL LOSS

3.1 INTRODUCTION

In open quantum systems, a competition between coherent and incoherent processes, as discussed in Ch. 1, can lead to unexpected phenomena. In certain cases, it may even lead to a binding mechanism [54, 96, 97], which is qualitatively different to the one resulting from coherent forces that bind the constituent particles, in for example molecules or atoms [98].

In Ref. [54] the creation of dissipatively bound complexes was shown to be due to the quantum Zeno effect [72, 85, 99–102]. The quantum Zeno effect is where through strong dissipation or measurement, i.e. the non-unitary rates are large in comparison to the coherent rates, the state space of the system is reduced as it is projected onto no-dissipation subspaces. This in turn leads to an effective dynamics on the so called Zeno subspace, this is discussed in more detail later.

In this chapter, we look at the situation of strong non-local particle loss introduced to a lattice system featuring coherent tunnelling, and study the constrained behaviour resulting in a particle binding. We focus on a one-dimensional lattice filled with hard-core bosons in a Mott insulating state. We find that the evolution proceeds in two stages. The first stage is characterised by a purely dissipative dynamics that leads to a strongly correlated loss of bosons until the system reaches a highly degenerate Zeno subspace. The second stage is governed by the competition between the dissipation and coherent particle hopping that leads to the formation of dissipatively bound complexes. We identify two qualitatively different types which naturally occur in the Zeno subspace. Their dispersion relations depend strongly on the number of constituent bosons and we find for some configurations the emergence of so-called flat bands [103] which result from an effective spin-orbit coupling and give rise to immobile complexes [104]. Such flat bands are of interest in the study of exotic topological states of matter e.g. in quantum Hall physics [105]. We further analyse the effect of interactions among neighboring bosons and between complexes.

This work was published in Physical Review B in collaboration with M. Hush and I. Lesanovsky [106].

3.2 QUANTUM ZENO EFFECT

The quantum Zeno effect [85] gains its name from the Greek philosopher Zeno of Elea who believed that motion was an illusion, and in aid of this belief invented three paradoxes of motion [107]:

1. **Achilles and the tortoise** - The story goes that Achilles has a footrace with a tortoise. He lets the tortoise have a head start, and then begins pursuing. He moves to where he saw the tortoise, but upon arrival he finds it has progressed further. So he moves to it again, and once more finds the same. This continues ad infinitum, thus the pursuer may never catch the pursued.

2. **Dichotomy** - When crossing a distance one may choose to travel it in halves. So first one moves halfway, and then another half, getting you to within one-quarter of your destination. If this is continued the destination is never reached rather one only gets incrementally closer.

3. **The arrow** - An arrow is fired through the air, at any one time it occupies a singular position. If time was frozen the arrow would be found precisely at a single spot and would be seen as equivalent to a motionless arrow at the same position, i.e. without time the arrow is not in motion.

All of these paradoxes are about the division of a dimension into finite parts and whether or not motion in that dimension can be described continuously or discretely.

The first two paradoxes can be resolved by considering an infinite geometric series. Taking the Dichotomy paradox, if the total distance to travel is $d = 1$ then it is easily shown that $\sum_{i=1}^{\infty}(1/2)^i = 1$ converges. Furthermore, if we assume a constant speed of travel the time taken for each subsequent step will reduce, converging towards 0. This means that the individual will travel distance d in a finite time when employing this strategy. The same exact reasoning applies to the resolution of Achilles and the tortoise.

The third paradox found a natural home in quantum physics. The quantum Zeno effect is where the evolution of a system, or part of it, may be "frozen" if under the influence of rapid dissipation or measurement. A simple example is demonstrated by a two-level system with Hamiltonian

$$H = \Omega\sigma_x \tag{3.1}$$

where $\{\sigma^x, \sigma^y, \sigma^z\}$ are the standard Pauli matrices with states $|0\rangle$ and $|1\rangle$. We consider this system's state as being measured in a Markovian setting meaning the system is well modelled by the Lindblad master

equation, as discussed in Sec. 2.1.1. A measurement or jump operator can be used to detect which state it is in at a rate γ,

$$L = \sqrt{\gamma} n, \tag{3.2}$$

where n is the density operator defined as $n = \sigma^+\sigma^-$, where $\sigma^\pm = (\sigma^x \pm i\sigma^y)/2$. When $\gamma = 0$ the system will undergo a Rabi oscillation causing the probability of it being found in the excited state to oscillate as $P(\uparrow) = \sin^2(\Omega t/2)$. For $\gamma \neq 0$, the measurement will cause the collapse of the state into either $|\downarrow\rangle$ or $|\uparrow\rangle$ with no coherences. If the rate of the measurement is fast i.e. $\gamma \gg \Omega$, then using the technique described in Sec. 2.1.2, we find that the system is projected onto the subspace of states $\mu = a\,|\downarrow\rangle\langle\downarrow| + b\,|\uparrow\rangle\langle\uparrow|$. Furthermore we see that it is now governed by an effective master equation

$$\partial_t \mu = \frac{4\Omega^2}{\gamma}\left(\sigma^-\mu\sigma^+ + \sigma^+\mu\sigma^- - \left\{\sigma^+, \sigma^-\right\}\mu\right). \tag{3.3}$$

This is equivalent to a Lindblad master equation with no coherent terms and jump operators

$$L_0 = \frac{4\Omega^2}{\gamma}\sigma^- \tag{3.4a}$$

$$L_1 = \frac{4\Omega^2}{\gamma}\sigma^+. \tag{3.4b}$$

The system dynamics effectively follows an incoherent flipping action between the two states at a rate $\frac{4\Omega^2}{\gamma}$. In the limit $\gamma \gg \Omega$ this rate is very low, such that when compared to the coherent action, $\gamma = 0$, the system will appear frozen in its initial state. This idea can be extended to all instances where the rate of decoherence is rapid relative to the coherent processes as will be presented in Ch. 4.

3.3 THE MODEL

We consider a one-dimensional lattice with L sites filled with hard-core bosons [80]. Hard-core bosons are when the on-site interaction is strong in comparison to other coherent processes. If the system then starts in a state with either zero or one boson per site then the probability of a double or more occupation of a site is negligible, meaning that the system can be projected onto a spin system with states $|\downarrow\rangle$, $|\uparrow\rangle$ representing an unoccupied and occupied site respectively. This scenario can, for example, be realized with optically trapped cold atoms [3].

We consider the bosons tunnelling between adjacent sites at a rate J under Hamiltonian

$$H = J\sum_{k=1}^{L}(\sigma_k^-\sigma_{k+1}^+ + \sigma_k^+\sigma_{k+1}^-), \tag{3.5}$$

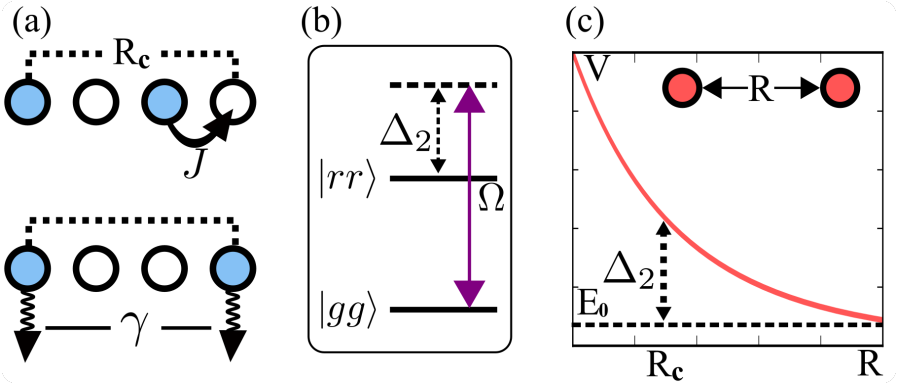

Figure 3.1: (a) Illustration of the non-local distance-selective pair loss, where the atoms may tunnel at rate J and if at a distance R_c they are ejected from the lattice a rate γ. (b) Show the level structure resulting in this dissipation as the ground state of the pair, $|gg\rangle$, is resonantly coupled to the double-Rydberg state, $|rr\rangle$, at distance R_c. (c) Illustrates the Rydberg-Rydberg interaction and the dependence of the position of the critical distance, R_c, on the detuning Δ_2.

In addition to the coherent Hamiltonian evolution we consider non-local dissipation which is given by distance-selective pair loss. Two bosons separated by the critical distance R_c are ejected from the lattice at a rate γ. This is shown in Fig. 3.1(a). This type of dissipation can for instance be physically realised in cold atom experiments by exploiting the properties of Rydberg states [54]. By utilising the anti-blockade described in Ch. 1, a laser couples the atoms in the system to a Rydberg state $|r\rangle$ with Rabi frequency Ω and detuning Δ. Considering two Rydberg atoms, $|rr\rangle$, on sites at a distance R, the interaction between the pair will detune the state from the bare value by $\Delta_2(r) = 2\Delta + V(r)$. This means that by adjusting Δ the value of R_c may be selected as the position where $\Delta_2(R_c) = 0$, causing the double Rydberg state of this pair to be resonant with the excitation laser meaning they will be rapidly excited to that state, as illustrated in Fig. 3.1(b). The excited pair then experience two decay channels. The first is due to the interaction between the pair which puts a strong mechanical force on them, i.e. $F = -\nabla V(R)$, thus causing the atoms to escape the lattice and be lost. The second channel is that as a Rydberg atom undergoes radiative decay back to its ground state, it will tend to follow a long decay path. With each decay the atom receives a momentum kick which as it occupies non-trapped states on its relaxation path it will be pushed out of the lattice.

This interaction can lead to off-resonant processes as well. Atoms that are at a single lattice site away from the critical distance i.e. $R_c + 1$,

will have the most significant rate. Using Eq. (1.4), the detuning of these processes will be

$$\Delta_2 = V(R_c)(1-(1+1/R_c)^{-6}). \tag{3.6}$$

This leads to the adjusted Rabi frequency for this process to be $\Omega_1 \approx \sqrt{\Omega_0^2+\Delta_2^2}$, with Ω_0 being the Rabi frequency of the resonant pair excitation. The max probability of this off-resonant double excitation occurring is $\approx \Omega_0^2/4\Delta_2^2$ which as $V(R_c)$ is large, as discussed in Ch. 1, this will be a highly improbable process meaning we can neglect it for the following analysis as we will not be considering the long time dynamics.

We assume that the Markovian approximation is valid, which is true for the proposed experimental implementation [54], allowing the dynamics of the density matrix ρ of the system to be described by a Lindblad master equation, discussed in Sec. 2.1.1, with distance-selective pair loss jump operators of the form

$$L_k = \sqrt{\gamma}\sigma_k^- \sigma_{k+R_c}^-. \tag{3.7}$$

for $k \in [1, L]$. Here we focus on the limit of strong dissipation, i.e. $\gamma \gg J$. The strength of the decay may be adjusted using the coupling of the double-ground state to the double-Rydberg state, such that we work in the limit of resonance i.e. $\Delta_2(R_c) = 0$. This leads to a separation of the two timescales on which the coherent and dissipative dynamics proceed.

3.4 FAST DISSIPATIVE DYNAMICS AND THE ZENO SUBSPACE

We begin by analysing the fast initial dissipative dynamics carried out by the Liouvillian

$$\mathcal{L}_d\rho = \sum_k (L_k\rho L_k^\dagger - \frac{1}{2}\{L_k^\dagger L_k, \rho\}). \tag{3.8}$$

Its stationary subspace — the Zeno subspace — is spanned by all states $|s\rangle$ that satisfy

$$L_k|s\rangle = 0 \ \forall\, k, \tag{3.9}$$

i.e. they do not contain any two bosons at the critical distance R_c. To understand the dissipative non-equilibrium evolution into the Zeno subspace we consider our system starting in a Mott insulator state, which features a single boson on each site, $|\psi_i\rangle = |\uparrow\rangle^{\otimes L}$. The corresponding evolution of the average boson density,

$$p(t) = \sum_k \frac{\langle n_k(t)\rangle}{L}, \tag{3.10}$$

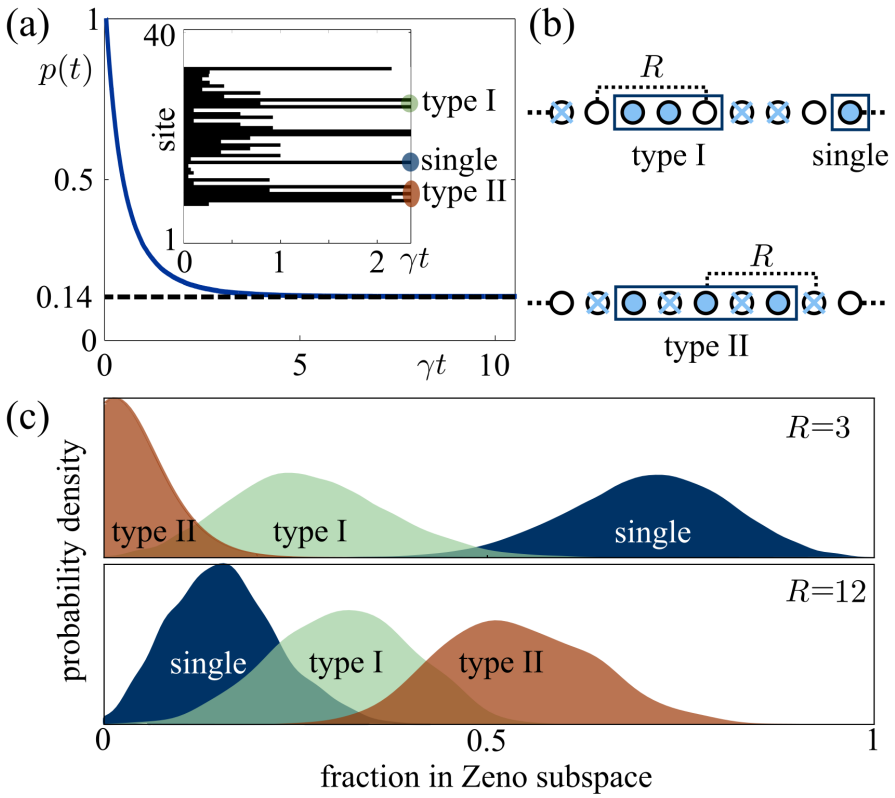

Figure 3.2: (a) Evolution of the boson density $p(t)$ under the dissipative dynamics $\mathcal{L}_d$ from an initial Mott insulator. The stationary density is $p(t \to \infty) = e^{-2} \approx 0.14$ marked by the dashed line. The inset shows a single trajectory with 40 bosons on a lattice of $L = 40$ with $R_c = 3$ and periodic boundary conditions. (b) Representative boson arrangements in the stationary state with $R_c = 3$, where single free bosons and two types of particle complexes emerge. The circles indicate sites, a filled circle indicates an occupied site, a cross indicates a site whose occupation is forbidden, as the resulting configuration would not lie in the Zeno subspace, and a box indicates the "size" of a complex. The type I complex — defined as having a size smaller than R_c — is, in this example, consists of two bosons. These bosons are unable to tunnel away from each other without running into a forbidden site which leads to an effective binding. The type II complex has a spatial extent that is larger than R_c. It is qualitatively different to type I in the sense that the removal of one boson (in the center) destroys the binding for the remaining ones. (c) Probability distributions for single bosons, type I and type II complexes in the stationary state that is reached from a Mott insulator for the cases of $R_c = 3, 12$. The relative abundances of the species change once R_c becomes comparable to the mean interparticle distance, e^2, in the stationary state. This Fig. originally appeared in Ref. [106].

can be found analytically: The mean value of the density on site k evolves under the fast dynamics of $\mathcal{L}_d$, found using Eq. (2.8), according to

$$\langle \dot{n_k} \rangle = -\gamma(\langle n_k n_{k+R_c} \rangle + \langle n_{k-R_c} n_k \rangle), \tag{3.11}$$

i.e. it depends on a two-point correlation function set by the critical distance of the pair loss. Defining the correlators $C_j = \langle \prod_{l=0}^{j} n_{k+lR_c} \rangle$ and using translational invariance, i.e. $n_{k+R_c} \equiv n_{k-R_c}$, we obtain the hierarchy

$$\dot{C}_j = -\gamma(jC_j + 2C_{j+1}). \tag{3.12}$$

This equation is solved by introducing (see Ref. [108]) the generating function

$$G(x,t) = \sum_{j=0}^{\infty} \frac{x^j C_j}{j!} \tag{3.13}$$

which evolves according to

$$\dot{G}(x,t) = -\gamma(2+x)\partial_x G(x,t). \tag{3.14}$$

For a Mott insulator state we have the initial condition $C_j = 1 \; \forall j$ and therefore $G(x,0) = \sum_{k=0}^{\infty} x^j/j! = e^x$. For this initial condition the solution becomes $G(x,t) = e^{(2+x)e^{-\gamma t}-2}$, giving the density evolution as

$$p(t) = C_0 = G(x=0,t) = e^{2(e^{-\gamma t}-1)}. \tag{3.15}$$

Numerical Monte Carlo simulations, shown in Fig. 3.2(a), confirm the rapid exponential decay of the boson density on a timescale $\sim \gamma^{-1}$. The inset shows a generic trajectory which displays the fast removal of boson pairs and a stationary configuration in which boson pairs at a distance R_c are absent. This is one configuration of many that span the high dimensional stationary Zeno subspace, the projector onto which is explicitly written as

$$Q_0 = \prod_{k=1}^{L} (1 - n_k n_{k+R_c}). \tag{3.16}$$

The average density in the stationary state reached from a Mott insulator is given by

$$p(t \to \infty) = e^{-2} \approx 0.14. \tag{3.17}$$

Note, that this result is in fact *independent* of the value of R_c.

3.5 EFFECTIVE COHERENT DYNAMICS IN THE ZENO SUBSPACE

Once having reached the Zeno subspace the dissipative evolution governed solely by $\mathcal{L}_d$ comes to a halt. Due to,

$$\mathcal{L}_c\rho = -i[H,\rho], \tag{3.18}$$

introducing quantum tunnelling to the Zeno subspace, non-trivial coherent dynamics emerges taking place on a timescale J^{-1}. As shown in Ref. [54] the effective master equation for the projected density matrix in the Zeno subspace, $\mu \equiv P_0\rho P_0$, for the limit $\gamma \gg J$, is obtained by means of Kato perturbation theory [80, 90] discussed in Sec. 2.1.2.

For this limit we only need to go to second-order in Eq. (2.24), the only actions of interest are those which exit the Zeno subspace via a single tunnelling event and return to it also with a single event. This limits the states outside of the Zeno subspace necessary to study to a single pair of bosons, and a double pair which share the central boson all at the critical distance. We define the pseudo-projectors, P_i, of $\mathcal{L}_d$ on this truncated space as:

$$\begin{aligned} P_0\rho =& Q_0\rho Q_0 + \sum_k \sigma_k^- \sigma_{k+R_c}^- Q_1\rho Q_1 \sigma_{k+R_c}^+ \sigma_k^+ \\ &+ \sum_k \sigma_{k-R_c}^- \sigma_k^- \sigma_{k+R_c}^- Q_2\rho Q_2 \sigma_{k+R_c}^+ \sigma_k^+ \sigma_{k-R_c}^+ \end{aligned} \tag{3.19a}$$

$$P_1\rho = P_0\rho Q_1 + Q_1\rho P_0, \tag{3.19b}$$

$$P_2\rho = P_0\rho Q_2 + Q_2\rho P_0 \tag{3.19c}$$

where:

$$Q_1 = \sum_m n_m n_{m+R_c} \prod_{k\neq m} (1 - n_k n_{k+R_c}), \tag{3.20a}$$

$$Q_2 = \sum_m n_{m-R_c} n_m n_{m+R_c} \prod_{k\neq m,m-R_c} (1 - n_k n_{k+R_c}). \tag{3.20b}$$

Q_0 was introduced in Eq. (3.16) and projects onto states of no pairs, Q_1 projects onto states with a single pair and Q_2 projects onto instances with two pairs which share the central boson. P_0 projects onto the steady state space of $\mathcal{L}_d$, i.e. $P_0 \equiv \lim_{t\to\infty} \mathcal{L}_d$, as it includes only states with no pairs of bosons at the critical distance. Using the assumption that the system starts in the steady state space, P_0 may be reduced to only the first term in Eq. (3.19a). It may also be shown that P_0, P_1 and P_2 project onto the eigenspaces of $\mathcal{L}_d$ with eigenvalues, $0, -\gamma/2, -\gamma$ respectively.

Using the property, $Q_iQ_j = \delta_{i,j}Q_i$, from the first term in Eq. (2.24) an effective Hamiltonian, H_Z, is derived as

$$H_Z = Q_0 H Q_0, \tag{3.21}$$

We then formulate the projected jump operators from the second term of Eq. (2.24). We first rewrite this term as:

$$\begin{aligned}-\sum_{\lambda}\frac{1}{k_\lambda}P_0\mathcal{L}_c P_\lambda \mathcal{L}_c P_0\mu(t) = P_0(&-\frac{2}{\gamma}[H,Q_1[H,\mu]Q_0]\\ &-\frac{2}{\gamma}[H,Q_0[H,\mu]Q_1]-\frac{1}{\gamma}[H,Q_2[H,\mu]Q_0]\\ &-\frac{1}{\gamma}[H,Q_0[H,\mu]Q_2]),\end{aligned} \tag{3.22}$$

where λ runs over the non-zero eigenvalues k_λ. Upon expansion of Q_0HQ_1 and Q_0HQ_2 we find

$$\dot{\mu} = -i[H_Z,\mu] + \sum_{k,\alpha}(L^{(Z)}_{k,\alpha}\mu L^{(Z)\dagger}_{k,\alpha} - \frac{1}{2}\{L^{(Z)\dagger}_{k,\alpha}L^{(Z)}_{k,\alpha},\mu\}), \tag{3.23}$$

with

$$L^{(Z)}_{k,1} = \sqrt{2\Gamma}(A_k - \sigma^+_{k-R_c}B_k - \sigma^+_{k+2R_c}B_{k+R_c}) \tag{3.24}$$

$$L^{(Z)}_{k,2} = \sqrt{\Gamma}B_k, \tag{3.25}$$

where the effective decay rate $\Gamma = 2J^2/\gamma$ and the operators

$$A_k = \sigma^-_{k+R_c+1}\sigma^-_k + \sigma^-_{k+R_c-1}\sigma^-_k + \sigma^-_{k+R_c}\sigma^-_{k+1} + \sigma^-_{k+R_c}\sigma^-_{k-1} \tag{3.26}$$

$$B_k = \sigma^-_{k-R_c}\sigma^-_{k-1}\sigma^-_{k+R_c} + \sigma^-_{k-R_c}\sigma^-_{k+1}\sigma^-_{k+R_c}. \tag{3.27}$$

By construction the dynamics under H_Z is restricted to the Zeno subspace. Dissipation within the Zeno subspace affects boson pairs, $L^{(Z)}_{k,1}$, or triples, $L^{(Z)}_{k,2}$, in configurations that are one tunnelling event away from containing bosons at the critical distance R_c. Such configurations undergo an incoherent evolution at a rate Γ, which is strongly suppressed for fast two-body decay $\gamma \gg J$. Therefore the evolution within the Zeno subspace becomes predominantly coherent despite the strong dissipation present.

3.6 FAMILIES OF COHERENT PARTICLE COMPLEXES

The approximately coherent evolution under H_Z has interesting consequences. Due to the explicit appearance of the projector Q_0, the simultaneous occupation of two sites at a distance of R_c is forbidden. This is the quantum Zeno effect in action as the system may not coherently evolve into states outside of the reduced Zeno subspace; or put differently, measurements are done at a high frequency to check the system for pairs of bosons at the critical distance which in turn prevents their development. This leads to strong correlations and the formation of bound complexes. These complexes contain a varying

number of bosons, but there are two qualitatively different configuration sets in which they can form.

Let us start with the simplest case — which we refer to as *type I*. Here m bosons are localised in a region with spatial extent smaller than R_c, an example of which is shown in Fig. 3.2(b). These bosons are effectively bound since they cannot separate by more than $R_c - 1$ sites. The second class — *type II* — are distinguished by having a spatial extent greater than R_c. These complexes form when the bosons and their associated critical distances overlap. Here, unlike for type I, not every particle binds all the others. There are even situations in which the removal of one boson destroys the entire complex, an example of which is shown in Fig. 3.2(b). By defining the complexes in this manner it is possible to classify each self-contained object present in the Zeno subspace. Both type I and II complexes appear naturally in the stationary state that is reached from an initial Mott insulator state an example of which is shown in Fig. 3.2(a).

The relative abundances of complexes in the system is dependant on the critical distance. As the mean inter particle distance is fixed by Eq. (3.17) to be e^2, there is a crossover in the relative abundances at $R_c \approx e^2$: When $R_c < e^2$ single bosons dominate with a significant proportion of bosons populating type I complexes. When $R_c > e^2$ complexes are more abundant than single bosons, with type II becoming more and more dominant with increasing R_c. Examples are shown in Fig. 3.2(c).

As the only acting Hamiltonian on the particles is hopping, which cannot create critical pairs, the primary point of interest of these complexes is their motion on the lattice. We calculate their dispersion relations, which defines the speeds of the different frequencies of a plane wave,

$$\omega(\chi) = v(\chi)\chi \tag{3.28}$$

where ω is the angular frequency, χ is the wavenumber and $v(\chi)$ are the wave-speeds or phase-velocities. The dispersion relation can then be used to calculate the group-velocity,

$$v_g = \frac{d\omega(\chi)}{d\chi}. \tag{3.29}$$

i.e. the speed of the total amplitude of the plane wave, which in our case is the speed of the complex. When working with lattice systems and crystal structures it becomes simpler to express these quantities in momentum-space. In momentum-space particles are described by their respective momenta rather than their position. This gives the complex a quasi-momentum, q and a dispersion relation $\varepsilon(q)$. The group velocity is now found by

$$v_g = \frac{d\varepsilon(q)}{dq}. \tag{3.30}$$

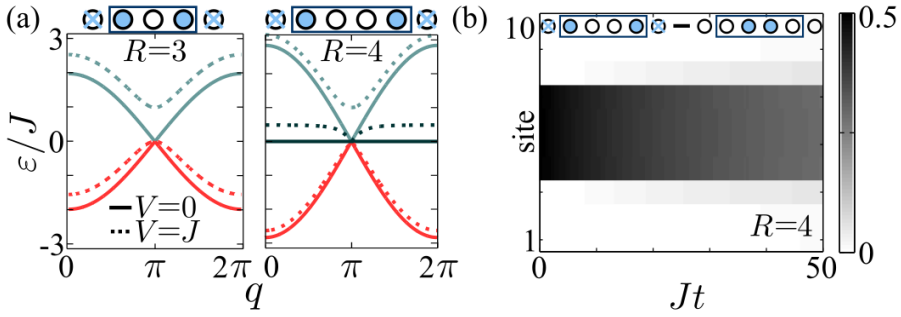

Figure 3.3: (a) Dispersion relations (solid curves) for type I complexes of two bosons with $R_c = 3$ and $R_c = 4$. Both cases show a crossing at $q = \pi$, and when $R_c = 4$ a flat band occurs. In the presence of nearest neighbor interactions (here $V = J$) the degeneracy is lifted and the flat bands are distorted (dashed curves). The sketches above the panels show a particular internal state of the respective complex. Panel (b) shows the evolution of the boson density of a type I complex formed by two bosons in the state $|F_k^{(I)}\rangle$ with $R_c = 4$ (see sketch above the panel) and $\gamma = 100J$ on a lattice of $L = 10$ sites simulated with the full master equation. This Fig. originally appeared in Ref. [106].

3.6.1 *Type I complexes*

We first characterise the type I complexes by limiting our study to the dynamics of a single complex on the lattice, addressing the interactions between complexes in the later Sec. 3.7. In the following we will provide three qualitatively different examples: immobile complexes without internal structure, complexes with an internal structure and effective spin-orbit (SO) coupling, and complexes whose dispersion relations feature a flat band arising from this effective SO coupling.

We start with the simplest type I state: two bosons, $m = 2$, and a critical distance $R_c = 2$. The only possible configuration of these bosons, in a type I state, is to be adjacent. Thus, the basis states are $|k, 1\rangle = \sigma_k^+ \sigma_{k+1}^+ |\Phi\rangle$, where $|\Phi\rangle$ is the vacuum state. In this notation k denotes the position on the lattice of the complex, and the second index labels the "internal state" of the complex. The projected Hamiltonian H_Z in this basis is identically zero. Hence the basis states $|k, 1\rangle$ are trivially eigenstates and this is an example of an immobile type I complex. These type I solutions emerge whenever $R_c = m$.

In order to see non-trivial physics we require a complex with internal states coupled via H_Z. The simplest case of this is $m = 2$ with $R_c = 3$. To calculate the spectrum of this complex, a basis of the internal states is defined as $|k, 1\rangle = \sigma_k^+ \sigma_{k+1}^+ |\Phi\rangle$ and $|k, 2\rangle = \sigma_k^+ \sigma_{k+2}^+ |\Phi\rangle$. We may also define a creation operator $|k, \alpha\rangle \equiv b_k^{(\alpha)\dagger} |\Phi\rangle$, allowing us to re-express the effective Hamiltonian as $H_Z = J \sum_k [b_k^{(2)\dagger} b_k^{(1)} + b_{k+1}^{(1)\dagger} b_k^{(2)} + \text{H.c.}]$, which now works to evolve the complex as a single

object. This can then be used to calculate the dispersion relation by first defining a generic state of the system in terms of these internal states separating the spin position parts as

$$|\psi\rangle = \sum_{k,j} A_{k,j} |j\rangle \otimes |k\rangle = \sum_{k} \begin{pmatrix} A_1(k) \\ A_2(k) \end{pmatrix} |k\rangle \tag{3.31}$$

where $A_{k,j}$ are the associated amplitudes for states $|k,j\rangle$, where for this case $j = \{1,2\}$. We then perform a discrete Fourier transform using periodic boundary conditions to find a generic quasi-momentum state as

$$|K\rangle = \frac{1}{\sqrt{L}} \sum_{k,j} e^{ikq} A_{k,j} |j\rangle \otimes |k\rangle \tag{3.32}$$

where $q = 2\pi K/L$ where K runs from 0 to $L-1$. We then transform the action of H_Z onto this basis by considering its action on the state $|K\rangle$, which we then find the associated eigensystem to get the dispersion relation of the complex as $H_Z |K\rangle = \varepsilon(q) |K\rangle$. When done on this complex the dispersion relations and eigenstates $|K_\pm\rangle$ are found to be

$$\varepsilon_\pm(q) = \pm 2J \cos\left(\frac{q}{2}\right), \tag{3.33}$$

$$|K_\pm\rangle = \frac{1}{\sqrt{2L}} \sum_{k} e^{ikq} \left[|k,2\rangle \pm e^{-iq/2} |k,1\rangle\right], \tag{3.34}$$

which are shown in Fig. 3.3(a). We see that the internal state of the complex is strongly linked to its motion on the lattice, namely the group velocity of the internal states is always in the opposite direction for the same quasi-momentum. This is termed as an effective SO-coupling, where the internal state is directly linked to its motion. Note that this spectrum has a degeneracy, or crossing, that occurs at $q = \pi$, which implies that a state transformed through quasi-momentum space will feature a discontinuous change at this point.

Lastly we consider a complex where the effective SO coupling results in a flat band, namely the case of two bosons with $R_c = 4$. We define a basis of three internal states as: $|k,1\rangle = \sigma_k^+ \sigma_{k+1}^+ |\Phi\rangle$, $|k,2\rangle = \sigma_k^+ \sigma_{k+2}^+ |\Phi\rangle$ and $|k,3\rangle = \sigma_k^+ \sigma_{k+3}^+ |\Phi\rangle$. The resulting dispersion relations, shown in Fig. 3.3(a), and eigenstates are given by

$$\varepsilon_\eta(q) = \eta\, 2\sqrt{2} J \cos\left(\frac{q}{2}\right), \tag{3.35}$$

$$|K_0\rangle = \sum_{k} \frac{e^{ikq}}{\sqrt{2L}} \left[|k,3\rangle - e^{-iq} |k,1\rangle\right], \tag{3.36}$$

$$|K_\pm\rangle = \sum_{k} \frac{e^{ikq}}{2\sqrt{L}} \left[e^{-iq} |k,1\rangle \pm \sqrt{2} e^{-iq/2} |k,2\rangle + |k,3\rangle\right]. \tag{3.37}$$

This complex has three branches labelled by $\eta = \{0,+,-\}$. The branch $\eta = 0$ is a flat band. Dispersion relations featuring flat bands result in immobile localised states which in contrast to the first type

I example are non-trivial. These localised states are formed by superimposing many quasi-momentum eigenstates and hence for non-flat dispersion relations immobile states cannot form. In a flat band all quasi-momentum states have the *same* energy and the resulting superposition state is thus still an eigenstate of the Hamiltonian.

A concrete example is given by the states

$$\left|F_k^{(I)}\right\rangle = \sqrt{\frac{2}{R_c}} \sum_{i=k}^{k+R_c/2-1} [(-1)^i \sigma_i^+ \sigma_{R_c-i+1}^+] \, |\Phi\rangle \, . \tag{3.38}$$

Using one of these states as the initial condition and propagating it under the *full master equation* we find indeed that it remains immobile as shown in Fig. 3.3(b). The simulation of the master equation is greatly simplified in these cases as we are interested in the evolution of the complex and once a dissipation event occurs, removing a pair of bosons, the lattice either has a single boson, whose behaviour is well understood, or is left empty. This means we only need to evolve the system by the effective Hamiltonian described in Sec. 2.3, and the loss of normalisation corresponds to the average dissipation in the system such that there is no need for a stochastic evolution. We see that the boson density is slowly decreasing on a timescale $1/\Gamma$. This clearly shows that the flat bands are not an artefact of infinitely strong dissipation but instead that they indeed have a drastic effect on the boson dynamics in a system with competing coherent and dissipative evolution.

Let us make some general remarks on the emergence of flat bands in the case of type I complexes: For complexes consisting of two bosons, flat bands exist provided that R_c is even. Furthermore, we find that for two, three and four bosons a flat band emerges when $R_c/m \in \mathbb{N}$. Interactions among bosons also play an important role. In order to illustrate this we consider nearest-neighbor interactions of the form $H_{nn} = V \sum_k n_k n_{k+1}$ which might, for instance, emerge in cases where non-local loss is engineered via Rydberg dressing [54]. Such interactions modify the dispersion relations as shown in Fig. 3.3(a) lifting the degeneracy point observed for $R_c = 3$, and distorting the flat band in the case of $R_c = 4$.

3.6.2 *Type II complexes*

We now move our study to type II complexes, i.e. complexes that are larger than R_c. We give two examples, one without internal structure and one with effective SO coupling.

First we consider three bosons and a critical distance $R_c = 3$. The only possible type II complexes have the basis $|k, 1\rangle = \sigma_k^+ \sigma_{k+2}^+ \sigma_{k+4}^+ |\Phi\rangle$. They are immobile — similar to the first type I example — as each boson's movement is inhibited by its nearest bosons. This is confirmed by numerical simulations shown in Fig. 3.4(a). Such immobile states

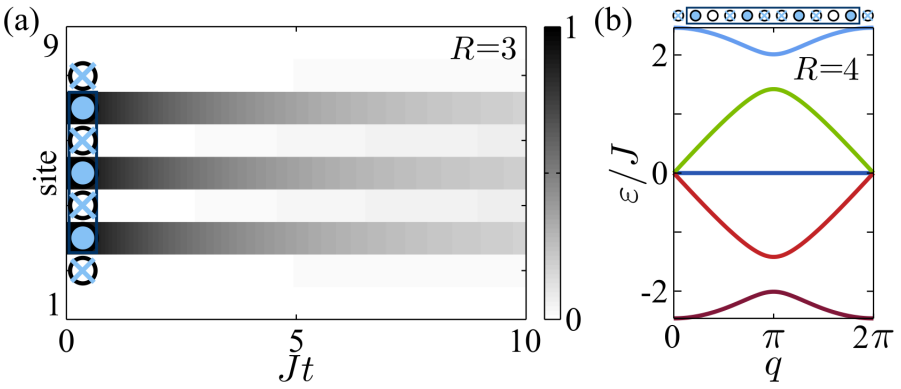

Figure 3.4: (a) Evolution of boson density for a type II complex in the immobile state $|F_3^{(II)}\rangle$, with $R_c = 3$ and $\gamma = 100J$. (b) Dispersion relation for a type II complex consisting of four bosons with $R_c = 4$. This Fig. originally appeared in Ref. [106].

can be straight-forwardly generalised to larger boson numbers, e.g. in the given example by attaching bosons to either end of the complex keeping a separation of one site.

Next we consider four bosons and a critical distance $R_c = 4$. The resulting complex has five internal states:

$$\begin{aligned}
|k,1\rangle &= \sigma_k^+\sigma_{k+3}^+\sigma_{k+6}^+\sigma_{k+9}^+|\Phi\rangle,\\
|k,2\rangle &= \sigma_k^+\sigma_{k+3}^+\sigma_{k+6}^+\sigma_{k+8}^+|\Phi\rangle,\\
|k,3\rangle &= \sigma_k^+\sigma_{k+3}^+\sigma_{k+5}^+\sigma_{k+8}^+|\Phi\rangle,\\
|k,4\rangle &= \sigma_k^+\sigma_{k+2}^+\sigma_{k+5}^+\sigma_{k+7}^+|\Phi\rangle,\\
|k,5\rangle &= \sigma_k^+\sigma_{k+2}^+\sigma_{k+5}^+\sigma_{k+8}^+|\Phi\rangle
\end{aligned}$$

and the dispersion relations shown in Fig. 3.4(b):

$$\varepsilon_0(q) = 0, \tag{3.39}$$

$$\varepsilon_{\eta,\delta}(q) = \eta\sqrt{3+\delta\sqrt{5+4\cos(q)}}, \tag{3.40}$$

with $\eta, \delta = \pm$. Hence, this type II complex features a flat band and spatially localised states of the form

$$|F_k^{(II)}\rangle = [-\sigma_k^+\sigma_{k+3}^+\sigma_{k+6}^+\sigma_{k+9}^+ + \sigma_{k+1}^+\sigma_{k+3}^+\sigma_{k+6}^+\sigma_{k+8}^+]|\Phi\rangle. \tag{3.41}$$

Again let us conclude with some more general remarks: A flat band of similar structure exists for five bosons with $R_c = 4$. For $R_c = 3$ and 4, a flat band exists provided the number of bosons is equal to or greater than R_c. The dispersion relation of this type II complex is not modified by the presence of nearest neighbour interactions. This is due to the fact for the given arrangement of bosons the simultaneous occupation of neighbouring sites is forbidden, thus the flat bands of certain type II complexes are protected from interaction effects in contrast to the type I case.

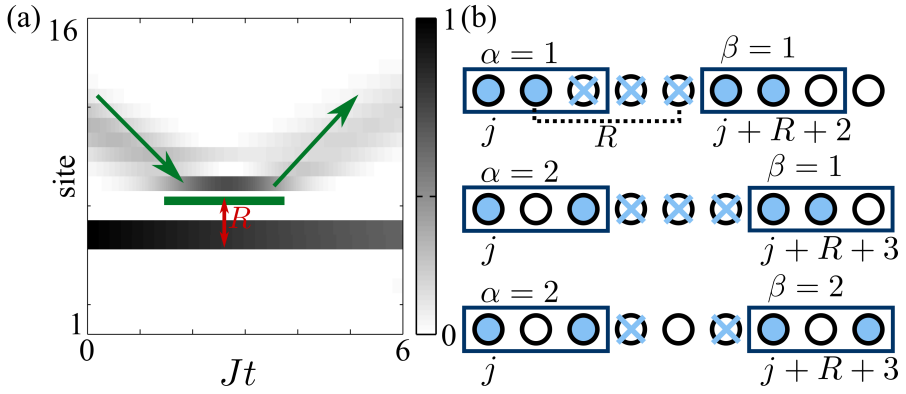

Figure 3.5: (a) Evolution of the boson density for a single boson impinging an immobile type II complex ($R_c = 2$). The single boson is in the wave packet state $|G\rangle$ with initial central quasi-momentum of $q_0 = \pi/2$ and width $\sigma = 2$. The two-particle loss rate is $\gamma = 100J$. The single boson is reflected elastically off the type II complex due to the presence of an effective next nearest neighbor exclusion interaction. (b) We show three examples of two type I complexes, in different internal states, interacting with one another. We see that the distance of the interaction depends on the internal state of the complexes. This Fig. originally appeared in Ref. [106].

3.7 INTERACTION BETWEEN COMPLEXES

As can be seen in the inset of Fig. 3.2(a) complexes are typically not isolated in the stationary subspace of $\mathcal{L}_d$ and so interactions between complexes and single bosons will occur in a normal system. A general form of the interaction was not found as each interaction is dependant on the internal state of the complex, but we can make some observations. First we study a numerical simulation of an interaction between a single boson in the wave packet state

$$|G\rangle = \frac{1}{\sqrt{2\pi\sigma^2}} \sum_k e^{-iq_0 k} e^{(k-k_0)^2/2\sigma^2} |k\rangle, \tag{3.42}$$

where k_0, q_0, σ are the initial central position, quasi-momentum, and width of the wave packet, respectively, which collides with an immobile type I complex with $R_c = 2$ shown in Fig. 3.5(a). In much the same way that the dissipation acts to bind the bosons, it also results in a hard core exclusion interaction between isolated bosons and complexes that in this example extends over R_c sites. In the case at hand this leads to an elastic collision with the type I complex essentially acting as a hard boundary. Using this mechanism one could imagine a situation where two immobile complexes enclose a boson, thereby acting as a trap.

For the type I complex of two bosons with $R_c = 3$ we can define an effective complex-complex interaction for a single pair as

$$H_{\text{int}}^{(I)} = \lim_{W\to\infty} W \sum_{m>k} \sum_{\{\alpha,\beta\}} \Theta(R_c + \alpha - |k-m|) n_k^{(\alpha)} n_m^{(\beta)}, \quad (3.43)$$

with the internal states of the complexes being indexed by $\alpha, \beta = [1, 2]$ for the left and right complex respectively, $n_k^{\alpha} = b_k^{(\alpha)\dagger} b_k^{(\alpha)}$, and $\Theta(x)$ is the Heaviside step function. This interaction is illustrated in Fig. 3.5(b). The Heaviside step function puts an infinite potential barrier on states which would have bosons of the two complexes at a distance R_c. The interaction only depends on the internal state of the left complex as it is governed by the positions of the nearest bosons, as shown in Fig. 3.5(b). For the internal state $\alpha = 1$ the bosons of the left complex are neighbouring allowing the complexes to move within $R_c - 1$ of one another. Whilst for $\alpha = 2$ the complexes can only be within distance $R_c - 2$ due to the extra site between the boson's of the left complex. This shows the interesting relationship between the internal states and relative positions of the complexes when interacting.

3.8 CONCLUSIONS

We have shown that in a system of hard-core bosons the interplay between distance-selective particle loss and coherent hopping results in rich out-of-equilibrium dynamics. The quasi-stationary Zeno subspace reached from an initial Mott insulator state features two families of coherently bound complexes, that exhibit a number of interesting properties, such as effective effective SO coupling, flat dispersion relations and state-dependent interactions. Such pure systems could be experimentally prepared in the ultracold atom lattice experiments discussed in Refs. [109, 110].

4

EMERGENT KINETIC CONSTRAINTS, ERGODICITY BREAKING AND COOPERATIVE DYNAMICS IN NOISY QUANTUM SYSTEMS

4.1 INTRODUCTION

A central goal in the study of interacting many-body systems is to understand settings which undergo a complex collective relaxation, such as glass formers. These systems, under certain conditions, typically, below a certain temperature, display extremely long relaxation times [5, 15, 111–115]. A characteristic feature of glassy systems is a intermediary meta-stable period. One approach proposed to explain this dynamical behaviour assumes that on the microscopic level local transitions are only permitted when certain conditions, e.g. very specific arrangements of particles, are satisfied. As we saw in the previous chapter, long relaxation times can be achieved in quantum settings by use of the quantum Zeno effect, reducing the state space and, by a similar logic, restricting certain configurations in the system.

The field of kinetically constrained models (KCMs) [4, 8, 15, 16, 116], as discussed in Ch. 1, has been employed as a possible explanation of glassy dynamics. They typically feature a trivial and non-interacting steady-state ρ_{ss} but their dynamics is found to be complex at sufficiently high densities or low temperatures as severe restrictions are placed on the allowed pathways that connect different many-body configurations. This causes their approach to equilibrium to be highly intricate and often result in the emergence of meta-stability [8, 13–16], leading to their application in glasses and supercooled liquids.

Kinetic constraints are in practice achieved, for example, by the energetic suppression of straightforward rearrangements forcing the remaining transitions to assume a highly cooperative character. Depending on the specific mechanism, KCMs can be grouped into classes [15]. One set of examples are constrained dynamic lattice gases [117, 118], where a particle's diffusion, by hopping, is hindered by its neighbours, mimicking excluded volume in dense fluids. Another instance is given by facilitated spin models, such as the so-called East [14] and Fredrickson-Andersen (FA) models [13], in which a spin's ability to change its state depends on the configuration of the ones nearby, for both $\rho_{ss} \propto e^{-\beta N}$ where N is the number of excited (up) spins and β is the inverse temperature

Despite their success in capturing hierarchical relaxation, it was only very rarely possible to derive kinetic constraints from first principles and they appeared to remain an effective construct [120]. It was

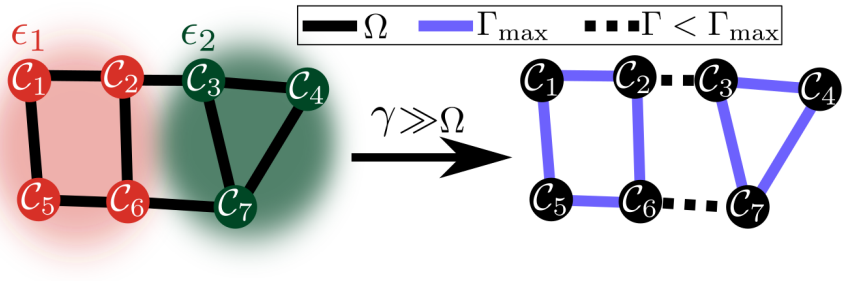

Figure 4.1: Connectivity of the configuration space. Without noise (left), i.e., dephasing rate $\gamma = 0$, classical configurations, $|\mathcal{C}_m\rangle$, shown as circles, are connected to each other by H_Q with coupling strength $\propto \Omega$. In this example H_C is constructed such that the energy landscape in configuration space is separated into two plateaus with energies ϵ_1 (red) and ϵ_2 (green). This choice leads, in the presence of strong noise (right hand side), to two weakly connected spaces. The transition rates within and between the domains are Γ and $\Gamma_{\max}$, respectively. For $\Gamma_{\max} \gg \Gamma$ this results in an (approximate) ergodicity breaking. For further explanation see Sec. 4.2. This Fig. originally appeared in Ref. [119].

recently shown however that they naturally emerge in quantum optical systems [10, 63, 121], specifically cold atomic gases, in the presence of strong interactions and dephasing noise. In certain regimes, these systems show aspects of the facilitation dynamics [56, 122] inherent to the FA, as highlighted in recent experiments [57, 123]. Kinetic constraints moreover govern the non-equilibrium dynamics of nuclear ensembles undergoing so-called Dynamic Nuclear Polarisation [124] — a process used to enhance the signal in magnetic resonance imaging applications. Further to that, a connection between kinetically constrained models and many-body localisation (MBL) in the absence of disorder was also established [125, 126]. In Ch.5, we will also look at their application to the study of the effect of interactions on the decay of the MBL state in open systems [127].

In this chapter we explore the kinetic constraints that emerge in noisy quantum systems from a more general perspective. Typically, KCMs rely on suppressed thermal activation to induce the kind of dynamical cooperativity mentioned above. This suppression mechanism is often absent in the quantum optical setting we consider. For instance, atoms in optical lattices subject to dephasing noise are driven towards an effective infinite temperature state. Here we show that, nevertheless, strongly cooperative and glass-like behaviours may emerge in this framework. The underlying mechanism hinges upon the presence of (approximate) conservation laws. The resulting fragmentation of the space of states can then make even the evolution towards an infinite temperature state highly complex. To demonstrate this, we discuss an example of an effective reaction-diffusion process

in which the interplay between these conservation laws and the lattice geometry induces cooperative diffusion. This experimentally realisable case displays pronounced collective behaviour, timescale separation as well as dynamical reducibility of the state space — features that are typically present in glassy dynamics.

This work was published in Physical Review E in collaboration with M. Marcuzzi, J.P. Garrahan and I. Lesanovsky [119].

4.2 CONSTRUCTION OF KINETICALLY CONSTRAINED SPIN SYSTEMS

We focus here on spin$-\frac{1}{2}$ systems, with internal states $|\uparrow\rangle$, $|\downarrow\rangle$, arranged on a regular lattice. The L sites are labelled by an index k, with the spin operators $\sigma_k^{\pm} = (\sigma_k^x \pm i\sigma_k^y)/2$, where $\{\sigma^x, \sigma^y, \sigma^z\}$ are the standard Pauli matrices. The coherent evolution of the spins is governed by a Hamiltonian $H = H_C + H_Q$ which we separate into a "classical" and a "quantum" part. The former assumes the form

$$H_C = \sum_k u_k n_k + \sum_{k\neq j} \frac{v_{kj}}{2} n_k n_j + \sum_{k\neq j\neq i} \frac{w_{kjl}}{3!} n_k n_j n_l + \ldots, \qquad (4.1)$$

with $k, j, i \in [1, L]$ and where $n_k = \sigma_k^+ \sigma_k^-$ and u_k, v_{kj}, w_{kjl} can be interpreted as one-, two-, three-body interaction couplings. In general, it can be any function of the number operators n_k. H_C defines an energetic landscape E_m over the classical Fock configurations $|\mathcal{C}_m\rangle = |\cdots \uparrow_{k-1} \uparrow_k \downarrow_{k+1} \cdots\rangle$ $(m = 1 \ldots 2^L)$ via $H_C |\mathcal{C}_m\rangle = E_m |\mathcal{C}_m\rangle$. In Fig. 4.1, these configurations are represented as circles and grouped in domains of equal energy.

The quantum part acts as $H_Q |\mathcal{C}_m\rangle = \sum_{n\neq m} a_{mn} |\mathcal{C}_n\rangle$ and defines the dynamical connectivity of the configurations. This is illustrated in Fig. 4.1 where the solid lines correspond to the cases in which $a_{mn} \neq 0$ i.e. states which are connected by the quantum Hamiltonian. We define a generic Hamiltonian acting on a spin state as

$$H_Q = \sum_\nu l_\nu + l_\nu^\dagger \qquad (4.2)$$

where

$$l_\nu = c_\nu \bigotimes_k A_k^\nu \qquad A_k^\nu \in \{\sigma_k^+, \sigma_k^-, n_k, p_k, I_k\} \qquad (4.3)$$

with I_k being the identity operator and $p_k = I_k - n_k$. Each A_k^ν is a local operator acting only on site k, and c_ν are constants. This form allows for the definition of any Hamiltonian which features no diagonal components i.e. each l_ν features a single $\sigma_k^\pm$ for some k. We require any diagonal elements to be contained in the classical Hamiltonian.

We will focus on two prototypical examples: Spin-flipping, induced for example by a laser on a two-level atomic transition which is commonly implemented in Rydberg atomic systems [37, 128, 129]; and quantum tunnelling of hard-core bosons between nearest neighbours [3, 80], which are described by the Hamiltonians

$$H_Q^{(f)} = \Omega \sum_k \sigma_k^x \quad \text{and} \quad H_Q^{(t)} = \Omega \sum_{\langle k,j \rangle} \sigma_k^- \sigma_j^+, \tag{4.4}$$

respectively. Here $\langle k, j \rangle$ is shorthand for summing over the nearest neighbours of site k, and Ω is the coupling strength of the two processes i.e. depending on the realisation: the laser Rabi frequency or lattice tunnelling amplitude. These two processes can also be defined as having: $l_k = \Omega \sigma_k^+$ for spin flipping with $\nu \equiv k$, and $l_{kj} = (\Omega/2)\sigma_k^+ \sigma_j^-$ for the quantum tunnelling example with $\nu \equiv \langle k, j \rangle$.

We consider the system in contact with an environment which induces fast decoherence of quantum superpositions. We assume the Markovian approximation, so that the evolution of the density matrix ρ is governed by the Lindblad master equation, see Sec. 2.1.1, with jump operators defined as

$$L_k = \sqrt{\gamma} n_k \tag{4.5}$$

for $k \in [1, L]$ and where γ is the dephasing rate. This form of dissipation occurs naturally in cold atom lattice experiments, stemming for example from the off-resonant scattering of photons from the optical-trapping laser field [130], or from phase noise of the laser driving [57, 123, 131]. The dephasing rate may be tuned relative to the coherent rates as shown in Refs. [3, 130] and briefly reported in App. A.

We look at the limit $\gamma \gg \Omega$ in order to project the system onto a reduced state space. This allows for the adiabatic elimination of H_Q using the method described in Sec. 2.1.2. We start by splitting the master equation into two terms, a dominant $\mathcal{L}_0$ which contains the classical Hamiltonian's action and the dephasing, and a perturbative $\mathcal{L}_1$ which contains the quantum terms, as $\mathcal{L}\rho = (\mathcal{L}_0 + \mathcal{L}_1)\rho$. $\mathcal{L}_0$ projects the dynamics onto its steady state space, the subspace of diagonal density matrices $P\rho = \mathrm{diag}(\rho) = \mu$ in the $|\mathcal{C}_m\rangle$ basis [10, 132–136]. Substitution of these composite parts into Eq. (2.24) leads to the necessity of the evaluation of the object in the integral of

$$P\mathcal{L}_1 e^{\mathcal{L}_0 t}\mathcal{L}_1 \mu = -P \sum_\nu [l_\nu^\dagger, e^{\mathcal{L}_0 t}[l_\nu, \mu]] + [l_\nu, e^{\mathcal{L}_0 t}[l_\nu^\dagger, \mu]]. \tag{4.6}$$

As $e^{\mathcal{L}_0 t}$ is acting upon states which experience a single action of l_ν, it means that they will be outside the diagonal subspace. First we decompose this into the dephasing and classical interaction terms, $e^{\mathcal{L}_0 t} = e^{\mathcal{L}_{\mathrm{deph}} t} e^{\mathcal{L}_H t}$. The dephasing term, $e^{\mathcal{L}_{\mathrm{deph}} t}$, will act to pull out a $e^{\frac{-\gamma t}{2}}$ on every off-diagonal component generated by the l_ν's, i.e., for every site k on which $A_k^\nu = \sigma_k^\pm$, according to the definition in

Eq. (4.3). We classify the number of these terms by s. In the case of spin flipping $s = 1$ while for tunnelling $s = 2$.

The effect of $e^{\mathcal{L}_H t}$ is more complicated, but can be understood by carefully considering the ordering with which the operators are applied. As H_C is a generic function of n_k operators, it has a well defined value E_m on every classical configuration $|\mathcal{C}_m\rangle$. If we consider the action of the two terms in Eq. (4.6) on a single configuration we find

$$\begin{aligned}\left(e^{\mathcal{L}_H t} l_\nu |\mathcal{C}_i\rangle \langle\mathcal{C}_i|\right) l_\nu^\dagger =& e^{-iH_C t} l_\nu |\mathcal{C}_i\rangle \langle\mathcal{C}_i| e^{iH_C t} l_\nu^\dagger \\ =& e^{-i(E_f - E_i)t} l_\nu |\mathcal{C}_i\rangle \langle\mathcal{C}_i| l_\nu^\dagger,\end{aligned} \tag{4.7}$$

and

$$l_\nu \left(e^{\mathcal{L}_H t} |\mathcal{C}_i\rangle \langle\mathcal{C}_i| l_\nu^\dagger\right) = e^{i(E_f - E_i)t} l_\nu |\mathcal{C}_i\rangle \langle\mathcal{C}_i| l_\nu^\dagger. \tag{4.8}$$

We see that this acts to extract the energy difference $\delta E = E_f - E_i$, corresponding to the final and initial energies of the transition caused by l_ν respectively. Eq. (4.6) is then evaluated as

$$\begin{aligned}&P\mathcal{L}_1 e^{\mathcal{L}_0 t} L_1 \mu = \\ &\quad - P \sum_\nu e^{\frac{-\gamma s t}{2}} 2\cos(\delta E t)(\{l_\nu, l_\nu^\dagger\}\mu - (l_\nu^\dagger \mu l_\nu + l_\nu \mu l_\nu^\dagger)),\end{aligned} \tag{4.9}$$

which after the integration gives a classical master equation for the evolution of μ as

$$\partial_t \mu = \sum_\nu \frac{4}{s\gamma} \Gamma_\nu \left(l_\nu^\dagger \mu l_\nu + l_\nu \mu l_\nu^\dagger - \{l_\nu, l_\nu^\dagger\}\mu\right). \tag{4.10}$$

The rates Γ_ν are configuration-dependent and read as

$$\frac{1}{\Gamma_\nu} = 1 + \left(\frac{2\,\delta E}{s\gamma}\right)^2. \tag{4.11}$$

δE can be viewed as the "energy cost" of performing the l_ν-induced transition allowing the dynamics of the system to be understood in terms of the energetic landscape. Note that the inverse process induced by $l_\nu^\dagger$ occurs at the same rate; therefore, Eq. (4.10) satisfies detailed balance at infinite temperature and the steady-state distribution μ_{ss} is uniform i.e. $\propto \mathbb{1}$ under ergodic conditions.

4.3 "HARD" AND "SOFT" KINETICALLY CONSTRAINED MODELS

According to Eq. (4.11) the rate of a transition is maximal when both involved states are on resonance, i.e. $\delta E = 0$. Conversely, if $|\delta E| \gg \gamma$ the transition rate is greatly suppressed. This implies that depending

on the precise form of H_C, particular processes are favoured over others, thereby creating a constrained dynamics which favours specific pathways in the configuration space.

In the limit $|\delta E|/\gamma \to \infty$ the suppression is total and the corresponding transition is "blocked". Ideally, the energy differences will be either vanishing or infinite meaning transitions induced by H_Q either take place at rate $\Gamma_{max} = 1$ or never occur ($\Gamma = 0$) giving a *hard* constraint. As highlighted in Fig. 4.1, this causes the space to fragment into disconnected parts corresponding to different energies, making the system go from an ergodic one, where each state can be connected to any-other by a series of transitions, to a non-ergodic one producing a reducible dynamics, this is known as ergodicity breaking.

Necessarily, any kinetic constraint prohibiting a transition between two configurations, $|\mathcal{C}_1\rangle \not\to |\mathcal{C}_2\rangle$, can only admit a hard realisation if these belong to dynamically-disconnected sub-spaces, i.e., if there is no sequence of allowed transitions connecting them. If such a pathway exists, e.g. $|\mathcal{C}_1\rangle \to |\mathcal{C}_3\rangle \to |\mathcal{C}_4\rangle \to |\mathcal{C}_2\rangle$, the realisation of a *soft* constraint [137] might still be possible. In this case direct transitions between $|\mathcal{C}_1\rangle$ and $|\mathcal{C}_2\rangle$ cannot be forbidden but merely suppressed. The maximal degree of suppression is determined by the minimal number, q, of allowed transitions joining $|\mathcal{C}_1\rangle$ and $|\mathcal{C}_2\rangle$ and is $\Gamma_{suppressed}/\Gamma_{allowed} \gtrsim 1/q^2$, assuming that all allowed rates are equal.

Hard KCMs tend to live in the realm of the purely mathematical, which focus on capturing singular aspects of a physical system. These are used to test hypotheses that the hard constraint is at the root of the interesting phenomena. This has been particularly important in the study of glasses as it allows a focus on the structure of the dynamics rather than the statics of the system. Soft constrained KCMs on the other-hand are viewed as closer and more representative of physical systems. By studying the transition of a KCM from hard to soft, insight can be gained into what features persist and which properties rely upon the rigid nature of the hard model and are thus unlikely to be found in nature. Here, any model which may be achieved in a hard setting can be made soft by considering the reduction in the energy barrier on the forbidden transitions.

4.4 REACTION-DIFFUSION MODEL WITH CONSTANT BONDS

Based on the above discussion, we construct here a KCM which mimics a lattice gas with excluded volume effects. This model admits a hard realisation and is simple enough to be experimentally realisable with cold atoms in an optical lattice [130, 138] in a range of settings such as polar molecules and Rydberg atoms. It consists of particles arranged on a triangular lattice which feature nearest neighbour tunnelling, as given by $H_Q^{(t)}$ in Eq. (4.4), and strong nearest-neighbour interactions, $H_C = V \sum_{\langle k,j \rangle} n_k n_j$. In the presence of dephasing this

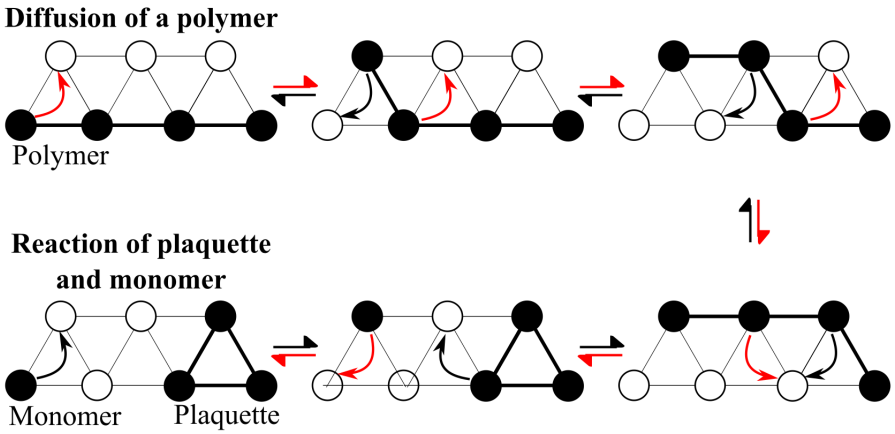

Figure 4.2: Illustrations of key processes governing the dynamics of the reaction diffusion model with constant bonds. The black dots represent excitations and a thick line on the lattice represents a bond. Arrows denote possible moves and point at the resulting configurations. A polymer (top) is a chain of connected excitations, and shown is the way in which it can diffuse across the lattice. A plaquette (bottom-left) is formed by three excitations filling the vertices of a triangular tile. We showcase its reaction with a monomer. This Fig. originally appeared in Ref. [119].

leads to a stochastic process of excitations hopping with rates that depend on the interaction strength V. By construction the number of excitations N is conserved. Taking the limit $V/\gamma \to \infty$ introduces a further conserved quantity, namely the number of neighbouring pairs of excitations or bonds, B. Consequently, excitations can only hop if doing so preserves the number of bonds between them.

Clusters of excitations become bound structures, whose dynamical behavior strongly depends on their shape. Two primary examples are shown in Fig. 4.2. On the top is a "polymer", consisting of two or more excitations arranged along a chain, which can only diffuse via slow, cooperative motion [9]. The second, on the bottom row, is a "plaquette", three excitations at the vertices of the same triangular tile. The plaquette is the simplest example of an immobile structure which cannot diffuse by itself, since any hop would result in the net loss of a bond. It can, however, react with "monomers", isolated excitations, or other mobile structures. This leads to an assisted diffusion which is reminiscent of the strongly cooperative motion found in many glassy models [8, 13–16].

Interestingly, N and B do not exhaust all the conservation laws of this model. There are additional, subtler ones that further split the space of configurations. The easiest way to realise this is to consider the case $N = B = 3$, which encompasses all possibilities of placing a single plaquette in the lattice: since plaquettes are unable to move on their own, all these states are dynamically disconnected. This finer

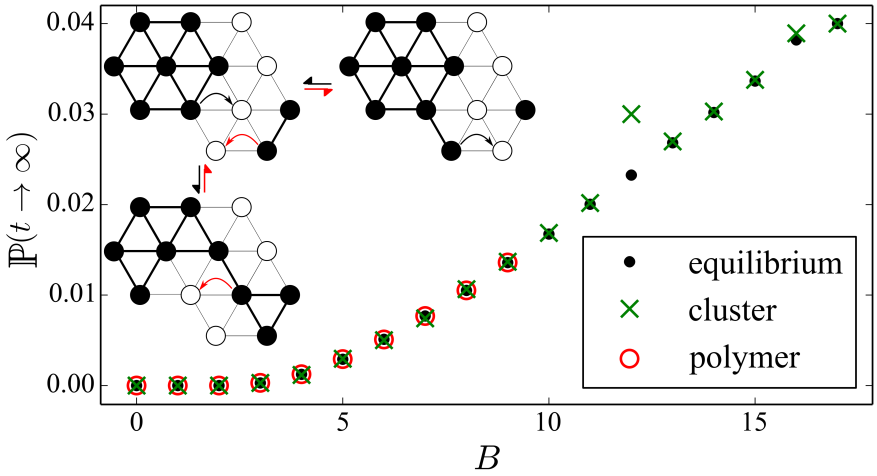

Figure 4.3: Stationary plaquette density $\mathbb{P}(t \to \infty)$ against the number of bonds B for a 10×10 lattice with $N = 10$, obtained via two different averaging procedures: black dots are calculated from a uniform random sampling of configurations at fixed (N, B). The remaining data points are averages over different realisations of the dynamics via a kinetic Monte Carlo procedure, differing by the initial condition: (green crosses) a single maximally compact cluster plus monomers, (red circles) a single polymer plus monomers. The inset shows how the cluster present at $B = 13$ can react with a monomer and the one at $B = 12$ with a dimer. The numerical error here is smaller than the size of the markers and thus is not displayed. This Fig. originally appeared in Ref. [119].

structure is generally related to the formation of immobile clusters and thus emerges at high numbers of bonds $B \gtrsim N$. This is exemplified in Fig. 4.3, where we compare results obtained from dynamical simulations with estimates based upon assuming that the steady state is an equilibrium "microcanonical shell" at fixed (N, B). Without this additional dynamical reduction, the two predictions would coincide. Shown is the plaquette density $\mathbb{P} = (\#\text{ of plaquettes}/2L)$ in a 10×10 lattice with $N = 10$ excitations and values of B from 0 to 17. The black dots are averages obtained from uniform random samplings of states at fixed (N, B). The other data sets correspond to long-time values of $\mathbb{P}$ extracted from kinetic Monte Carlo simulations of the dynamics. The initial conditions are chosen either to have all bonds taken by a single polymer structure (red circles), which is only possible up to $B = N - 1 = 9$, or to have all bonds taken by the smallest possible cluster (green crosses). In both cases, the remaining excitations are introduced as monomers.

At sufficiently low numbers of bonds there are no appreciable deviations; furthermore, the result does not depend on the choice of the initial condition, which shows that most configurations with the same (N, B) are dynamically connected. For $B = 12$ and 16, however, the "cluster initialisation" displays a higher stationary plaquette density than the naive equilibrium value. For instance, the initial cluster at $B = 12$ is chosen to be the "filled hexagon" displayed in the top-left corner of Fig. 4.3. Monomers cannot react with it, since each of the outer excitations form three bonds. In order to break it apart, the assistance of a dimer, or longer polymer, is required. Therefore, for $B = 12$ this structure is inert, while the remaining monomers explore the rest of the lattice via ordinary diffusion. Note however that adding bonds does not necessarily make a structure less prone to dissolution: for $B = 13$ the initial cluster can react with monomers via the mechanism displayed in Fig. 4.3, starting from the top-right configuration. Other examples of "protected" states causing ergodicity breaking are system-spanning configurations, such as a ring of neighbouring excitations which loops around a cylindrical or toroidal system. However, in general these are only encountered at high densities.

The presence of complex structures which cannot move by themselves and can only undergo assisted diffusion results in a separation of timescales in the dynamics. Displayed in Fig. 4.4 is the evolution of the *imbalance*

$$\mathbb{I}(t) = \sum_{\langle k,j \rangle} |\langle n_k \rangle - \langle n_j \rangle|^2, \tag{4.12}$$

a measure of the non-uniformity of the system, and the plaquette density $\mathbb{P}(t)$ as a function of time for a 20×20 lattice, $N = 10$, and prepared at $t = 0$ in a single-polymer state with $B = 3$, 4, 8 and 9. These configurations are able to explore the entire lattice and thus to restore translational invariance at sufficiently long times, implying

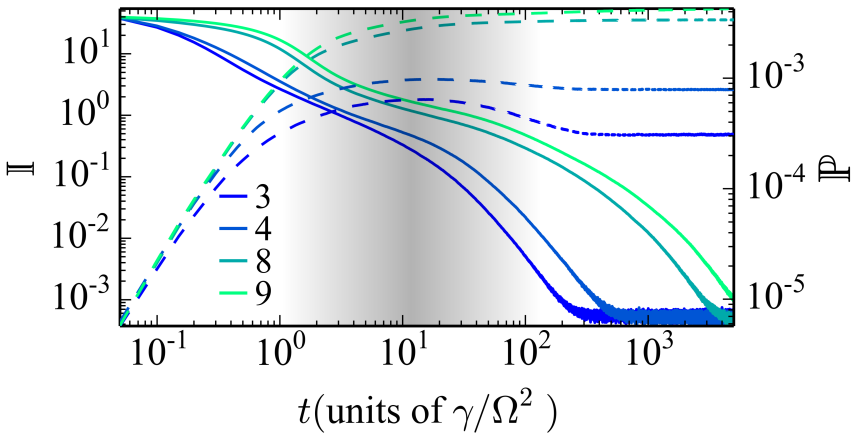

Figure 4.4: Dynamics of the imbalance $\mathbb{I}$ (solid) and plaquette density $\mathbb{P}$ (dashed) for a 20×20 lattice with $N = 10$. All cases are initialised with a single $(B+1)$ polymer and $N-B-1$ monomers for $B = 3, 4, 8$ and 9. The relaxation time increases with B. At low B, the plaquette density overshoots its stationary value and correspondingly the decay of the imbalance speeds up. This highlights the advantage in liberating monomers (or smaller structures) by forming plaquettes. The subsequent assisted diffusion of plaquettes acts on much longer timescales and eventually reduces $\mathbb{P}$ to its stationary value. The shaded area marks the separation between two regimes in the dynamics, the earliest dominated by plaquette creation and monomer diffusion, the latest by assisted diffusion of plaquettes. The errors on $\mathbb{I}$ and $\mathbb{P}$ are of order 10^{-5} and 10^{-6}, respectively. This Fig. originally appeared in Ref. [119].

$\mathbb{I}(t \to \infty) \to 0$. The early dynamics is dominated by diffusion of the original structures and the formation of plaquettes. For the low-B cases, around $t \approx 10\gamma/\Omega^2$ the plaquette density reaches its maximum, which is higher than its stationary value. Correspondingly, the imbalance relaxation speeds up, which can be understood as follows: the formation of clusters such as plaquettes breaks down polymers to shorter ones, which display higher mobility and diffuse faster. For instance, for $B = 3$, once a plaquette is formed an additional monomer is released (see Fig. 4.2) and monomers are the most efficient objects at exploring the lattice. Consequently, the higher the plaquette density, the higher the rate of relaxation of the imbalance. On longer time scales, further plaquette-monomer reactions relax $\mathbb{P}$ to its actual stationary value. The separation of time-scales of the different dynamics present in the system is another example of this system's constrained behaviour.

4.5 FACILITATED SPIN MODELS

We now consider the application of our model to the most well known KCMs, the FA and East models [15]. Both feature facilitated spin flipping, $H_Q^{(f)}$ in Eq. (4.4), whereby an excitation (up spin) enables the flipping of its neighbours e.g. $\uparrow\uparrow\downarrow \rightleftarrows \uparrow\downarrow\downarrow$ (whereas $\downarrow\uparrow\downarrow \not\rightleftarrows \downarrow\downarrow\downarrow$). In the East model, facilitation is further constrained and can only take place to an excitation's right. Neither model admits a hard realisation. To see this we consider the transition $\uparrow\downarrow\downarrow\downarrow \to \uparrow\downarrow\uparrow\downarrow$ which must be forbidden in both models. Both configurations can however be connected via a sequence of allowed steps $\uparrow\downarrow\downarrow\downarrow \to \uparrow\uparrow\downarrow\downarrow \to \uparrow\uparrow\uparrow\downarrow \to \uparrow\downarrow\uparrow\downarrow$.

The FA model still admits an obvious soft realisation by choosing $H_C = V \sum_k n_k (1 - 2n_{k+1}/3)$ such that $\Gamma_{\text{suppressed}}/\Gamma_{\text{allowed}} \gtrsim 1/9$. When simulated the basic behaviour is observable, but the suppression is not sufficient to appear hard.

For the facilitated dynamics inherent to the FA and East models to display glassy features, it is crucial that the density of excitations remains low. Conversely, under Eq. (4.10) the state invariably evolves towards equilibrium at infinite temperature, which poses a severe restriction to its applicability in this case. Introducing additional noise sources however might provide a way around this problem, as it may change the nature of the stationary state [10, 64, 122, 131, 139] an example of this is studied in Ch.6.

4.6 CONCLUSIONS

Kinetically constrained models were originally introduced to capture the basic properties of slow-relaxing materials, yet have largely remained an idealised construct. Here we have shown that in the pres-

ence of strong noise these constraints emerge rather naturally in the dynamics of open quantum systems.

The construction employed in this chapter results in effectively classical models which are realisable in experiment. The interesting question is however the behavior of those changes when quantum coherence is not entirely washed out by the noise. This could be systematically addressed in an experimental realisation of the discussed reaction-diffusion model with cold atoms in lattices [109, 140, 141], thereby providing a handle for exploring quantum effects in glassy relaxation [142, 143]. This could also shed light on the interplay between quantum and classical fluctuations on collective phenomena, as e.g. recently discussed in [144, 145].

5

ROLE OF INTERACTIONS IN A DISSIPATIVE MANY-BODY LOCALISED SYSTEM

5.1 INTRODUCTION

Constrained systems, as we have shown, often feature ergodicity breaking. A prime example of this same phenomena is that of many-body localisation (MBL). MBL stems off the field introduced in quantum systems originally with Anderson Localisation [146, 147]. One of the key identifiers of a localised system is a signature of its initial state in a local observable that persists for infinite time. Localisation is typically achieved in quantum systems via the introduction of a random field, e.g. a field that is randomised over space for each iteration of the ensemble, which prevents the system from thermalising. Anderson localisation and other studies have focussed on non-interacting particle systems and as such can be understood via single particle considerations. MBL features interacting particles and current evidence suggests that the same localisation phenomena is observed. The MBL phase exists in many-body quantum systems in the presence of quenched disorder, featuring a transition between an ergodic and a many-body localised phase [148–152]. While the transport properties of the MBL phase are still debated [153] it is generally accepted that it is characterised by a slow growth of entanglement entropy [154–157], and ergodicity breaking which has been observed in numerical studies [152, 158, 159] and experiments [145, 160–162]. Theoretical studies have focussed on one-dimensional models and there is experimental evidence of the MBL phenomena existing in two-dimensions [145, 161]. For a general review of MBL see Ref. [86].

While most literature has focused on closed quantum systems, the open nature of the cold atomic ensembles used in recent experimental observations of MBL calls for an understanding of the effect of dissipation on the MBL phase [163, 164]. In Ref. [165] a chain of interacting fermions in contact with an infinite temperature dephasing bath was studied numerically. At conditions where the closed system would be in the MBL phase, a slow approach to the infinite temperature state was observed in the open system, characterised by a stretched exponential decay of self-correlations. Stretched exponential behaviour was confirmed analytically in Ref. [166] in terms of a non-interacting (Anderson) system, valid for large disorder. Similarly, in Ref. [167] the scaling properties of the same system were studied in the large disorder limit, finding independence of the dynamics from interactions.

A central question is therefore whether interactions play any role in the relaxation to the ergodic state due to dephasing in an otherwise MBL system. In this chapter we address this question by studying the dissipative dynamics of a disordered XXZ chain in its MBL phase [165]. Through the application of the technique described in Ch. 4 we show that depending on the interaction strength the system explores two different regimes within the MBL phase. We observe a crossover from a disorder dominated regime to an interaction dominated regime, whose observable signature is a change in behaviour of the self-correlators from a stretched exponential to a compressed exponential dependence with time. This latter behaviour is due to the nucleation and growth of relaxing regions. A crossover of this sort is often the manifestation of non-equilibrium and aging behaviour in soft matter and glassy systems [7, 168–171].

The work presented was published in Physical Review B in collaboration with E. Levi, I. Lesanovsky, and J.P. Garrahan [127].

5.2 THE MODEL

We consider a paradigmatic MBL system, the disordered XXZ chain in a spinless fermion description in one-dimension for L sites,

$$H = J \sum_{k=1}^{L} \left(\hat{c}_k^\dagger \hat{c}_{k+1} + \hat{c}_{k+1}^\dagger \hat{c}_k \right) + V \sum_{k=1}^{L} \hat{n}_k \hat{n}_{k+1} + \sum_{k=1}^{L} h_k \hat{n}_k, \quad (5.1)$$

where $\hat{c}_k^\dagger$ is the fermion creation operator, $\hat{n}_k = \hat{c}_k^\dagger \hat{c}_k$, and the random field $h_k \in [-h, h]$ is independently drawn for each site from a uniform distribution. This model exhibits an MBL transition for $h_c/J \simeq 7.2$ [152, 157, 172] when $V \approx J$. The dependence of the transition point on V has yet to be fully evaluated.

We couple the system to an infinite temperature Markovian dephasing bath with weak coupling meaning the dynamics is described by a Lindblad Master equation, see Sec. 2.1.1, with jump operators defined as

$$L_k = \sqrt{\gamma} \hat{n}_k \quad (5.2)$$

for $k \in [1, L]$ and where γ is the dephasing rate. This form of dephasing and Hamiltonian is experimentally relevant, as it can be derived from microscopic principles for experiments on both cold fermionic [130] and hard-core bosonic gases [173].

The dephasing is caused by the off-resonant scattering of photons forming the lattice potential, and the dissipation rate γ is controlled by the detuning and intensity of the trapping laser as discussed in App. A. The dynamics conserves the fermion number and in what follows we will focus on the half-filling sector i.e. $\sum_{k=1}^{L} n_k = L/2$, where we assume an even number of sites.

5.3 RATE EQUATION DESCRIPTION

In Ref. [165] it was observed that the decay of the imbalance collapsed when time was rescaled according to γ, implying that the properties of the decay are independent of the value of γ. This means for times $t \gg 1/\gamma$ the master equation may be reduced to a classical master equation, using the technique described in Sec. 4.2, for either the situation of large dephasing, $\gamma \gg J$ [10, 119, 122, 133, 174] or large interactions and/or large longitudinal fields, $V, h \gg J$ [167]. This effective dynamics describes the evolution of the diagonal elements of the density matrix p_α when expressed in the σ^z basis. Expressing the diagonal as a vector, $|p\rangle = \sum_\alpha p_\alpha |\alpha\rangle$, where $|\alpha\rangle$ represents the $L!/(L/2)!^2$ Fock states in the half-filling sector [167], the master equation reduces to [119]

$$\partial_\tau |p\rangle = \sum_{k=1}^{L} \Gamma_k \left[\hat{c}_k^\dagger \hat{c}_{k+1} + \hat{c}_{k+1}^\dagger \hat{c}_k - \hat{\mathcal{P}}_k\right] |p\rangle \tag{5.3}$$

where $\mathcal{P}_k = \hat{n}_k + \hat{n}_{k+1} - 2\hat{n}_k\hat{n}_{k+1}$. Eq. (5.3) describes classical hopping of particles on the lattice, with a rescaled time $\tau = J^2\gamma t/h^2$ [166, 167]. The rate of hopping between sites k and $k+1$ is given by

$$\Gamma_k = \frac{h^2}{\gamma^2 + [V(n_{k+2} - n_{k-1}) + \Delta h_k]^2}, \tag{5.4}$$

where $\Delta h_k = h_{k+1} - h_k$ and $n_k = \mathrm{Tr}(\hat{n}_k |p\rangle)$ is the total probability of having an excitation on site k. In the following we will fix the energy scale to $\gamma = 1$. The rates Γ_k are configuration-dependent, as shown in Fig. 5.1(a) and act as a *kinetic constraint* [10, 119], as often encountered in systems with a complex relaxation dynamics, like glasses [116]. The form of the rates Γ_k does not determine the properties of the stationary state, but rather the relaxation pathways.

For each iteration, the rates Γ_k between any two configurations are random due to the field h_k. The specific distribution of these rates depends on the strength of the interactions and on the specific transition under consideration. We consider the distribution of these rates of transition shown on the left hand side of Fig. 5.1(a) between sites k and $k+1$ as they represent the two primary configurations. In both cases, the hop will result in a change of energy of $\pm V$, the sign depending on the direction, plus the difference in the random field, $\Delta h_k = h_{k+1} - h_k$. We focus on the $+V$ case, with the opposite sign following an identical argument, meaning that the rate is given by

$$\Gamma_k = g(\Delta h) = \frac{h^2}{1 + [V + \Delta h_k]^2}. \tag{5.5}$$

The distribution of Δh is defined as

$$P(\Delta h) = \frac{1}{4h^2}(2h - |\Delta h|), \quad \text{with} \quad \Delta h \in [-2h, 2h]\,. \tag{5.6}$$

Changing variables as

$$P(\Gamma) = \sum_{s\in\{+,-\}} \left|\frac{dg^{-1}(\Gamma)_s}{d\Gamma}\right| p(g_V^{-1}(\Gamma)_s), \tag{5.7}$$

where

$$g^{-1}(\Gamma_k)_\pm = V \pm \sqrt{\frac{h^2}{\Gamma_k} - 1}, \tag{5.8}$$

and the limits of Γ_k are defined as

$$\Gamma \in \left[\frac{h^2}{1+(2h+V)^2}, 1\right]. \tag{5.9}$$

To resolve Eq. (5.7) we need to consider the value of V in comparison to that of $2h$. For $V < 2h$ the inverse function is multivalued in the region $\Delta h \in [-2h, 2h-2V]$ meaning that s in Eq. (5.7) needs to be summed over. In the region $\Delta h \in (2h-2V, 2h]$ on the other hand the inverse function is single-valued only having a contribution from $g_V^{-1}(\Gamma_k)_+$. This gives the distribution of the rates as

$$\begin{aligned}
&\text{if } \frac{h^2}{1+(V+2h)^2} \leqslant \Gamma < \frac{h^2}{1+(V-2h)^2}: \\
&P(\Gamma) = A(\Gamma)\left(2h - \left|V + \sqrt{\frac{1}{\Gamma}-1}\right|\right) \\
&\text{if } \frac{h^2}{1+(V-2h)^2} \leqslant \Gamma \leqslant 1: \\
&P(\Gamma) = A(\Gamma)\left(4h - \left|V - \sqrt{\frac{1}{\Gamma}-1}\right| - \left|V + \sqrt{\frac{1}{\Gamma}-1}\right|\right),
\end{aligned} \tag{5.10}$$

where $1/A(\Gamma) = 8h^2\Gamma^{3/2}\sqrt{1-\Gamma}$. This means the distribution is bimodal for $V < 2h$, with a peak at $\Gamma/h^2 = 1$ resulting from when the random field exactly cancels the interactions field, and another peak, which for $V \ll 2h$ is found at $\Gamma/h^2 \sim 4/(3h)^2$.

For $V > 2h$ the inverse function is never multivalued meaning that the distribution is only defined by the first line of Eq. (5.10) with a single peak which for $V \gg 2h$ is found at $\Gamma \sim V^{-2}$. This implies that with increasing V the dynamics becomes slower. Crucially, as will be discussed later, the fast processes present at $V < 2h$ disappear hinting at different dynamical regimes. The form of $P(\Gamma)$ for these configurations is plotted in Fig. 5.1(b) for various values of V.

5.4 DISTINCT DYNAMICAL REGIMES WITHIN THE MANY-BODY LOCALISED PHASE

To explore the relaxation dynamics we focus on the case in which the initial state is the *charge density wave* (CDW) state, $|p(\tau = 0)\rangle =$

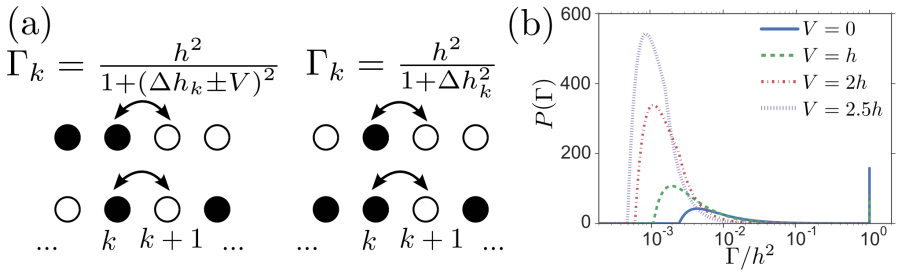

Figure 5.1: (a) The dependence of the classical hopping rates Γ_k on the configuration. We denote with $\bullet$ and $\circ$ the occupied and empty states respectively. (b) The normalised probability density function of rates $\sqrt{2/V}P(\Gamma)$ is displayed for different values of the interactions and $h = 10$. The unnormalised distribution is depicted in the case $V = 0$. This Fig. originally appeared in Ref. [127].

$|\circ\bullet\circ\bullet\ldots\circ\bullet\rangle$, with $\circ,\bullet$ denoting empty and occupied sites respectively. This initial state is ideal as every occupied site is capable of hopping but at the cost of now interacting with a neighbour and is translationally invariant. It is also relevant to recent experiments [145, 160–162]. The ergodicity properties can be quantified by the evolution of the *imbalance*, as was also used in Ch. 4,

$$\mathbb{I}(\tau) = \frac{2}{L}\sum_k (-1)^k n_k = \frac{4}{L}\sum_k \hat{n}_k(\tau)\hat{n}_k(0) - 1, \tag{5.11}$$

which gives a direct readout of the self-correlations.

We simulate Eq. (5.3) with kinetic Monte Carlo, see Sec. 2.2, averaging over disorder and measure $\langle\mathbb{I}\rangle$, examples of which are shown in the inset of Fig. 5.2. The decay of $\langle\mathbb{I}\rangle$ becomes slower for increasing interactions. We quantify this slowing down by defining the saturation time $\mathbb{T}$ such that $\langle\mathbb{I}(\mathbb{T})\rangle = e^{-2}$. As shown in Fig. 5.2, we observe two different regimes: For $V < 2h$ the saturation time shows little dependence on V, while for $V > 2h$ it increases rapidly with the interaction, signalling a slowdown of the dynamics. The inset shows that in the region $V < 2h$, $\mathbb{T}$ is approximately independent of V but the shape of the relaxation still varies.

Our data is well fitted by the function $\langle\mathbb{I}(\tau)\rangle \sim \exp\left[-(\tau/T)^\beta\right]$. This form is motivated by the analytical arguments below. The results on the exponent β and the time-scale T are reported in Fig. 5.4 and Fig.5.3. We find that at $V \simeq 2h$ the relaxation of the imbalance switches from a *stretched exponential* behaviour ($\beta < 1$) to a *compressed exponential* behaviour ($\beta > 1$) (see Fig. 5.4).

A stretched exponential occurs when a system is governed by a distribution of exponential decays. So the "faster" decaying terms will finish quickly leading to an initial rapid relaxation followed by a long tail of slowly decaying processes. This behaviour is commonly observed in glassy systems and the relaxation of disordered systems [4,

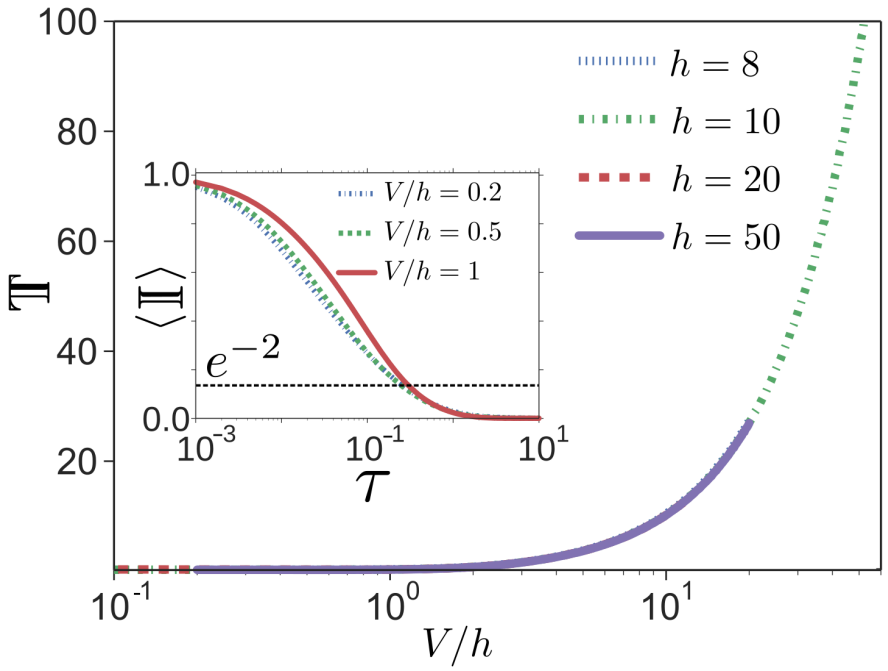

Figure 5.2: Plot of the dependence of the relaxation time $\langle \mathbb{I}(\mathbb{T}) \rangle = e^{-2}$ on the interactions V for various values of the disorder h for a chain of length $L = 1000$ averaged over 10000 realisations of the disorder. The inset shows the relaxation dynamics for $h = 10$, and different values of $V < 2h$. Standard errors are below the line width. This Fig. originally appeared in Ref. [127].

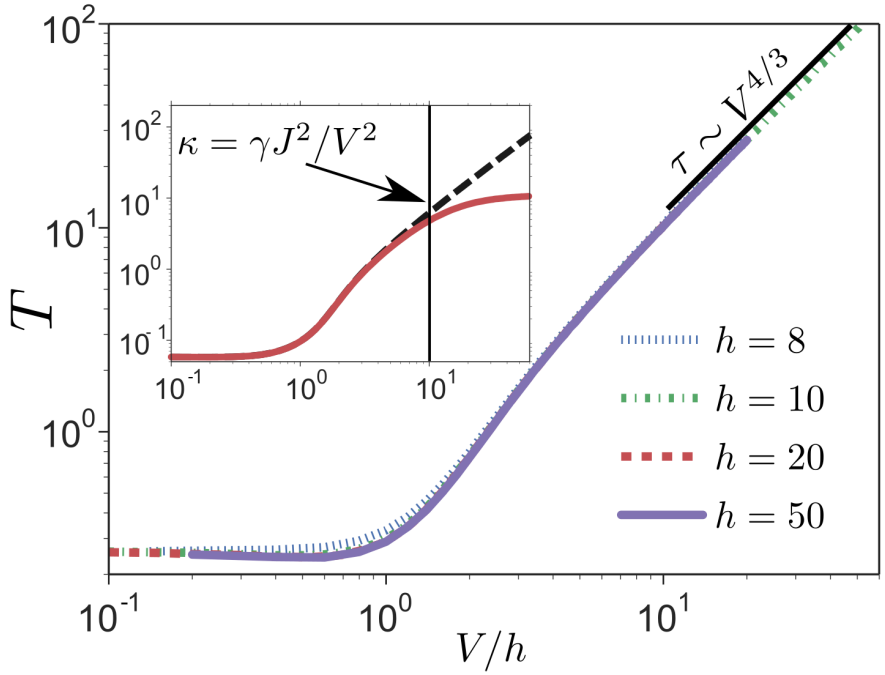

Figure 5.3: Plot of the time-scale T as a function of V for different values of h for a chain of length L = 1000 averaged over 10000 realisations of the disorder. The analytical value in the limit of strong interaction $T = 0.32V^{4/3}$ is shown. In the inset the comparison between the small particle loss limit $\kappa = 10^{-4}\gamma$ (red), and the $\kappa = 0$ case (black dashed) is displayed. Standard errors are below the line width. This Fig. originally appeared in Ref. [127].

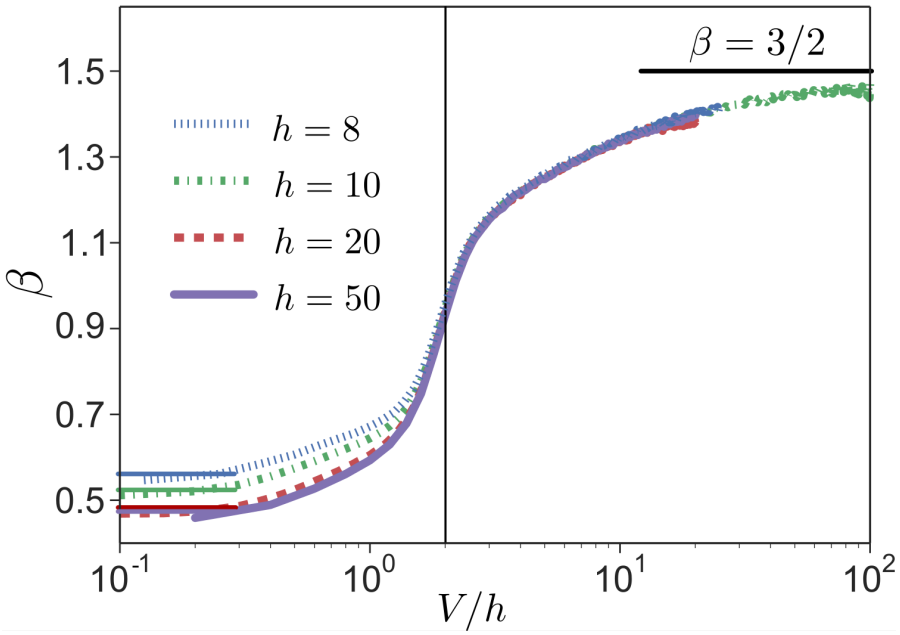

Figure 5.4: Plot of the dependence of the exponent β on V displayed for various values of h for a chain of length L = 1000 averaged over 10000 realisations of the disorder. The crossover between $\beta < 1$ and $\beta > 1$ at $V \simeq 2h$ is highlighted by a vertical line. The analytical values obtained for large and vanishing V are displayed as solid lines in the relevant regimes. Standard errors are below the line width. This Fig. originally appeared in Ref. [127].

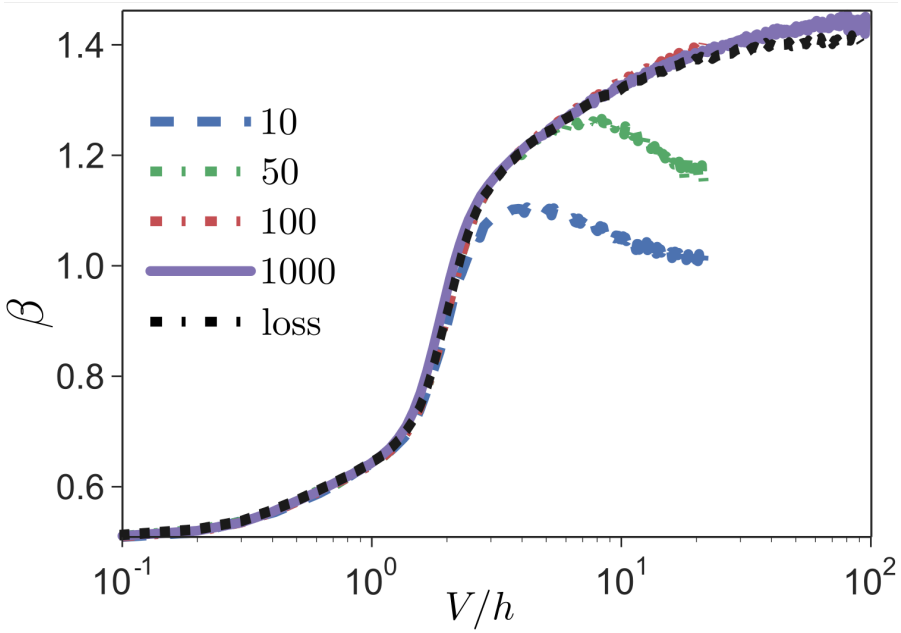

Figure 5.5: Plot of the dependence of the exponent β on V/h for $h = 10$ displayed for various lengths of the chain, averaged over 10000 realisations of the disorder, alongside the effect of a small particle loss $\kappa = 10^{-4}\gamma$. Standard errors are below the line width. This Fig. originally appeared in Ref. [127].

175]. Compressed exponential behaviour is often described as "caged" or "collective". Its hallmark is a slow initial decay followed by a rapid relaxation. This tends to occur when there is a slow initial process that has to first take place before a rapid relaxation can occur. This behaviour is observed in soft glassy matter systems under special conditions [7, 175, 176].

Despite the rapid increase in β at $V \simeq 2h$ which suggests a sharp acceleration of the dynamics, the increase in the time-scale T combines to give the slowing down observed in Fig. 5.2. The minimum in T at $V \sim 0.3h$ in the numerical results, and the large V behaviour are compatible with the results in Ref. [166]. A finite size study for the exponent β is shown in Fig. 5.5. Although in the stretched exponential regime ($V < 2h$) finite size effects have a marginal impact, in the compressed exponential regime ($V > 2h$) they cause a saturation of the exponent to lower values. The origin of this behaviour will become clear below.

5.4.1 *Low-interaction regime*

When $V \ll 2h$ the dynamics is dominated by disorder. For this study we will assume the limit of $V = 0$. In this case, the long time dynamics is characterised by large portions of the chain in which the system

has relaxed, giving null contributions to the imbalance, with isolated non-relaxed pairs corresponding to those with the largest Δh_k. The approach of $\langle \mathbb{I}(\tau) \rangle$ to equilibrium is first governed by these fast pairs and then the slow pairs. We study the dynamics of slow pairs by focusing on, sites k and $k+1$ with a single excitation between them with relaxed neighbours serving as a bath i.e. the slow pair is neighboured by fast pairs. That is, we set $n_{k'}$ for $k' > k+1$ and $k' < k$. This setting is sketched in Fig. 5.6(a).

The population on a single site is found by $\langle n_k \rangle \equiv n_k = \mathrm{Tr}(\hat{n}_k |p\rangle)$, where we consider an initial condition of $n_k(0) = 1$ and $n_{k+1} = 0$. Since the dynamics conserves the number of excitations we set $p_{\uparrow\uparrow} = p_{\downarrow\downarrow} = 0$. This leaves the evolution of the population as

$$\dot{n}_k = \mathrm{Tr}(\hat{n}_k \hat{p}_{k+1} \partial_\tau |p\rangle), \tag{5.12}$$

where $\hat{p}_k = \mathbb{1} - \hat{n}_k$. Using Eq. (5.3) gives

$$\dot{n}_k = \Gamma_{k-1}(n_{k-1} - n_k) + \Gamma_k(n_{k+1} - n_k). \tag{5.13}$$

We set n_{k-1} and n_{k+2} to the stationary average, $1/2$, and obtain the equations for the density of the pair as

$$\dot{n}_k = \Gamma_{k-1}\left(\frac{1}{2} - n_k\right) + \Gamma_k\left(n_{k+1} - n_k\right), \tag{5.14}$$

$$\dot{n}_{k+1} = \Gamma_k\left(n_k - n_{k+1}\right) + \Gamma_{k+1}\left(\frac{1}{2} - n_{k+1}\right). \tag{5.15}$$

Which can be expressed in terms of the local imbalance $\mathbb{I}_k = n_{k+1} - n_k$ giving

$$\dot{\mathbb{I}}_k = -2\Gamma_k \mathbb{I}_k + \frac{\Gamma_{k+1} - \Gamma_{k-1}}{2} - \left(\Gamma_{k+1} n_{k+1} - \Gamma_{k-1} n_k\right). \tag{5.16}$$

In this case, the rates in Eq. (5.4) depend only on the difference of the random fields on the sites they are connecting. The rates associated to two contiguous links, e.g. Γ_k and Γ_{k+1}, are therefore not statistically independent, since they both depend on the field on the site they share, but those of links further apart are i.e. when solving Eq. (5.16) we treat $\Gamma_{k-1} \equiv \Gamma_{k+1} \equiv \Gamma'$. This gives

$$\langle \mathbb{I}_k(\tau) \rangle = \int d\Gamma_k d\Gamma' P\left(\Gamma_k, \Gamma'\right) e^{-(2\Gamma_k + \Gamma')\tau}, \tag{5.17}$$

where $P\left(\Gamma_k, \Gamma'\right)$ is the joint probability which can be expressed in a form for numerical integration as

$$P(\Gamma_k, \Gamma') = \frac{1}{8h^3} \int_{-h}^{h} dh_k \, dh_{k+1} \, dh' \quad \delta\left(\Gamma_k - \frac{h^2}{1 + (h_{k+1} - h_k)^2}\right) \delta\left(\Gamma' - \frac{h^2}{1 + (h' - h_{k+1})^2}\right), \tag{5.18}$$

where h' is the random field on the relaxed sites. Numerically integration of Eq. (5.17) gives a stretched exponential behaviour. In Fig. 5.4 the results on β obtained by fitting are compared with the numerical data in the weak interaction regime, showing good agreement. The local imbalance is a good approximation of the total imbalance in this regime as slow relaxing links are rare in comparison to fast relaxing ones meaning that slow pairs will be far enough apart on average to be considered independent.

5.4.2 *Large-interaction regime*

In the $V \gg 2h$ limit, when starting from the CDW state the first step always costs $V + \Delta h_k$. This sets the time-scale $\sim V^2$ to observe the transitions of the kind $|...\circ\bullet\circ\bullet\circ\bullet...\rangle \to |...\circ\bullet\circ\circ\bullet\bullet...\rangle$. This creates a pair of holes and occupied sites, which each contribute zero to the imbalance. We pair off the lattice in this way and coarse grain it such that we instead label states by their contribution to the imbalance i.e. $|\circ\bullet\rangle \to |1\rangle$, $|\circ\circ\rangle \to |0\rangle$, $|\bullet\bullet\rangle \to |0\rangle$, and $|\bullet\circ\rangle \to |-1\rangle$. The above transition can then be written as $|1,1,1,1\rangle \to |1,0,0,1\rangle$. We refer to these transitions as *nucleation* events, as further transitions, e.g. $|...\circ\bullet\circ\circ\bullet\bullet...\rangle \to |...\circ\circ\bullet\circ\bullet\bullet...\rangle$ or $|1,0,0,1\rangle \to |0,-1,0,1\rangle$ are independent of V, which in the large-interaction regime makes them rapid events. These nucleation events happen at a homogeneous rate, $\Gamma_n \simeq 2(h/V)^2$, across the lattice. A nucleation event will either create two $|0\rangle$ sites or a $|-1\rangle$ site, but the two are translationally equivalent and they only need to be separated when interactions between two nucleation events are considered.

Once a nucleation event has occurred the process $|0,1\rangle \rightleftharpoons |-1,0\rangle$, and $|1,0\rangle \rightleftharpoons |0,-1\rangle$ are possible with the non-interacting rate $\Gamma_k = h^2/(1+\Delta h_k^2)$. This pair of reversible processes implies that the $|0\rangle$ sites can be treated as random walkers, which when moving away from each other create a growing region of $|-1\rangle$ sites. The site dependent differences between these rates are small for the time-scales we are considering ($V \gg 2h$), and we will assume a constant rate Γ_e. When averaged over random realisations the region between the $|0\rangle$ sites expands following the law $\langle G_e(\tau)\rangle \sim \sqrt{\Gamma_e \tau}$, contributing a net zero imbalance since the sites falling in this region are now equally likely to be a $|1\rangle$ or $|-1\rangle$. There are no possible interactions between neighbouring $|1\rangle$ states, nor between neighbouring $|-1\rangle$ states. The interaction between neighbouring $|1\rangle$ and $|-1\rangle$ states will be detailed in Sec. 5.5 where they are a relevant process.

This growth dynamics together with the initial nucleation events, reminiscent for example of a crystallisation process, is well described by the so-called Avrami law [177–181]. Here we give a sketch of the derivation in our case. The average number of nucleation events up to a given time $\langle \nu(\tau)\rangle$ is then found by integrating $\langle \dot{\nu}(\tau)\rangle = L\Gamma_n/2$. Not

accounting for overlap of the expanded regions, the total number of transformed sites, i.e. pairs which contribute 0 to the imbalance, is

$$\langle \mathcal{N}(\tau) \rangle = \int_0^\tau dt \quad \langle \dot{\nu}(t) \rangle \langle G_e(\tau - t) \rangle . \tag{5.19}$$

This dynamics is sketched in Fig. 5.6(b) for a single expanding region of transformed sites. Overlaps are excluded by assuming the increment in transformed sites $d\langle L_{tr} \rangle$ is proportional to $d\langle \mathcal{N} \rangle$ multiplied by the probability of not having an already transformed site $(1 - 2\langle L_{tr} \rangle / L)$, giving

$$\frac{2\langle L_{tr}(\tau) \rangle}{L} = 1 - \exp\left[\frac{2}{3} \sqrt{\Gamma_e} \left(\frac{h}{V} \right)^2 \tau^{\frac{3}{2}} \right]. \tag{5.20}$$

Initialising our dynamics in the CDW the imbalance at a given time is found as $\langle \mathbb{I}(\tau) \rangle = 1 - 2\langle L_{tr}(\tau) \rangle / L$, leading to

$$\langle \mathbb{I}(\tau) \rangle = \exp\left(\frac{\tau}{T} \right)^{\frac{3}{2}} \tag{5.21}$$

with $T = (V/h)^{4/3} (3/2\sqrt{G_e})^{2/3}$. This shows the compressed exponential behaviour with exponent $\beta = 3/2$ observed in Fig. 5.4 with the functional dependence of the time-scale $T \sim (V/h)^{4/3}$ for large V/h also being confirmed by our numerical results in Fig. 5.3.

This picture breaks when the time between nucleation events becomes comparable to the time taken for a single one to expand to the system's length. In this case we consider the expansion of a nucleated region as instantaneous and the imbalance as fully relaxed after a single nucleation event. In a single realisation we then model the imbalance as $\mathbb{I}(\tau|\tau') = 1 - \theta(\tau - \tau')$, where τ' is the time at which the first nucleation event happens. The probability of nucleation at this time is given as $\pi(\tau') = L \exp\left(-L\tau'/V^2\right)/V^2$, such that the imbalance averaged over realisations is

$$\langle \mathbb{I}(\tau) \rangle = \int d\tau' \, \pi(\tau') \, \mathbb{I}(\tau|\tau') = \exp\left(-\frac{L\tau}{V^2} \right). \tag{5.22}$$

This is the origin of the strong size dependence of the dynamics for large V, such as the saturation of the exponent β to 1 in Fig. 5.5 in for e.g. a system of length $L = 10$.

5.5 PARTICLE LOSS

In atomic experiments, additional to dephasing a common source of noise is that of particle loss from the lattice due to imperfect trapping and heating from the surrounding cloud. This corresponds to the addition of the process $|\bullet\rangle \to |\circ\rangle$, which is modelled in our effective description by adding to the r.h.s. of Eq. (5.3) the term

$$\frac{h^2}{J^2 \gamma} \kappa \sum_{k=1}^{L} (\hat{c}_k - \hat{n}_k) , \tag{5.23}$$

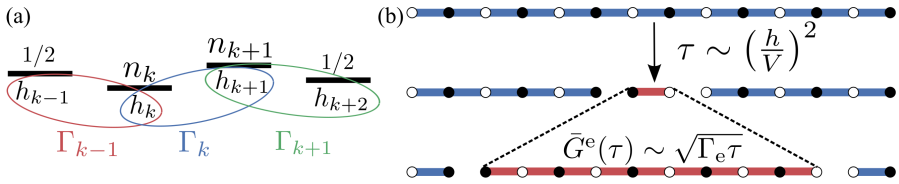

Figure 5.6: (a) An illustration of the non-interacting limit is displayed: The focus is on the sites k and $k+1$, while sites $k-1$ and $k+2$ serve as a bath in the relaxed state. Two contiguous rates are statistically correlated since they share the value of an on-site random field. (b) A cartoon of the nucleation and expansion of a transformed region in the strongly interacting limit. The transformed and untransformed regions are depicted respectively in red and blue. This Fig. originally appeared in Ref. [127].

where κ is the loss rate. Loss acts to relax the local imbalance to 0 in a non-collective manner by reducing the number of particles in the system. For $\kappa \gg \gamma J^2 h^{-2}$ the imbalance decays as $\mathbb{I} \approx e^{-\kappa t}$, and none of the above features survive. In contrast, for $\kappa \lesssim \gamma J^2 h^{-2}$ only the nucleation-expansion dynamics is significantly modified: decay acts as a nucleation event i.e. $|1,1,1\rangle \to |1,0,1\rangle$. In this relaxation process the states $|1\rangle$ and $|-1\rangle$ will interact following the rules $|-1,1,1\rangle \rightleftharpoons |-1,-1,1\rangle$, $|-1,1,0\rangle \rightleftharpoons |-1,-1,0\rangle$, note a $|1,1,-1\rangle \rightleftharpoons |1,-1,-1\rangle$ is slow as the transition involves a change in energy of V.

The nucleation by decay is dominant when $\kappa \gg \gamma J^2/V^2$. This affects marginally the value of the compressed β, but results in a saturation of the time scales T, $\mathbb{T}$ for large enough V, see Fig. 5.5 and the inset of Fig. 5.3.

5.6 CONCLUSIONS

In this chapter we have considered the effect of interactions on the dynamics of a MBL system subject to dephasing noise. We found two relaxation regimes, one dominated by disorder, and one dominated by the interactions. The physical manifestation is a crossover in the decay of time correlators, from stretched to compressed exponential in time. While the stretched exponential regime was expected for weak interactions [165, 166], the crossover to compressed exponential is a new prediction and as it requires large system sizes was not observable before in quantum simulations. These results could be confirmed via experimental analysis in systems akin to those in Ref. [162, 182, 183]. This again shows the constrained dynamics present in noisy many-body quantum systems, and using the techniques described in the previous chapter has provided answers to debated topics.

6

ATOMIC LOSS AND GAIN AS A RESOURCE FOR NON-EQUILIBRIUM PHASE TRANSITIONS IN OPTICAL LATTICES

6.1 INTRODUCTION

In nature, stochastic systems are ubiquitous and of particular interest are those which feature collective behaviour. A key example is in the field of continuous phase transitions, where the collective behaviour and the resulting long-range correlations are governed by the system's symmetries rather than its microscopic details. This allows for systems which share these reduced sets of symmetric properties to be placed in what are called *universality classes*. Although the systems in one class may be strikingly different in their origin and microscopic nature, their behaviour about their phase transitions is universal, in the sense that the scaling behaviours of observables around the critical point are the same throughout the class.

6.1.1 *Directed Percolation*

For non-equilibrium systems, the universality class of directed percolation (DP) [87] holds particular significance. DP is considered one of the simplest non-equilibrium classes found in stochastic systems, describing critical phenomena in the fields of biology, physics, chemistry, economics, etc. DP has the following required properties of each member of its class:

- *An absorbing state transition* - an absorbing state is one which once the system enters it cannot leave. This means that all DP models are non-equilibrium as they do not satisfy detailed balance.
- *Competing processes* - members of the class have two or more competing processes which have the quality of one set pushing the system towards the absorbing state and the other pushing away from it.
- *A one-component order parameter* - it requires that the system's state, with respect to the phase transition, be characterised by a single scalar value, e.g. the magnetisation of an Ising chain.
- *Short-range interactions* - the interactions must decay sufficiently fast as to not change the extensive nature of the energy.
- *No additional symmetries.*

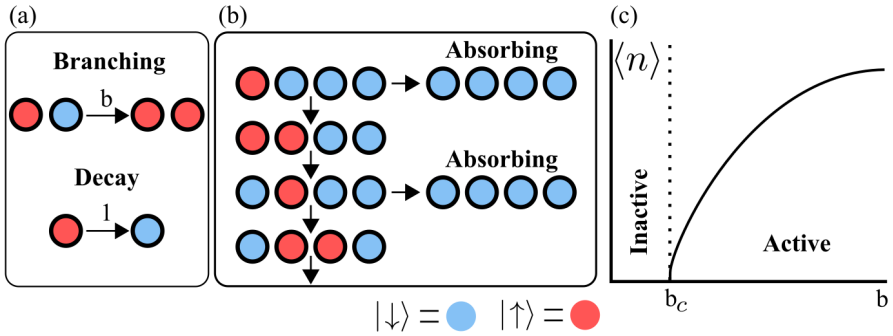

Figure 6.1: (a) Illustrations of the contact process branching and decay events. b is the branching rate, taken relative to the decay rate set to 1. (b) Shows possible trajectories of the a contact process, with states connected to the absorbing state shown. When a trajectory enters the absorbing state the dynamics ends. (c) Shows the transition of the contact process from and inactive to an active phase measured using the order parameter of average active site density $\langle n \rangle$ as defined in the text.

The DP phase transition is between an active and inactive phase, an illustration of which is shown in Fig. 6.1(c). On the inactive side, the processes which force the system into the absorbing state are dominant which causes the stationary state to be exclusively the absorbing state. In the active phase the rate of the processes pushing away from the absorbing state are dominant resulting in the stationary state no longer being the absorbing state but remaining in a dynamically-active phase.

A well known member of the DP class is the *contact process* [87, 184, 185]. The contact process can be applied to many models such as water percolation in granular media under the effect of gravity and epidemic models. The model features systems with a lattice of spin-1/2 particles with states, $|\uparrow\rangle$ and $|\downarrow\rangle$. These sites undergo two processes: branching and decay as shown in Fig. 6.1. Branching is when a $|\uparrow\rangle$ facilitates the excitation of a neighbouring $|\downarrow\rangle$; Decay is when a $|\uparrow\rangle$ transitions to a $|\downarrow\rangle$, i.e.

$$|\uparrow\downarrow\rangle \xrightarrow{b} |\uparrow\uparrow\rangle \qquad |\uparrow\rangle \xrightarrow{1} |\downarrow\rangle \tag{6.1}$$

respectively, with b being the branching rate considered relative to the rate of decay set to 1. Crucially the transition $|\downarrow\rangle \to |\uparrow\rangle$ may only occur by the facilitation from a neighbouring $\uparrow$-state. The absorbing state is thus where all sites are in a $|\downarrow\rangle$ state. The branching process attempts to maintain a population of $|\uparrow\rangle$'s and if its rate is sufficiently high it can do so, constituting the contact process's active phase. The phase transition from an inactive to active phase of the contact process is observed in the density of the $|\uparrow\rangle$'s i.e. $n = \sum_k n_k / L$ where $n_k = |\uparrow_k\rangle \langle\uparrow_k|$ and L is the number of sites, as shown in Fig. 6.1(c),

where $\langle n \rangle$ is the average of n over many trajectories. The phase transition is only strictly true in the limit of a infinite sized system at infinite time. For a finite system it is always possible for a fluctuation to occur which removes all excitations, therefore making the active phase unstable, meaning the length of time to run a finite simulation has to be carefully considered.

The nature of the phase transitions of universality classes are characterised by critical exponents applied to both the stationary and dynamical properties of the transition [87]. For DP these critical exponents are irrational and cannot be calculated analytically for dimension 4 or less. This has lead to most of the study of DP to be done numerically. Full experimental verification in all dimensions has yet to be achieved as these systems have proven to be very sensitive to quenched spatial disorder and to perturbations breaking the absorbing property of the empty state. Success was found in one and two dimensions [186, 187].

6.1.2 *Atomic systems and DP*

With the improvements in atomic experiments, the quantum simulation of complex non-equilibrium models is achievable, examples of which we have already seen in previous chapters. In this chapter we introduce a new scenario for the study of out-of-equilibrium phases and phase transitions with Rydberg atoms. The setting presented consists of a background gas, acting as a large reservoir, from which Rydberg states are only excited at given spatial positions which are arranged in a regular lattice, as produced, e.g., by employing spatial light modulators [188]. Atoms from the background dynamically enter and leave these excitation spots. In conjunction with the laser-excitation and the strong inter-atomic interactions this local loss and gain dynamics leads to the emergence of non-trivial many-body dynamics.

We show that the system possesses compatible static critical exponents with DP in multiple dimensions. In the presence of strong decoherence the loss and gain dynamics creates an absorbing space, rather than the usual single absorbing state which leads to a partial loss of universality [87]. This unusual behaviour, to our knowledge, has never been observed or considered in an open quantum system.

The presented scenario could be implemented in two rather different settings: first, a lattice of optical traps is immersed in a cold cloud of atoms and the traps are continuously filled and depleted [189]. Current experiments aim at progressively slowing down this local dynamics by, for example, reducing the pressure of the background gas or increasing the strength of the optical confinement [45, 190, 191]. These attempts could be relaxed and, in principle, the set-up could be "worsened" to the point that the timescale of the loss/-

gain dynamics becomes comparable with the other relevant dynamical processes. The second experimental setting consists of hot atomic gases confined in thermal vapour cells. Recently it has been shown that they allow for the observation of correlated many-body dynamics [57, 69] when Rydberg states are excited. Our envisioned set-up is then realised by restricting the laser excitation to a regular array of addressed spots. Thermal motion would move atoms in and out of these laser-illuminated regions, yielding the desired loss/gain dynamics.

Beyond introducing additional dynamical processes the consideration of local atom loss and gain might actually relax a number of challenges that are currently faced by experimentalists when studying collective many-body behaviour in dissipative Rydberg lattices. It might also simplify the modelling of Rydberg gases in which typically radiative decay is accounted for as a dominant decoherence mechanism:

(i) It is not necessary to have: (uniformly) deterministically loaded lattices, equal lattice confinement of ground state and Rydberg atoms, and very low temperature states. In fact it is required that atoms are not trapped over an entire experimental run.

(ii) One can employ very strongly interacting and high-lying Rydberg states that are typically long-lived. For such states the corresponding decay rate might simply be too small. In other words, it might be difficult to reach a regime in which the decay dynamics is able to properly compete with the laser excitation and inter-atomic interactions, which thus almost entirely characterise the evolution.

(iii) Even when acting on timescales that set it in competition with the driving, radiative decay is inevitably accompanied by momentum kicks from photon recoil. Even when a Rydberg atom eventually decays to the desired electronic ground state the resultant heating might lead to loss of the atoms which can be accounted for in our description. A similar process was discussed in Ch. 3.

For the sake of simplicity and in order to focus on the new aspects introduced by the loss/gain dynamics we will not consider radiative decay processes. The underlying assumption is that the loss/gain dynamics is faster than that of the decay and/or that decay effectively induces a loss process via the mechanism described in point (iii) above.

This work was published in Physical Review A in collaboration with M. Marcuzzi and I. Lesanovsky [122].

6.2 THE MODEL

We employ the standard description of a Rydberg lattice gas where each atom is modelled in terms of an effective two-level system. The

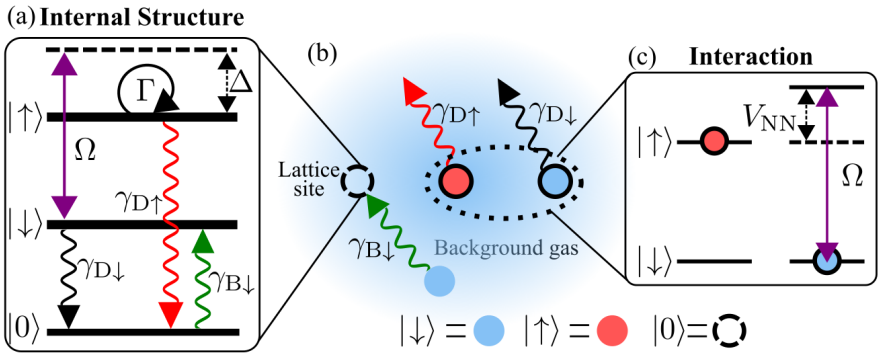

Figure 6.2: Schematic representation of the system: (a,b) an optical lattice is realised within a background cloud of atoms. Atoms within the sites undergo laser-induced coherent transitions between their ground state $|\downarrow\rangle$ and a high-lying (Rydberg) state $|\uparrow\rangle$. The corresponding Rabi frequency and laser detuning are Ω and Δ, respectively. A third state, $|0\rangle$, describes an empty site. Atoms are captured in and released from the sites with rates $\gamma_{B\downarrow}$ (capturing a ground-state atom), $\gamma_{D\downarrow}$ (losing a ground-state atom) and $\gamma_{D\uparrow}$ (losing a Rydberg atom). The atomic states are furthermore subject to dephasing at a rate Γ and radiative decay from the Rydberg state into their ground state at rate κ. (c) Rydberg atoms interact with a van der Waals potential V_{km}, whose value for nearest neighbours is denoted by V_{NN}. The corresponding energy shift of the Rydberg state in the vicinity of an excited atom is sketched. This Fig. originally appeared in Ref. [122].

ground state $|\downarrow\rangle$ is coupled to a Rydberg nS-state $|\uparrow\rangle$ through a laser with Rabi frequency Ω and detuning Δ with respect to the atomic transition, this is illustrated in Fig. 6.2(a). Within the rotating wave approximation the many-body Hamiltonian is then given by

$$H = \Omega \sum_k \sigma_k^x + \Delta \sum_k n_k + \frac{1}{2} \sum_{k \neq m} V_{km} n_k n_m, \tag{6.2}$$

where $V_{km} = C_6 / |\mathbf{r}_k - \mathbf{r}_m|^6$ represents the van der Waals (vdW) potential between pairs of excited atoms at positions $\mathbf{r}_k$ and $\mathbf{r}_p$, and the sums run over all lattice sites $k, m \in [1, L]$. Interactions among ground-state atoms or between ground-state and Rydberg atoms are significantly weaker and will therefore be neglected. The operators $\{\sigma^x, \sigma^y, \sigma^z\}$ are the standard Pauli matrices and the local density of excitations is defined as $n_k = |\uparrow_k\rangle \langle\uparrow_k|$ and the density of ground state atoms as $p_k = |\downarrow_k\rangle \langle\downarrow_k|$.

In order to account for atom gain/loss in the lattice sites we add an effective third state $|0\rangle$, denoting an empty site. We also introduce the corresponding local densities of occupied sites $e_k = n_k + p_k$. The local loss and gain takes place with atoms from a background gas which is assumed to act as a bath. In other words, the surrounding cloud contains a much higher number of atoms than can be accommodated in the lattice and the recapture of a lost one is an unlikely event. First of all, this suppresses correlations between loss and gain processes and allows us to treat them as being independent. Secondly, since atoms are constantly exchanged with new ones no correlations can be produced in the system via these processes. Thirdly, their occurrence probabilities are not appreciably affected by the history of occupation of a given site, and can thus be considered Markovian.

The relevant processes are schematically displayed in Fig. 6.2 and summarised as:

$$|\uparrow\rangle \xrightarrow{\gamma_{D\uparrow}} |0\rangle \quad , \quad |\downarrow\rangle \xrightarrow{\gamma_{D\downarrow}} |0\rangle \quad , \quad |0\rangle \xrightarrow{\gamma_{B\downarrow}} |\downarrow\rangle \, . \tag{6.3}$$

with $\gamma_{D\uparrow}$, $\gamma_{D\downarrow}$ and $\gamma_{B\downarrow}$ being the corresponding rates. The first two processes describe the loss of a Rydberg and ground state atom, respectively. The third process corresponds to the capture of a ground state atom from the background gas. Note, that we do not consider the eventuality of Rydberg atoms being captured. The reason is that laser excitation to Rydberg states is restricted to local sites and consequently Rydberg atoms are not produced in the background gas. Hence, the transition $|0\rangle \rightarrow |\uparrow\rangle$ could only occur if a Rydberg atom is captured which had been previously expelled from another site, which from the above discussion is unlikely. By themselves, these dissipative processes would push the density of ground state atoms to an equilibrium value of $\gamma_{B\downarrow}/(\gamma_{B\downarrow} + \gamma_{D\downarrow})$, in contrast to the tendency towards depletion experienced by the excitations.

Note, that we are also neglecting processes which lead to the occupation of a given site with multiple atoms. In fact, in experiments with microtraps such multi-occupancies are suppressed due to the collisional blockade [192, 193]. In circumstances where such suppression is not taking place the Rydberg blockade [44, 45, 194] discussed in Ch. 1 ensures that each site can only feature a single Rydberg excitation.

In addition to the loss/gain dynamics we consider the presence of noise, which dephases local superpositions between the states $|\uparrow\rangle$ and $|\downarrow\rangle$ at a rate Γ. The origin of this noise can be fluctuating background fields that result in random atomic level shifts, the broadening of atomic lines due to Doppler broadening [57] or interaction effects [195], or a spectrally broad excitation laser [128].

In the presence of the described coherent and dissipative processes the evolution of the density matrix ρ of the system is governed by a Lindblad master equation, see Sec. 2.1.1, with jump operators:

$$L_{D\downarrow,k} = \sqrt{\gamma_{D\downarrow}}\,|0_k\rangle\langle\downarrow_k| \tag{6.4a}$$

$$L_{D\uparrow,k} = \sqrt{\gamma_{D\uparrow}}\,|0_k\rangle\langle\uparrow_k| \tag{6.4b}$$

$$L_{B\downarrow,k} = \sqrt{\gamma_{B\downarrow}}\,|\downarrow_k\rangle\langle 0_k| \tag{6.4c}$$

$$L_{\mathrm{deph},k} = \sqrt{\Gamma} n_k \tag{6.4d}$$

where $k \in [1, L]$.

6.3 PERTURBED CLASSICAL MASTER EQUATION

We are interested in the limit of strong dephasing i.e. Γ much larger than the Rabi frequency, Ω and all other aforementioned dissipative rates. In this regime, the dynamics is effectively described by means of a classical stochastic equation [10, 119, 133, 196, 197]: the underlying separation of timescales permits the adiabatic elimination of the portion of the phase space subject to dephasing, as also seen in Ch. 4. Correspondingly, the evolution of the density matrix ρ of the system is projected onto the dissipation-free subspace [134, 198, 199], which in this case corresponds to the sole diagonal components in the σ^z basis, i.e. a basis of classical spin configurations [133]. At the leading order in a perturbative expansion in powers of γ_i/Γ and Ω/Γ the truncated density matrix μ evolves according to

$$\partial_t \mu = \sum_k \Lambda_k(\sigma_k^x \mu \sigma_k^x - e_k \mu) + \sum_{i,k} \gamma_i \left[L_{i,k} \mu L_{i,k}^\dagger - \frac{1}{2}\left\{ L_{i,k}^\dagger L_{i,k}, \mu \right\} \right] \tag{6.5}$$

where i runs over the atomic loss and gain operators (Eqs. (6.4a-6.4c)) and

$$\Lambda_k = \Omega^2\Gamma\left[\left(\frac{\Gamma}{2}\right)^2 + \left(\Delta + \sum_{q\neq k} V_{kq} n_q\right)^2\right]^{-1} \tag{6.6}$$

is a configuration-dependent rate, this is derived using the technique described in Sec. 2.1.2 but with additional dissipative processes which do not enter the expansion and appear only as additions. Defining the diagonal part of the Hamiltonian ($H|_{\Omega=0}$) as the "classical" component, the second term in the brackets of Eq. (6.6) corresponds to the square of the classical energy change accompanying a spin-flip at site k. Spin-flips that result in a significant increase or decrease in energy are therefore strongly suppressed. In the scenario investigated, in order to achieve DP-like behaviour we choose the detuning Δ such that it is opposite to the interaction energy V_{NN} between neighbouring excited atoms $\Delta = -V_{NN}$, see Fig. 6.2(c). Hence, exciting an atom right next to an *isolated* already excited one incurs no energy difference and therefore occurs at the maximal rate $\Lambda_k^{(max)} \equiv \lambda = 4\Omega^2/\Gamma$, leading to the branching shown in Fig. 6.1(a). This is known as the anti-blockade effect as discussed in Ch. 1. We further assume to be working in a regime where $|\Delta| = |V_{NN}| \gg \Gamma$, i.e. the interaction surpasses the dephasing strength. In this regime any atom that has more than 1 excitation in its neighbourhood, or none at all, can only change its internal state at a rate $\Lambda_k \propto \Omega^2\Gamma/\Delta^2$. This rate is significantly smaller than $\Lambda_k^{(max)}$ and thus such processes are strongly suppressed. For brevity, we shall refer to all of them as "off-resonant" processes.

In order to gain some first insight into the expected many-body dynamics we assume for a moment that all off-resonant processes can be neglected. In this regime Eq. (6.5) displays features close to that of the contact process and other branching-annihilating ones [87]. It is important to note that in the present case the absorbing phase does not consist of a unique state, but rather an absorbing space that is spanned by the entire set of configurations of sites which are either in state $|0\rangle$ or $|\downarrow\rangle$. In general there is dynamics taking place within the absorbing manifold as all the absorbing configurations can be visited via the interplay of the local loss and gain processes. This requires us to consider also the density of occupied sites $\eta = \sum_k \langle e_k\rangle / L$ when analysing the dynamics of the system.

6.4 MEAN-FIELD APPROACH

The mean-field approximation discards correlations between different sites, i.e. for every local observable $\mathcal{O}_k$ we substitute $\langle \mathcal{O}_k \mathcal{O}_p\rangle \to \langle \mathcal{O}_k\rangle \langle \mathcal{O}_p\rangle$ if $k \neq p$, and permits the formulation of closed equations

of motion for the expectation values of the densities of excitations n and of occupied sites η. We start by rewriting Eq. (6.6) as

$$\Lambda_k = \sum_{j=0}^{z} \lambda_j \sum_{\mathbb{C}} \prod_{\langle k,i\rangle}^{z-j} p_i \prod_{\langle k,i\rangle}^{j} n_i, \tag{6.7}$$

where z is the lattice coordination number, the number of nearest neighbours per site, $\mathbb{C}$ is a sum over all possible configurations of the excitations on the neighbours, and λ_j is shorthand for the rate of a flipping process occurring in the presence of j excited neighbours. This means that λ_1 characterises the resonant processes introduced above with $\lambda_1 = \lambda = 4\Omega^2/\Gamma$, whereas the remaining values refer to the off-resonant processes and read

$$\lambda_{j\neq 1} = \frac{\Omega^2\Gamma}{\left(\frac{\Gamma}{2}\right)^2 + \Delta^2\,(j-1)^2} \approx \frac{\Omega^2\Gamma}{\Delta^2\,(j-1)^2} \ll \lambda. \tag{6.8}$$

Using Eq. (6.5) we derive the equations

$$\partial_t n = -\gamma_{D\uparrow} n + \sum_{j=0}^{z} \binom{z}{j} \lambda_j n^j\,(\eta - 2n)\,(1-n)^{z-j} \tag{6.9a}$$

$$\partial_t \eta = \gamma_{B\downarrow} - \left(\gamma_{B\downarrow} + \gamma_{D\downarrow}\right)\eta + \left(\gamma_{D\downarrow} - \gamma_{D\uparrow}\right) n. \tag{6.9b}$$

In a first approximation we neglect the off-resonant terms, $j = 0$ and $j > 1$, and Eq. (6.9a) becomes

$$\partial_t n = -\gamma_{D\uparrow} n + \lambda z n\,(\eta - 2n)\,(1-n)^{z-1}. \tag{6.10}$$

This equation together with Eq. (6.9b) predicts a transition from the region $\lambda < \lambda_c = \gamma_{D\uparrow}(\gamma_{B\downarrow} + \gamma_{D\downarrow})/(z\gamma_{B\downarrow})$ which admits only the absorbing solution $n = 0$ to the region $\lambda > \lambda_c$ in which the system displays a finite density $n > 0$ in the long-time limit.

We look at the choice $\gamma_{D\uparrow} = \gamma_{D\downarrow} \equiv \gamma_D$ as the occupation dynamics decouples from the internal state dynamics, as seen in Eq. (6.9b), meaning the stationary density of occupied sites, $\bar{\eta}$, can be calculated exactly. In Fig. 6.3 we report the corresponding phase diagram in the $(\lambda, \bar{\eta})$ plane also setting $\Delta = -64\Gamma$. The threshold value λ_c identifies the critical point of a continuous transition between the two phases. For $\lambda > \lambda_c$, the density scales linearly, $n \sim \lambda - \lambda_c$, while at the critical point its value decays to 0 in time according to the power-law $n(t) \sim 1/t$. The density of occupied sites relaxes to the finite value $\gamma_{B\downarrow}/(\gamma_{B\downarrow} + \gamma_D)$. Consequently, at the mean-field level, this system undergoes a transition which shows some of the characteristic features of DP universality [87].

Let us now discuss the role of the off-resonant terms. Those with $j > 1$ in Eq. (6.9a) do not affect the fundamental properties of the transition, as they vanish for $n \to 0$. Therefore, they only shift the position of the critical point according to the relative statistical weights

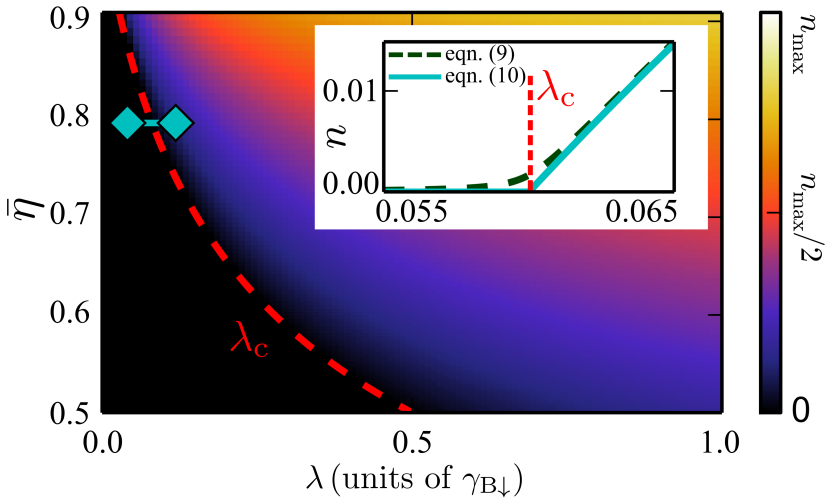

Figure 6.3: Stationary density of excitations n extracted from the mean-field equations (6.10) and (6.9b) for $-\Delta = V_{NN} = 64\Gamma$, $\gamma_{B\downarrow} = 0.01\Gamma$ and $\gamma_{D\uparrow} = \gamma_{D\downarrow}$. The data is shown as a function of the branching rate λ for resonant processes and the density of occupied sites $\bar{\eta} = \gamma_{B\downarrow}/(\gamma_{B\downarrow} + \gamma_{D\downarrow})$. The color scale is bounded by $n_{max} = 0.5$. The red dashed line corresponds to the values taken by the critical rate λ_c for different values of $\bar{\eta}$. A cross section is displayed in the inset for $\bar{\eta} = 0.8$ (along the cyan horizontal line in the main figure), which highlights the mean-field scaling behaviour $n \sim \lambda - \lambda_c$. The green, dashed line corresponds to the same curve calculated including the leading off-resonant processes relevant in a Rydberg gas. As expected, the introduction of the latter makes the transition smoother, but deviations are only visible in close vicinity to the critical point λ_c. This Fig. originally appeared in Ref. [122].

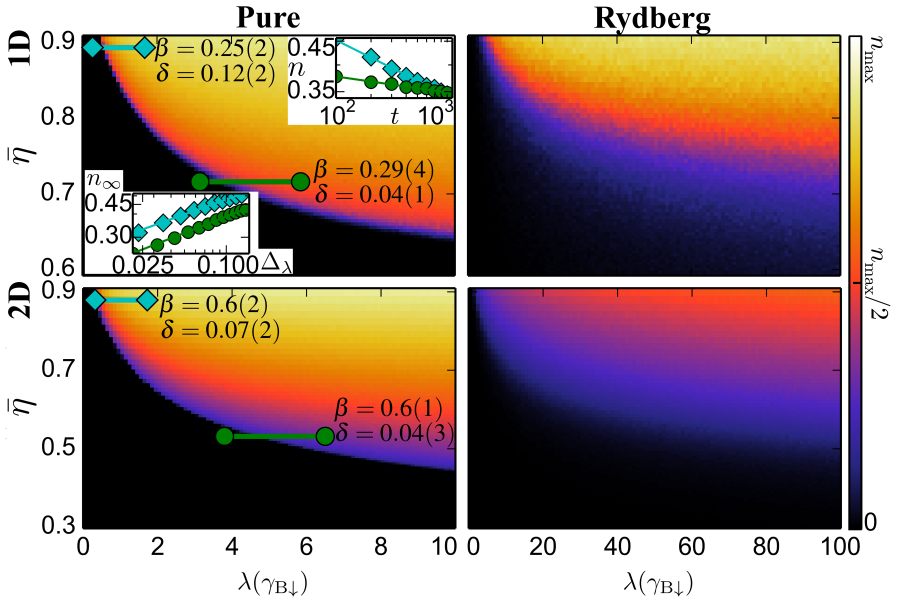

Figure 6.4: Phase diagrams of the pure and Rydberg processes (see text) in the $\bar{\eta}$-λ plane for a 1D chain of 100 sites and a 2D square lattice of 20×20 sites. The parameters are chosen as $-\Delta = V_{NN} = 64\Gamma$, $\gamma_{B\downarrow} = 0.01\Gamma$ and $\gamma_{D\downarrow} = \gamma_{D\uparrow} \equiv \gamma_D$. The color scale is set with respect to the maximal value the density can take, i.e., $n_{max} = 1$ for the pure process and $1/2$ for the Rydberg one. Numerically computed exponents β (static) and δ (dynamic) are displayed in the panels. The selected parameter ranges are shown as a cyan and a green line on the main plot. For the 1D pure process we also show (in log-log scale) the critical profiles of the stationary density n as a function of $\Delta_\lambda = \lambda - \lambda_c$ (lower-left inset) and of its evolution in time (upper-right inset) to highlight the scaling behaviour. For comparison we provide the known DP exponents [87]: $\beta_{1D} = 0.276$, $\beta_{2D} = 0.584$, $\delta_{1D} = 0.159$, and $\delta_{2D} = 0.451$. This Fig. originally appeared in Ref. [122].

λ_j. The $j = 0$ term, on the other hand, constitutes a relevant — albeit small — perturbation that brings the system away from the critical point. The reason is that it accounts for production of excitations in an empty neighbourhood and thus prevents the aforementioned subspace of configurations devoid of excitations from being strictly absorbing. This term smooths the transition into a crossover, as highlighted in the inset of Fig. 6.3. The magnitude of this effect can be suppressed by increasing the detuning Δ. When sufficiently small it allows the observation of the mean-field scaling behaviour for values of $\lambda \gtrsim \lambda_c$.

6.5 NUMERICAL ANALYSIS

In order to investigate the effect of fluctuations which are not captured by the mean-field treatment we perform numerical Monte Carlo simulations of Eq. (6.5), see Sec. 2.2 for the method, using a state in which all sites are occupied with a Rydberg atom as the initial condition. We set the rates $\gamma_{D\downarrow} = \gamma_{D\uparrow} \equiv \gamma_D$, $\gamma_{B\downarrow} = 0.01\Gamma$, $V_{NN} = 64\Gamma = -\Delta$ and collect data in the $(\lambda(\gamma_{B\downarrow}), \bar{\eta})$ plane by adjusting the values of γ_D and Ω. For this particular choice of parameters the loss and gain dynamics decouples from the excitation dynamics. This can be seen directly in Eq. (6.9b) which is valid beyond mean-field. Consequently, the density of occupied sites reaches on the low timescale of $(\gamma_{B\downarrow} + \gamma_D)^{-1}$, the steady-state value $\bar{\eta} = \gamma_{B\downarrow}/(\gamma_{B\downarrow} + \gamma_D)$.

For Rydberg gases one needs to account for the fact that the off-resonant production of excitations and the long-range tails of the vdW potential affect the emergence of the phase transition. As we discuss further below, these features actually constitute a source of additional noise which to some extent may obscure the anticipated scaling behaviours. In order to shed light on the fundamental critical properties of the transition we have therefore also simulated a dynamical process in which we replace the first term of the r.h.s. of Eq. (6.5) by

$$\sum_{\langle k,i\rangle} \frac{\lambda}{z} n_i \left(\sigma_k^+ \mu \sigma_k^- - p_k \mu\right), \tag{6.11}$$

with $\langle k, i\rangle$ denoting the set of nearest-neighbouring sites i of site k. After this replacement we have a pure branching process as found in, e.g., the contact process mentioned above [87] and shown in Eq. (6.1), producing excitations from nearby ones at a rate $b = \lambda/z$. The normalisation by the coordination number z is meant to compensate for the fact that in this case multiple excitations enhance the rate. We emphasise that, although different, the two processes we consider share the same fundamental properties: the absorbing subspace is the same and, apart from off-resonant events, branching is the only way to increase the number of excitations. Furthermore, in the presence of low-densities — as happens in the proximity of the critical point — the action of the branching terms in Eqs. (6.5) and (6.11) is analogous up to multiplicative rescaling of the rates. For brevity, in the following we shall refer to the new stochastic process as the "pure" instance and to the original process as the "Rydberg" one.

In Fig. 6.4 the pure and Rydberg processes display qualitatively the same behaviour. As expected, in the pure case the transition from the absorbing to the active phase is significantly sharper. Beyond that, two interesting features are observed. First, the simulations seem to suggest that the critical point λ_c diverges as the stationary density of occupied sites $\bar{\eta}$ decreases and that below a certain threshold $\bar{\eta}_c$

the transition disappears entirely. Second, there is a qualitative difference in the static and dynamic scaling behaviour when varying $\bar{\eta}$. The stationary properties remain unaffected and always display, within numerical accuracy, a scaling behaviour $n \sim (\lambda - \lambda_c)^\beta$ with a critical exponent β compatible with the DP one for both one- and two-dimensional processes as shown in Fig. 6.4. In contrast, the dynamical approach to the stationary state changes continuously. This means that when approaching the threshold value $\bar{\eta}_c$, the critical exponent of the algebraic decay $n(t) \sim t^{-\delta}$ smoothly decreases from a value which, in 1D, is comparable with the one of pure DP to 0.

The latter feature is strongly reminiscent of the behaviour of stochastic processes with multiple absorbing states as reported in Refs. [87, 200], which provide a qualitative explanation of our observations. Even though in our case the absorbing space is not made of individual absorbing states, the excitation dynamics effectively perceives them as such, since it stops completely as soon as the first absorbing configuration is reached. Moreover, in the cases discussed in Refs. [87, 200] the dynamic exponent is also not constant but instead varies continuously as a function of the initial conditions, e.g. the initial density. In our simulations we start from a fixed initial condition (all atoms present and excited). However, the fast loss/gain dynamics rapidly constructs an "effective initial condition" with an occupied site density $\bar{\eta}$ determined by the rates $\gamma_{B\downarrow}$ and γ_D. Since this initial condition is varied under a change of $\gamma_{B\downarrow}$ and γ_D this might be a possible explanation for the observed variation of the dynamic exponent.

The Rydberg case features off-resonant processes and thus displays a smoothed transition. Moreover, it requires stronger driving for the active phase to appear. This can be understood by noting how clusters of excitations actually hinder their own growth. For instance, if we consider a pair of nearby excitations, elongating it to a three-excitation segment, $\uparrow\uparrow\downarrow \to \uparrow\uparrow\uparrow$, faces the presence of next-nearest neighbour interactions. Because of them, the rate at which this process occurs is no longer λ but instead given by

$$\Lambda_k^{(NNN)} = \frac{\Omega^2 \Gamma}{\left(\frac{\Gamma}{2}\right)^2 + V_{NNN}^2}. \tag{6.12}$$

Our choice of parameters, $V_{NNN} = V_{NN}/2^6 = \Gamma$, implies $\Lambda_k^{NNN} = \lambda/5$ and hence the branching rate is effectively reduced. Further growth along the same direction experiences much smaller corrections and thus continues approximately at a rate $\lambda/5$. The situation worsens if we consider branching orthogonally with respect to the two original excitations, since in this case the distance between next-nearest neighbours is reduced to $\sqrt{2}$ times the lattice spacing, implying $V_{NNN} = V_{NN}/(\sqrt{2})^6 = 8\Gamma$ and yielding an effective rate $\Lambda_k^{NNN} = \lambda/257$. This explains the suppression of the stationary density in the 2D case with respect to the 1D one. The relevance of this effect can be drastically

reduced by partially removing the tails of the vdW interactions using a microwave dressing scheme [56, 201–203]. In other words, by coupling two Rydberg levels with a strong microwave field one can obtain a hybridisation of the relative interactions. For appropriate choices, it will feature a crossover threshold separating a short-distance regime displaying the usual vdW decay from a long-distance one which is instead suppressed with respect to the previous one and can be considered approximately flat. This length-scale thus acts as a cutoff for the potential tails and could then be set such that the vdW interaction does not occur beyond the distance of a single neighbouring site.

6.6 CONCLUSIONS

Here we have studied an example of a non-equilibrium system that could be realised in a Rydberg lattice gas with local loss and gain dynamics. Where these latter processes have been regarded as "negative" effects before but we have shown that, as with many other forms of dissipation [10, 64, 73, 74, 76, 81, 121, 143, 204], if utilised in the correct way they can be a powerful tool.

We have seen that by employing the anti-blockade effect a DP-like branching process can be produced and the loss and gain dynamics may be used in-place of a direct decay as it avoids the destructive decay of a Rydberg atom. In the limit of strong dephasing a perturbative classical master equation can model the system accurately allowing for direct numerical simulation of large-scale systems.

It is seen that this dynamics produces DP-like behaviour exhibiting paradigmatic dynamics and equal static exponents, but with the absorbing state becoming a space. This results in the dynamical exponent decaying with the average number of occupied sites, and there being the possibility of a critical point, η_c, below which the phase transition no longer occurs. This setting, as far as we are aware, has not been considered prior in open quantum systems and could be achieved experimentally in all dimensions [45, 57, 69, 189–191, 205].

7

ABSORBING STATE PHASE TRANSITION IN THE QUANTUM REGIME

7.1 INTRODUCTION

As the investigation of non-equilibrium systems continues to be a vibrant field both in classical and quantum physics, the study of the quantum-classical crossover is important. Through the employment of dephasing noise, a quantum system can be made to be governed by an effective classical master equation [119, 122, 127], as seen in Ch. 4. As this limit is softened the quantum nature returns. The study of the features on either the classical or quantum side, and which of those features survives the crossover, poses an interesting question theoretically but also is important in experimental study. In Ch. 6 we saw that a quantum system, namely in a Rydberg setting, can reproduce classical non-equilibrium phase transitions similar to that seen in the directed percolation (DP) universality class [87], which was discussed in Sec. 6.1.1. In Ref. [144] an open quantum model for DP was investigated, namely its action in the quantum regime was probed and signatures of a change in the transition, described below, were predicted.

Here we address the applicability of a Rydberg system to reproduce a quantum DP model from both a mean-field and numerical perspective. We find that the transition changes from second-order to first-order the more "quantum" the system is. As the classical side has been addressed in Ch. 6 and in Ref. [56] we focus our numerical study on the quantum side displaying similar predicted behaviour.

The numerical study was published in Physical Review B as part of a collaboration with M. Buchhold, M. Marcuzzi, I. Lesanovsky, S. Diehl [206] and the mean-field study is to appear in a future publication.

7.2 DIRECTED PERCOLATION AND RYDBERG SYSTEMS

Discussed in Ref. [144] was a system which had the key actions of the contact process, shown in Eq. (6.1) and discussed in detail in Sec. 6.1.1, as dissipative events and a quantum Hamiltonian which reproduces a coherent version of branching, such that a site will only undergo a Rabi oscillation when in the presence of excited neighbours. Its "classical" and "quantum" limits were found to feature similar behaviour with an absorbing state transition. The classical limit is defined as where the quantum processes are vanishing leaving a

purely DP model; the quantum limit is defined as when the dephasing is vanishing. A phase transition between inactive and active is seen in both the quantum and classical limits but its nature changes. This was studied from a mean-field approach and a numerical one and it was observed that the quantum limit transition was first-order, whilst it is known that in the classical limit it is second-order.

Here we look at a possible implementation of this dynamics in a Rydberg system utilising the anti-blockade effect, discussed in Ch. 1. We use the standard approach by modelling it as a two-level system. The ground state, $|\downarrow\rangle$, is coupled to the Rydberg nS-state, $|\uparrow\rangle$, by a coupling laser with Rabi frequency Ω and detuning Δ. We will only consider a 1D lattice of atoms on L sites giving a Hamiltonian

$$H = \Omega \sum_k \sigma_x^k + \Delta \sum_k n_k + \frac{1}{2} \sum_{k \neq m} V_{k,m} n_k n_m \tag{7.1}$$

where $V_{k,m} = V_{NN}/|k-m|^6$ is the van der Waals(vdW) interaction between the Rydberg atoms with $V_{NN} = C_6/a^6$ where a is the lattice spacing i.e. V_{NN} is the nearest-neighbour interaction, and the sums run over all lattice sites $k, m \in [1, L]$. We consider the system to be in contact with a bath with the only dissipative processes being dephasing noise and decay. The dephasing noise can be the result of fluctuating background fields that result in random atomic level shifts, the broadening of atomic lines due to Doppler broadening [57] or interaction effects [195], or a spectrally broad excitation laser [128]. The decay typically occurs from spontaneous radiative emission [128]. We also assume it to be Markovian in nature and can be modelled using the Lindblad master equation, discussed in Sec. 2.1.1, with jump operators

$$L_k^{\text{deph}} = \sqrt{\Gamma} n_k, \tag{7.2a}$$

$$L_k^{\text{decay}} = \sqrt{\kappa} \sigma_k^-, \tag{7.2b}$$

where Γ is the dephasing rate, κ is the decay rate and $k \in [1, L]$. A schematic diagram of this model is shown in Fig. 7.1(a-b).

In order to recreate the branching process we use the anti-blockade effect, by setting $\Delta = -V_{NN}$ i.e. the detuning is equal and opposite to the nearest neighbour interaction, and we move to the strongly interacting limit, $V \gg \Omega$. Isolated atoms, i.e. atoms far from any Rydberg atoms, will be very weakly coupled to the Rydberg state due to the large detuning, whilst atoms neighbouring a single Rydberg atom will be resonant with the laser, leading to a strong coupling. This is shown in Fig. 7.1(c). Those with two neighbouring Rydberg atoms will also be greatly off-resonant due to the doubled interaction. This creates a reversible coherent branching process.

As investigated in Ref. [56] in the limit of large dephasing this model features a DP-like transition, which is second-order, and as discussed in Ref. [144] there should be a first-order transition in the low

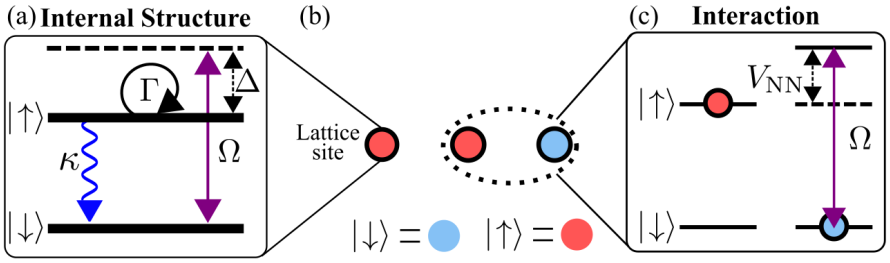

Figure 7.1: Schematic representation: (a,b) an optical lattice is realised within a background cloud of atoms in such a way that each trap is filled with a single atom. Atoms within the sites undergo laser-induced coherent transitions between their ground state $|\downarrow\rangle$ and a high-lying (Rydberg) state $|\uparrow\rangle$. The corresponding Rabi frequency and laser detuning are Ω and Δ, respectively. The atomic states are subject to dephasing noise at a rate Γ and decay at a rate κ. (c) Rydberg atoms interact via a van der Waals interaction, which has a strength V_{NN} for nearest neighbours. This shifts the Rydberg state of neighbouring atoms by V_{NN}, however due to the detuning being set such that $\Delta = -V_{NN}$, in an anti-blockade configuration, the laser couples resonantly to the shifted level.

dephasing limit. Here we investigate this model further and study the quantum to classical transition by using simplifying approximations which do not qualitatively modify the physics.

7.3 DOUBLE-BLOCKING APPROXIMATION

Unlike in the previous chapter, we do not consider the limit of large-dephasing as this has been heavily investigated in Ref. [56]. To study the properties of this model we make simplifications which gives the "double blocking" approximation. This makes the following assumptions:

- we neglect the van der Waals interactions beyond nearest neighbours,
- we set $\Delta = -V_{NN}$,
- and we assume the limit $V_{NN} \to \infty$.

This means that only atoms with a single neighbouring excitation have their ground state coupled to their excited state, making this a hard constraint. This gives the double blocking approximation a Hamiltonian

$$H = \Omega \sum_k \Pi_k \sigma_k^x, \tag{7.3}$$

with $\Pi_k = n_{k-1} + n_{k+1} - 2n_{k-1}n_{k+1}$. The final term in Π_k prevents coupling when there is more than a single excitation neighbouring a

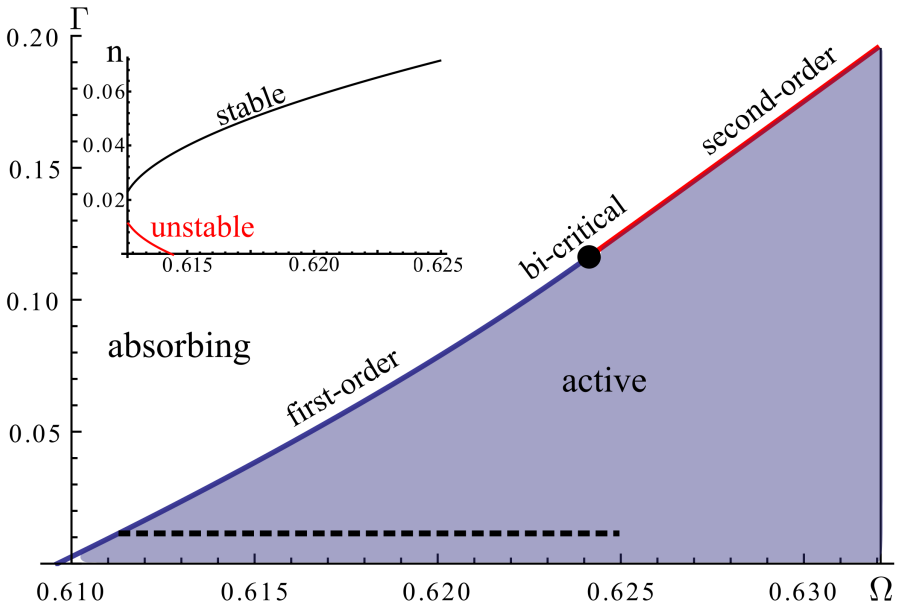

Figure 7.2: The augmented mean-field phase diagram with $\kappa = 1$. The white area on the left is absorbing, meaning the only solutions present are those for $n = 0$ while the shaded area is the active phase, with the steady state featuring solutions with finite population. The transitions are labelled as first (blue) and second-order (red) with the bi-critical point highlighted as a black dot. The solutions to the first order transition along the black dashed line at $\Gamma = 0.01$ are shown in the inset, with the unstable solution shown in red.

site. This will be important to the dynamics of dense systems due to the protection of surrounded objects from the quantum term. Once the system is sparse however it should only play a minor role, which should be true near to the transition from the inactive to active phase.

7.4 MEAN-FIELD APPROACH

We begin by applying a mean-field approach to the double blocking approximation. By using Eq. (2.8) the observables $(\langle n_k\rangle, \langle\sigma_k^y\rangle, \langle\sigma_k^x\rangle)$, which form a complete set for a single spin, are found to be governed by

$$\partial_t \langle n_k\rangle = \Omega \langle \Pi_k \sigma_k^y\rangle - \kappa \langle n_k\rangle , \tag{7.4a}$$

$$\partial_t \langle \sigma_k^y\rangle = -\Omega \langle 2\Pi_k(2n_k - 1) - \sigma_k^x \sigma_{k-1}^x (1 - 2n_{k-2})\rangle - \langle \sigma_k^x \sigma_{k+1}^x (1 - 2n_{k+2})\rangle - \frac{\kappa + \Gamma}{2} \langle \sigma_k^y\rangle , \tag{7.4b}$$

$$\partial_t \langle \sigma_k^x\rangle = -\Omega \langle \sigma_k^y \sigma_{k-1}^x (1 - 2n_{k-2}) + \sigma_k^y \sigma_{k+1}^x (1 - 2n_{k+2})\rangle - \frac{\kappa + \Gamma}{2} \langle \sigma_k^x\rangle . \tag{7.4c}$$

We consider the approximation that all correlations between sites are negligible i.e. for every local observable, $\mathcal{O}_k$, we assume that $\langle \mathcal{O}_k \mathcal{O}_j \rangle = \langle \mathcal{O}_k \rangle \langle \mathcal{O}_j \rangle$ whenever $k \neq j$. We also assume that the system is uniform such that $\langle \mathcal{O}_k \rangle = \mathcal{O} \; \forall \, k$. Applying these assumptions to Eqs. (7.4) we find

$$\partial_t n = 2\Omega(n - n^2)\sigma_y - \kappa n, \tag{7.5a}$$

$$\partial_t \sigma_y = \Omega(4n(1-2n)(1-n) + 2\sigma_x^2(1-2n)) - \frac{\kappa + \Gamma}{2}\sigma_y, \tag{7.5b}$$

$$\partial_t \sigma_x = -2\Omega(\sigma_y \sigma_x (1-2n)) - \frac{\kappa + \Gamma}{2}\sigma_x. \tag{7.5c}$$

As we are interested in the steady state solutions of the system we look at the case of $\partial_t \mathcal{O} = 0 \; \forall \mathcal{O}$. We also look at the case of $\sigma_x(t) = 0 \; \forall \, t$, which is true for $\sigma_x(0) = 0$, and it can be shown that for the valid range of n, i.e. $0 < n < 0.5$, σ_x is always decaying and its steady state will be exclusively 0. After substitution this gives

$$n^2(1-2n)(1-n)^2 = \nu n \tag{7.6}$$

where $\nu = \kappa(\kappa + \Gamma)/16\Omega^2$. Eq. (7.6) always features a stable zero population solution, and a first-order transition to finite population at $\nu = 1$. We know from previous studies [56] that a second-order transition exists in the limit of large Γ but due to strong correlations between nearest neighbours, caused by the Π operator, this mean-field approach fails to detect it.

7.4.1 *Augmented meanfield*

In order to include short range correlations we extend our description to the pair of operators $\langle n_{k+1}\sigma_k^y \rangle$ and $\langle n_{k-1}\sigma_k^y \rangle$, the primary components of $\langle \Pi_k \sigma_k^y \rangle$. This means that we retain their two-point correlations and discard all others i.e. $\langle n_{k\pm1}\sigma_k^y \rangle \neq \langle n_{k\pm1} \rangle \langle \sigma_k^y \rangle$, but higher orders may still be discarded. This allows the term $\langle \Pi_k \sigma_k^y \rangle$ to be re-expressed as

$$\begin{aligned}\langle \Pi_k \sigma_k^y \rangle = &\langle n_{k-1}\sigma_k^y \rangle (1 - 2\langle n_{k+1} \rangle) + \langle n_{k+1}\sigma_k^y \rangle (1 - 2\langle n_{k-1} \rangle) \\ &+ 2\langle n_{k+1} \rangle \langle n_{k-1} \rangle \langle \sigma_k^y \rangle .\end{aligned} \tag{7.7}$$

We then find the evolution of the additional terms, $\langle n_{k\pm1}\sigma_k^y \rangle$, as

$$\begin{aligned}\partial_t \langle n_{k\pm1}\sigma_k^y \rangle = &\Omega(\langle 2n_{k\pm1}(1-2n_k)(1-n_{k\mp1}) \rangle \\ &+ \left\langle \frac{\sigma_k^y \sigma_{k\pm1}^y + \sigma_k^x \sigma_{k\pm1}^x}{2}(1-2n_{k\pm2}) \right\rangle \\ &+ \langle \sigma_k^y \sigma_{k\pm1}^y n_{k\pm2} + \sigma_{k\mp1}^x \sigma_k^x n_{k\pm1}(1-2n_{k\mp2}) \rangle) \\ &- \frac{3\kappa + \Gamma}{2}\langle n_{k\pm1}\sigma_k^y \rangle\end{aligned} \tag{7.8}$$

Applying the same assumptions as before and defining $S_\pm = \langle n_{k\pm1}\, \sigma_k^y \rangle \; \forall\, k$ then Eqs. (7.8) become

$$\partial_t S_\pm = \Omega(2n(1-2n)(1-n) + \frac{\sigma_y^2}{2}) - \frac{3\kappa+\Gamma}{2} S_\pm. \tag{7.9}$$

The equations for $S_\pm$ have exactly the same form. Assuming the chain to be invariant under reflection with respect to its centre, mapping $S_+ \rightleftharpoons S_-$, we set $S_+ = S_- = S$. Using this we see that Eq. (7.5a) also becomes

$$\partial_t n = 2\Omega(S(1-2n) + n^2\sigma_y) - \kappa n. \tag{7.10}$$

When these equations are solved for their steady state solution we find

$$\begin{aligned} 0 =& n[4\alpha(1-2n)^2(1-n) + \alpha\beta^2 n(1-n)^2(1-2n)^3 \\ &+ \beta n^2(1-2n)(1-n) - \frac{\kappa}{\Omega}] \end{aligned} \tag{7.11}$$

where $\alpha = 2\Omega/(3\kappa+\Gamma)$ and $\beta = 8\Omega/(\kappa+\Gamma)$. Again we see the $n = 0$ solution present but now the inner function, within the square brackets of Eq. (7.11), depending on the values of α and β, features either a first or second order transition. This leads to the existence of a bi-critical point, highlighted in Fig. 7.2 as where the two lines meet. The position of which is found by when the derivative of the inner function is zero at $n = 0$, giving

$$\Omega = \frac{\kappa(\sqrt{5}+\sqrt{105})}{20}, \tag{7.12}$$

lying on the transition curve which for the second order transition, found as when the inner function is zero at $n = 0$, is given by

$$\Gamma = \frac{8\Omega^2}{\kappa} - 3\kappa. \tag{7.13}$$

An estimate for the position of the first-order transition is found by a perturbative expansion of the inner function of Eq. (7.11) about $n = 0$ to second-order. The lower the value of Γ the worse this approximation is as the transition shifts to larger finite values of n. The phase diagram is shown in Fig. 7.2, showing a qualitative representation of the transitions we expect in the (Ω, Γ) plane. We see at low Γ a first order transition, as Ω is scanned, from an inactive to active phase, and a second order transition at higher Γ, with a bi-critical point between them [144].

7.4.2 *Stability of solutions*

We look at the dynamical stability of the solutions to this augmented mean-field method. For an observable $\mathcal{O}$ this is calculated by considering the evolution of a perturbation about the steady state solution.

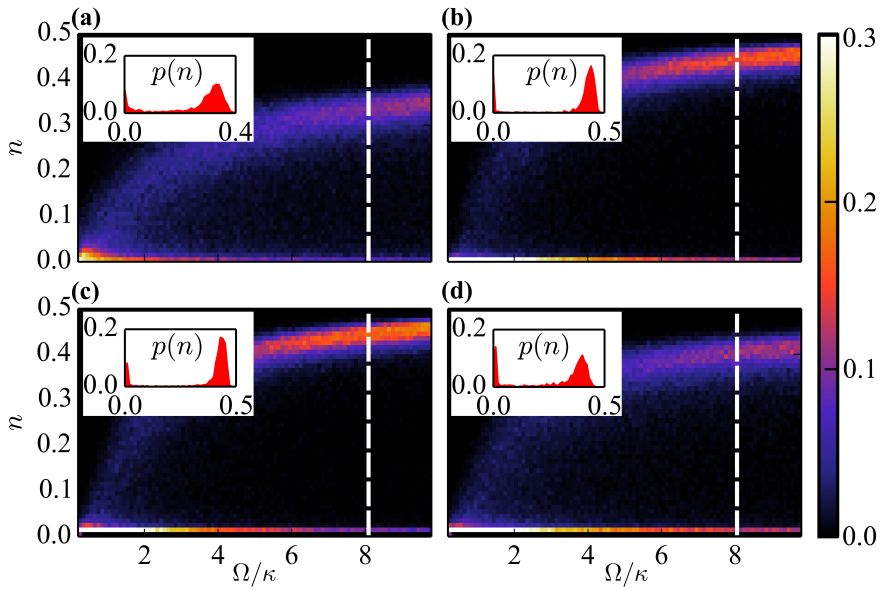

Figure 7.3: Signature of a first order transition in the quantum limit, $\Gamma = 0$. The panels show histograms of the excitation count for one-dimensional systems of 12 particles. (a) Idealised model using Eq. (7.15), (b) Effective model using Eq. (7.3) derived from the Rydberg Hamiltonian (c) Rydberg chain with nearest neighbor interaction, (d) Rydberg chain with the van-der-Waals tail. All plots display a crossover from an (almost) absorbing state at small Ω to a state with finite excitation density. For intermediate values of Ω the histograms feature a bimodal distribution which is a signature of the anticipated first order phase transition. This is shown in the insets that display intersections taken at $\Omega = 8\kappa$. All results are obtained via Quantum Jump Monte Carlo simulations and average over 1000 runs. The simulation times are $\kappa t = 4$ (a) and $\kappa t = 6$ (b-d). The calculations for the Rydberg systems [panels (c,d)] are done choosing the parameters $\Delta = V_{NN} = 10\Omega$. Note that the colorbar has been limited to a height of 0.3 to give a better color contrast. For $\Omega \lesssim 3\kappa$ the peaks around 0 exceed this limit. This Fig. originally appeared in Ref. [206].

A solution is considered stable in a regime if any small perturbation is decaying, i.e. $\delta O \partial_t \delta O < 0$. For simultaneous evolution equations this is done by considering the defining matrix and is stable if all eigenvalues are negative.

If we look at the $n = 0$ solution we find that it is only unstable at the points where

$$4\Omega^2 \geqslant \frac{\kappa(3\kappa + \Gamma)}{2} \tag{7.14}$$

corresponding to the active phase right of the second order line in Fig. 7.2. We numerically look at the stability of the finite n solutions and find that for the second-order transition the finite solution is always stable whilst for the first-order transition the lower population solution is unstable as shown in the inset of Fig. 7.2.

7.5 NUMERICAL ANALYSIS

As the classical limit, $\Gamma \gg \Omega$, was fully explored in Ref. [56] we choose to focus our numerical study on the quantum limit i.e. $\Gamma = 0$. We use the technique described in Sec. 2.3, which limits our study to small system sizes. We look at four instances. First the "pure" approximation which removes the single neighbouring excitation limit of the double blocking, meaning that when a site is neighboured by one or two excitations it has its ground and excited state coupled. This makes it closer to a "quantum" DP model, giving a Hamiltonian

$$H = \Omega \sum_k \left(n_{k-1} + n_{k+1}\right) \sigma_k^x. \tag{7.15}$$

From the above discussion, this should show qualitatively similar behaviour near the absorbing state transition. Followed by the double blocking approximation described using Eq. (7.3), the Rydberg chain including only nearest neighbour interactions, and the Rydberg chain with full interactions. Shown in Fig. 7.3 are the counting statistics of the average population, i.e. $n = \sum_{k=1}^{L} n_k/L$, at "long times" which shows a bifurcation in the statistics for each case, an indicator of the first-order phase transition predicted in the mean-field study in the quantum limit.

The double blocking approximation is closer to the Rybderg models than the pure further from the transition point due to the increase in density. Furthermore we see that the inclusion of the full interactions weakens the transition due to the tails affecting next to nearest neighbour transitions. This could be addressed by use of microwave dressing [56, 201–203]. Further details on this are given in Sec. 6.5. This suggests that Rydberg systems could prove a suitable platform for the study of DP-like quantum models.

7.6 CONCLUSIONS

Here we have looked at a DP-like quantum model, where we have started to test the grounds of using a Rydberg system to achieve it. The numerical results presented give good indication that the same behaviours in pure and double blocking approximations are present in the Rybderg model. The mean-field study shows what behaviour might be expected in the quantum-classical crossover, featuring a bi-critical point where the system goes from having a first-order transition to a second-order one. Work on this study is continuing and experimental platforms for its realisation appear promising [191, 205, 207].

8

CONCLUSIONS

In this thesis we have looked at examples of open non-equilibrium quantum systems that can all be realised in current experimental set-ups. They showcase different phenomena that can be observed by utilising dissipation as a resource, and, in certain cases, the strong interactions of Rydberg atoms.

In Ch. 3 we looked at the case of a selective-pair dissipation induced by a simultaneous excitation of a Rydberg pair, with the distance controlled by the anti-blockade effect. When this dissipative process is strong it results in a binding effect due to the quantum Zeno effect which in-turn creates two distinguishable complexes. Through their dispersion relations, these complexes were found to exhibit interesting physics in the role of effective spin-orbit coupling. Particularly the existence of a flat-band for certain complexes, which are localised and stable states. The ability to produce such states reliably in experimental set-ups [109, 110] could open interesting study into the quantum phases that result from these complexes possessing properties of interest in condensed matter physics.

We then moved onto study what kinetically constrained models (KCMs) can be achieved in open quantum lattice systems with strong dephasing noise in Ch. 4. KCMs have long remained an effective construct used to demonstrate slow-relaxing and glassy systems, but their physical realisation and application has been difficult. Although the method fails to capture some of the prototypical examples of KCMs due to the lack of temperature control, we show that other examples are possible and demonstrate that with simple ingredients a system which shows constrained physics, such as ergodicity breaking, can be achieved.

We then found a further application of the formalism from Ch. 4 in the study of dissipative many-body localised (MBL) systems. Observed in Ref. [165], the MBL state in an open system decays with a stretched exponential behaviour. It was shown that the decay collapsed when time was rescaled with dephasing noise, implying that the effect was in-fact classical in nature. Presented in Ch. 5 we found that the presence of interactions effects causes the decay to follow two distinct forms. For low interactions we observed the stretched exponential decay being governed by a pair relaxation process, this confirms that the observed phenomena is in-fact a purely classical process. For strong interactions the decay was compressed instead, resulting from an Avrami law [177–181]. This behaviour was not seen in previous theoretical studies as they utilised quantum simulation,

which due to the strong size dependence prevented observation. We also showed that this behaviour was only effected by particle loss for strong interactions, placing a limit on the timescale. Not only does this explain the observed features, but it opens up the study of a system which features a stretched to compressed exponential behaviour transition in experiments already studying MBL [145, 160–162].

We then focussed on the study of systems which display directed percolation (DP) behaviour. As previously studied in Ref. [56], Rydberg systems featuring strong dephasing noise and utilising the anti-blockade effect can reproduce a contact process and show DP-like behaviour. There however the standard decay channel for the decay process was used, which can be highly destructive often resulting in the loss of an atom. Instead in Ch. 6, we chose to exploit this atom loss and consider a denser cloud structure allowing a on-site loss and gain dynamics to take the place of the decay process. This created an absorbing space instead of a single state, resulting in a different DP-like behaviour that has previously not been observed. A key feature being the divergence of the DP phase transition as the average population was reduced. This system offers an effective way to realise DP-like dynamics in all dimensions in current experimental set-ups [45, 57, 69, 189–191, 205] and allows access to new, relatively unstudied physics.

In the final Ch. 7 we look at a quantum model which features DP-like behaviour in a Rydberg setting. We found that the model exhibits a first-order transition in the quantum limit, confirmed by mean-field and numerical results. From the mean-field study we also saw the existence of a tri-critical point, where as the system became more classical the transition went from first to second-order, as expected for a DP model. This shows further the viability of Rydberg systems to produce these constrained DP-like models and to probe the quantum and classical boundary that exists in them.

Overall, the work presented in this thesis contributes to the growing field of open quantum non-equilibrium systems in atomic lattice systems. We highlight key examples of where Rydberg properties allow for the realisation of both new and long-predicted models through use of their strong interactions. By engineering a anti-blockade effect, these interactions can be accurately controlled to facilitate particular processes, and block others. This gives a great deal of control, allowing for the production of models which reproduce the physics of interesting non-equilibrium and constrained systems. Crucially we utilise dissipation as a resource. Throughout the thesis we made use of dephasing noise to project a quantum system into a classical setting. This allows for the use of quantum systems to produce classical effects that are otherwise hard to engineer, allowing for models, such as DP, to be realised. We also use other decay channels, such as on-site loss and gain. Each of these decay channels are often

viewed as detrimental processes and a great deal of effort goes into minimising and controlling them. This implies that the "worsening" of systems to reintroduce them, and their control to certain values is attainable in current experimental set-ups.

BIBLIOGRAPHY

[1] P. W. Anderson. "More Is Different." In: *Science* 177.4047 (1972), pp. 393–396. ISSN: 00368075, 10959203. URL: http://www.jstor.org/stable/1734697.

[2] Philip W Anderson et al. "Twenty-five Years of High-Temperature Superconductivity – A Personal Review." In: *Journal of Physics: Conference Series* 449.1 (2013), p. 012001. ISSN: 1742-6596. DOI: 10.1088/1742-6596/449/1/012001.

[3] Immanuel Bloch and Wilhelm Zwerger. "Many-body physics with ultracold gases." In: *Reviews of Modern Physics* 80.885 (2008). ISSN: 0034-6861. DOI: 10.1103/RevModPhys.80.885.

[4] L. Berthier and G. Biroli. "Theoretical perspective on the glass transition and amorphous materials." In: *Reviews of Modern Physics* 83.2 (2011), pp. 587–645. ISSN: 0034-6861. DOI: 10.1103/RevModPhys.83.587.

[5] G. Biroli and J. P. Garrahan. "Perspective: The glass transition." In: *The Journal of Chemical Physics* 138.12 (2013), 12A301. ISSN: 1089-7690. DOI: 10.1063/1.4795539.

[6] R. Bowley and M. Sánchez. *Introductory Statistical Mechanics*. 2nd. Oxford Science Publications.

[7] Luca Cipelletti and Laurence Ramos. "Slow dynamics in glassy soft matter." In: *Journal of Physics: Condensed Matter* 17.6 (2005), R253.

[8] J. P. Garrahan, R. L. Jack, V. Lecomte, E. Pitard, K. van Duijvendijk, and F. van Wijland. "Dynamical First-Order Phase Transition in Kinetically Constrained Models of Glasses." In: *Phys. Rev. Lett.* 98.195702 (2007). DOI: 10.1103/PhysRevLett.98.195702.

[9] R. A. L. Jones. *Soft Condensed Matter*. Oxford University Press, 2011.

[10] Igor Lesanovsky and Juan P. Garrahan. "Kinetic Constraints, Hierarchical Relaxation, and Onset of Glassiness in Strongly Interacting and Dissipative Rydberg Gases." In: *Phys. Rev. Lett.* 111.215305 (2013). DOI: 10.1103/PhysRevLett.111.215305.

[11] M. Heyl, A. Polkovnikov, and S. Kehrein. "Dynamical Quantum Phase Transitions in the Transverse-Field Ising Model." In: *Phys. Rev. Lett.* 110.135704 (2013). DOI: 10.1103/PhysRevLett.110.135704.

[12] M. Heyl. "Dynamical Quantum Phase Transitions in Systems with Broken-Symmetry Phases." In: *Phys. Rev. Lett.* 113.205701 (2014). DOI: 10.1103/PhysRevLett.113.205701.

[13] G. H. Fredrickson and H. C. Andersen. "Kinetic Ising Model of the Glass Transition." In: *Phys. Rev. Lett.* 53.1244 (1984). ISSN: 0031-9007. DOI: 10.1103/PhysRevLett.53.1244.

[14] J. Jäckle and S. Eisinger. "A hierarchically constrained kinetic Ising model." In: *Z. Phys. B Condensed Matter* 84.1 (1991), pp. 115–124. ISSN: 0722-3277. DOI: 10.1007/BF01453764.

[15] P. Sollich F. Ritort. "Glassy dynamics of kinetically constrained models." In: *Advances in Physics* 52.4 (2003), pp. 219–342.

[16] J. P. Garrahan, R. L. Jack, V. Lecomte, E. Pitard, K. van Duijvendijk, and F. van Wijland. "First-order dynamical phase transition in models of glasses: an approach based on ensembles of histories." In: *Journal of Physics A: Mathematical and Theoretical* 42.7 (2009), p. 075007.

[17] Bose. "Plancks Gesetz und Lichtquantenhypothese." In: *Zeitschrift für Physik* 26.1 (1924), pp. 178–181. ISSN: 0044-3328. DOI: 10.1007/BF01327326.

[18] V S Letokhov, M A Ol'shanii, and Yu B Ovchinnikov. "Laser cooling of atoms: a review." In: *Quantum and Semiclassical Optics: Journal of the European Optical Society Part B* 7.1 (1995), p. 5.

[19] M. H. Anderson, J. R. Ensher, M. R. Matthews, C. E. Wieman, and E. A. Cornell. "Observation of Bose-Einstein Condensation in a Dilute Atomic Vapor." In: *Science* 269.5221 (1995), pp. 198–201. ISSN: 0036-8075. DOI: 10.1126/science.269.5221.198.

[20] C. C. Bradley, C. A. Sackett, J. J. Tollett, and R. G. Hulet. "Evidence of Bose-Einstein Condensation in an Atomic Gas with Attractive Interactions." In: *Phys. Rev. Lett.* 75.1687 (1995). DOI: 10.1103/PhysRevLett.75.1687.

[21] K. B. Davis, M. O. Mewes, M. R. Andrews, N. J. van Druten, D. S. Durfee, D. M. Kurn, and W. Ketterle. "Bose-Einstein Condensation in a Gas of Sodium Atoms." In: *Phys. Rev. Lett.* 75.3969 (1995). DOI: 10.1103/PhysRevLett.75.3969.

[22] B. DeMarco and D. S. Jin. "Onset of Fermi Degeneracy in a Trapped Atomic Gas." In: *Science* 285.5434 (1999), pp. 1703–1706. ISSN: 0036-8075. DOI: 10.1126/science.285.5434.1703.

[23] F. Schreck, L. Khaykovich, K. L. Corwin, G. Ferrari, T. Bourdel, J. Cubizolles, and C. Salomon. "Quasipure Bose-Einstein Condensate Immersed in a Fermi Sea." In: *Phys. Rev. Lett.* 87.080403 (2001). DOI: 10.1103/PhysRevLett.87.080403.

[24] Andrew G. Truscott, Kevin E. Strecker, William I. McAlexander, Guthrie B. Partridge, and Randall G. Hulet. "Observation of Fermi Pressure in a Gas of Trapped Atoms." In: *Science* 291.5513 (2001), pp. 2570–2572. ISSN: 0036-8075. DOI: 10.1126/science.1059318.

[25] Rudolf Grimm. "Ultracold Fermi gases in the BEC-BCS crossover: a review from the Innsbruck perspective." In: (2007). arXiv: 0703091 [cond-mat].

[26] R. P. Feynman. "Simulating Physics with Computers." In: *International Journal of Theoretical Physics* 21 (June 1982), pp. 467–488. DOI: 10.1007/BF02650179.

[27] Immanuel Bloch, Jean Dalibard, and Sylvain Nascimbène. "Quantum simulations with ultracold quantum gases." In: *Nature Physics* 8.4 (2012), pp. 267–276. ISSN: 1745-2473. DOI: 10.1038/nphys2259.

[28] Cheng Chin, Rudolf Grimm, Paul Julienne, and Eite Tiesinga. "Feshbach resonances in ultracold gases." In: *Rev. Mod. Phys.* 82.1225 (2010). DOI: 10.1103/RevModPhys.82.1225.

[29] Markus Greiner, Cindy A. Regal, and Deborah S. Jin. "Emergence of a molecular Bose–Einstein condensate from a Fermi gas." In: *Nature* 426.6966 (2003), pp. 537–540. ISSN: 0028-0836. DOI: 10.1038/nature02199.

[30] Michael Aizenman, Elliott H. Lieb, Robert Seiringer, Jan Philip Solovej, and Jakob Yngvason. "Bose-Einstein quantum phase transition in an optical lattice model." In: *Phys. Rev. A* 70.023612 (2004). DOI: 10.1103/PhysRevA.70.023612.

[31] Thilo Stöferle, Henning Moritz, Christian Schori, Michael Köhl, and Tilman Esslinger. "Transition from a Strongly Interacting 1D Superfluid to a Mott Insulator." In: *Phys. Rev. Lett.* 92.130403 (2004). DOI: 10.1103/PhysRevLett.92.130403.

[32] I. B. Spielman, W. D. Phillips, and J. V. Porto. "Mott-Insulator Transition in a Two-Dimensional Atomic Bose Gas." In: *Phys. Rev. Lett.* 98.080404 (2007). DOI: 10.1103/PhysRevLett.98.080404.

[33] I. B. Spielman, W. D. Phillips, and J. V. Porto. "Condensate Fraction in a 2D Bose Gas Measured across the Mott-Insulator Transition." In: *Phys. Rev. Lett.* 100.120402 (2008). DOI: 10.1103/PhysRevLett.100.120402.

[34] N. Poli, M. Schioppo, S. Vogt, St. Falke, U. Sterr, Ch. Lisdat, and G. M. Tino. "A transportable strontium optical lattice clock." In: *Applied Physics B* 117.4 (2014), pp. 1107–1116. ISSN: 1432-0649. DOI: 10.1007/s00340-014-5932-9.

[35] A Peters, K Y Chung, and S Chu. "High-precision gravity measurements using atom interferometry." In: *Metrologia* 38.1 (2001), p. 25.

[36] G. Rosi, F. Sorrentino, L. Cacciapuoti, M. Prevedelli, and G. M. Tino. "Precision measurement of the Newtonian gravitational constant using cold atoms." In: *Nature* 510.7506 (2014), pp. 518–521. ISSN: 0028-0836. DOI: 10.1038/nature13433.

[37] M. Saffman, T. G. Walker, and K. Mølmer. "Quantum information with Rydberg atoms." In: *Rev. Mod. Phys.* 82 (3 2010), pp. 2313–2363. DOI: 10.1103/RevModPhys.82.2313.

[38] T F Gallagher. "Rydberg atoms." In: *Reports on Progress in Physics* 51.2 (1988), p. 143.

[39] Jongseok Lim, Han-gyeol Lee, and Jaewook Ahn. "Review of cold Rydberg atoms and their applications." In: *Journal of the Korean Physical Society* 63.4 (2013), pp. 867–876. ISSN: 1976-8524. DOI: 10.3938/jkps.63.867.

[40] Sébastien Gleyzes, Stefan Kuhr, Christine Guerlin, Julien Bernu, Samuel Deléglise, Ulrich Busk Hoff, Michel Brune, Jean-Michel Raimond, and Serge Haroche. "Quantum jumps of light recording the birth and death of a photon in a cavity." In: *Nature* 446.7133 (2007), pp. 297–300. ISSN: 0028-0836. DOI: 10.1038/nature05589.

[41] D B Branden, T Juhasz, T Mahlokozera, C Vesa, R O Wilson, M Zheng, A Kortyna, and D A Tate. "Radiative lifetime measurements of rubidium Rydberg states." In: *Journal of Physics B: Atomic, Molecular and Optical Physics* 43.1 (2010), p. 015002. ISSN: 0953-4075. DOI: 10.1088/0953-4075/43/1/015002.

[42] Antoine Browaeys and Thierry Lahaye. "Interacting Cold Rydberg Atoms: A Toy Many-Body System." In: *Niels Bohr, 1913-2013: Poincaré Seminar 2013*. Ed. by Olivier Darrigol, Bertrand Duplantier, Jean-Michel Raimond, and Vincent Rivasseau. Springer International Publishing, 2016, pp. 177–198. ISBN: 978-3-319-14316-3. DOI: 10.1007/978-3-319-14316-3_7.

[43] D. Tong, S. M. Farooqi, J. Stanojevic, S. Krishnan, Y. P. Zhang, R. Côté, E. E. Eyler, and P. L. Gould. "Local Blockade of Rydberg Excitation in an Ultracold Gas." In: *Phys. Rev. Lett.* 93.063001 (2004). DOI: 10.1103/PhysRevLett.93.063001.

[44] E. Urban, T. A. Johnson, T. Henage, L. Isenhower, D. D. Yavuz, T. G. Walker, and M. Saffman. "Observation of Rydberg blockade between two atoms." In: *Nature Physics* 5.2 (2009), pp. 110–114.

[45] A. Gaetan, Y. Miroshnychenko, T. Wilk, A. Chotia, M. Viteau, D. Comparat, P. Pillet, A. Browaeys, and P. Grangier. "Observation of collective excitation of two individual atoms in the Rydberg blockade regime." In: *Nat. Phys.* 5 (2 2009), pp. 115–118. DOI: 10.1038/nphys1183.

[46] Matthias Weidemüller. "Rydberg atoms: There can be only one." In: *Nature Physics* 5.2 (2009), pp. 91–92. ISSN: 1745-2473. DOI: 10.1038/nphys1193.

[47] T. M. Weber, M. Höning, T. Niederprüm, T. Manthey, O. Thomas, V. Guarrera, M. Fleischhauer, G. Barontini, and H. Ott. "Mesoscopic Rydberg-blockaded ensembles in the superatom regime and beyond." In: *Nature Physics* 11 (2015), pp. 157–161. DOI: 10.1038/nphys3214.

[48] Antoine Browaeys, Daniel Barredo, and Thierry Lahaye. "Experimental investigations of dipole–dipole interactions between a few Rydberg atoms." In: *Journal of Physics B: Atomic, Molecular and Optical Physics* 49.15 (2016), p. 152001.

[49] Y.-Y. Jau, A. M. Hankin, T. Keating, I. H. Deutsch, and G. W. Biedermann. "Entangling atomic spins with a Rydberg-dressed spin-flip blockade." In: *Nature Physics* 12.1 (2015), pp. 71–74. ISSN: 1745-2473. DOI: 10.1038/nphys3487.

[50] Thibault Peyronel, Ofer Firstenberg, Qi-Yu Liang, Sebastian Hofferberth, Alexey V. Gorshkov, Thomas Pohl, Mikhail D. Lukin, and Vladan Vuletić. "Quantum nonlinear optics with single photons enabled by strongly interacting atoms." In: *Nature* 488.7409 (2012), pp. 57–60. ISSN: 0028-0836. DOI: 10.1038/nature11361.

[51] C. Ates, I. Lesanovsky, C. S. Adams, and K. J. Weatherill. "Fast and Quasideterministic Single Ion Source from a Dipole-Blockaded Atomic Ensemble." In: *Phys. Rev. Lett.* 110.213003 (2013). DOI: 10.1103/PhysRevLett.110.213003.

[52] C. Ates, T. Pohl, T. Pattard, and J. M. Rost. "Antiblockade in Rydberg Excitation of an Ultracold Lattice Gas." In: *Phys. Rev. Lett.* 98.023002 (2007). DOI: 10.1103/PhysRevLett.98.023002.

[53] Thomas Amthor, Christian Giese, Christoph S. Hofmann, and Matthias Weidemüller. "Evidence of Antiblockade in an Ultracold Rydberg Gas." In: *Phys. Rev. Lett.* 104.013001 (2010). DOI: 10.1103/PhysRevLett.104.013001.

[54] C. Ates, B. Olmos, W. Li, and I. Lesanovsky. "Dissipative Binding of Lattice Bosons through Distance-Selective Pair Loss." In: *Physical Review Letters* 109.233003 (2012). DOI: 10.1103/PhysRevLett.109.233003.

[55] I. Lesanovsky and J. P. Garrahan. "Out-of-equilibrium structures in strongly interacting Rydberg gases with dissipation." In: *Phys. Rev. A* 90.011603 (2014). DOI: 10.1103/PhysRevA.90.011603.

[56] M Marcuzzi, E Levi, W Li, J P Garrahan, B Olmos, and I Lesanovsky. "Non-equilibrium universality in the dynamics of dissipative cold atomic gases." In: *New Journal of Physics* 17.7 (2015), p. 072003.

[57] A. Urvoy, F. Ripka, I. Lesanovsky, D. Booth, J. P. Shaffer, T. Pfau, and R. Löw. "Strongly Correlated Growth of Rydberg Aggregates in a Vapor Cell." In: *Phys. Rev. Lett.* 114.203002 (2015). DOI: 10.1103/PhysRevLett.114.203002.

[58] Rainer Blatt and David Wineland. "Entangled states of trapped atomic ions." In: *Nature* 453.7198 (2008), pp. 1008–1015. ISSN: 0028-0836. DOI: 10.1038/nature07125.

[59] H. Häffner, C.F. Roos, and R. Blatt. "Quantum computing with trapped ions." In: *Physics Reports* 469.4 (2008), pp. 155–203. ISSN: 03701573. DOI: 10.1016/j.physrep.2008.09.003.

[60] J. I. Cirac and P. Zoller. "Quantum Computations with Cold Trapped Ions." In: *Physical Review Letters* 74.4091 (1995). DOI: 10.1103/PhysRevLett.74.4091.

[61] Bryce Gadway and Bo Yan. "Strongly interacting ultracold polar molecules." In: *Journal of Physics B: Atomic, Molecular and Optical Physics* 49.15 (2016), p. 152002. ISSN: 0953-4075. DOI: 10.1088/0953-4075/49/15/152002.

[62] T. D. Ladd, F. Jelezko, R. Laflamme, Y. Nakamura, C. Monroe, and J. L. O'Brien. "Quantum computers." In: *Nature* 464.7285 (2010), pp. 45–53. ISSN: 0028-0836. DOI: 10.1038/nature08812.

[63] M. Mattioli, A. W. Glätzle, and W. Lechner. "From classical to quantum non-equilibrium dynamics of Rydberg excitations in optical lattices." In: *New Journal of Physics* 17.11 (2015), p. 113039.

[64] Michael Hoening, Wildan Abdussalam, Michael Fleischhauer, and Thomas Pohl. "Antiferromagnetic long-range order in dissipative Rydberg lattices." In: *Physical Review A* 90.2 (2014), p. 021603. ISSN: 1050-2947. DOI: 10.1103/PhysRevA.90.021603.

[65] M. Höning, D. Muth, D. Petrosyan, and M. Fleischhauer. "Steady-state crystallization of Rydberg excitations in an optically driven lattice gas." In: *Phys. Rev. A* 87.023401 (2013). DOI: 10.1103/PhysRevA.87.023401.

[66] T. E. Lee, H. Häffner, and M. C. Cross. "Antiferromagnetic phase transition in a nonequilibrium lattice of Rydberg atoms." In: *Phys. Rev. A* 84.031402 (2011). DOI: 10.1103/PhysRevA.84.031402.

[67] C. Ates, B. Olmos, J. P. Garrahan, and I. Lesanovsky. "Dynamical phases and intermittency of the dissipative quantum Ising model." In: *Phys. Rev. A* 85.043620 (2012). DOI: 10.1103/PhysRevA.85.043620.

[68] T. E. Lee, H. Häffner, and M. C. Cross. "Collective Quantum Jumps of Rydberg Atoms." In: *Phys. Rev. Lett.* 108.023602 (2012). DOI: 10.1103/PhysRevLett.108.023602.

[69] C. Carr, R. Ritter, C. G. Wade, C. S. Adams, and K. J. Weatherill. "Nonequilibrium Phase Transition in a Dilute Rydberg Ensemble." In: *Phys. Rev. Lett.* 111.113901 (2013). DOI: 10.1103/PhysRevLett.111.113901.

[70] Miguel Orszag and Juan Carlos Retamal, eds. *Modern Challenges in Quantum Optics*. Vol. 575. Lecture Notes in Physics. Berlin, Heidelberg: Springer Berlin Heidelberg, 2001. DOI: 10.1007/3-540-45409-8.

[71] B. Kraus, H. Büchler, S. Diehl, A. Kantian, A. Micheli, and P. Zoller. "Preparation of entangled states by quantum Markov processes." In: *Physical Review A* 78.042307 (2008). DOI: 10.1103/PhysRevA.78.042307.

[72] Sabrina Maniscalco, Francesco Francica, Rosa L. Zaffino, Nicola Lo Gullo, and Francesco Plastina. "Protecting Entanglement via the Quantum Zeno Effect." In: *Physical Review Letters* 100.090503 (2008). DOI: 10.1103/PhysRevLett.100.090503.

[73] Frank Verstraete, Michael M. Wolf, and J. Ignacio Cirac. "Quantum computation and quantum-state engineering driven by dissipation." In: *Nature Physics* 5 (2009), pp. 633–636.

[74] Valeriy Brazhnyi, Vladimir Konotop, Víctor Pérez-García, and Herwig Ott. "Dissipation-Induced Coherent Structures in Bose-Einstein Condensates." In: *Physical Review Letters* 102.144101 (2009). DOI: 10.1103/PhysRevLett.102.144101.

[75] Hendrik Weimer, Markus Müller, Igor Lesanovsky, Peter Zoller, and Hans Peter Büchler. "A Rydberg quantum simulator." In: *Nature Physics* 6 (2010), pp. 382–388. DOI: 10.1038/nphys1614.

[76] Y Lin, J P Gaebler, F Reiter, T R Tan, R Bowler, A S Sørensen, D Leibfried, and D J Wineland. "Dissipative production of a maximally entangled steady state of two quantum bits." In: *Nature* 504 (2013), pp. 415–8. DOI: 10.1038/nature12801.

[77] B. Zhu et al. "Suppressing the Loss of Ultracold Molecules Via the Continuous Quantum Zeno Effect." In: *Physical Review Letters* 112.070404 (2014). DOI: 10.1103/PhysRevLett.112.070404.

[78] Roland Cristopher F. Caballar, Sebastian Diehl, Harri Mäkelä, Markus Oberthaler, and Gentaro Watanabe. "Dissipative preparation of phase- and number-squeezed states with ultracold atoms." In: *Physical Review A* 89.013620 (2014). DOI: 10.1103/PhysRevA.89.013620.

[79] N Syassen, D M Bauer, M Lettner, T Volz, D Dietze, J J García-Ripoll, J I Cirac, G Rempe, and S Dürr. "Strong dissipation inhibits losses and induces correlations in cold molecular gases." In: *Science (New York, N.Y.)* 320 (2008), pp. 1329–31. DOI: 10.1126/science.1155309.

[80] J J García-Ripoll, S Dürr, N Syassen, D M Bauer, M Lettner, G Rempe, and J I Cirac. "Dissipation-induced hard-core boson gas in an optical lattice." In: *New Journal of Physics* 11.013053 (2009). DOI: 10.1088/1367-2630/11/1/013053.

[81] M. Marcuzzi, E. Levi, S. Diehl, J. P. Garrahan, and I. Lesanovsky. "Universal Nonequilibrium Properties of Dissipative Rydberg Gases." In: *Phys. Rev. Lett.* 113.210401 (2014). DOI: 10.1103/PhysRevLett.113.210401.

[82] H. Weimer. "Variational Principle for Steady States of Dissipative Quantum Many-Body Systems." In: *Phys. Rev. Lett.* 114.040402 (2015). DOI: 10.1103/PhysRevLett.114.040402.

[83] H. Weimer. "Variational analysis of driven-dissipative Rydberg gases." In: *Phys. Rev. A* 91.063401 (2015). DOI: 10.1103/PhysRevA.91.063401.

[84] N. Malossi, M. M. Valado, S. Scotto, P. Huillery, P. Pillet, D. Ciampini, E. Arimondo, and O. Morsch. "Full Counting Statistics and Phase Diagram of a Dissipative Rydberg Gas." In: *Phys. Rev. Lett.* 113.023006 (2014). DOI: 10.1103/PhysRevLett.113.023006.

[85] B. Misra and E. C. G. Sudarshan. "The Zeno's paradox in quantum theory." In: *Journal of Mathematical Physics* 18.756 (1977). ISSN: 00222488. DOI: 10.1063/1.523304.

[86] Rahul Nandkishore and David A. Huse. "Many-Body Localization and Thermalization in Quantum Statistical Mechanics." In: *Annual Review of Condensed Matter Physics* 6.1 (2015), pp. 15–38. DOI: 10.1146/annurev-conmatphys-031214-014726.

[87] H. Hinrichsen. "Non-equilibrium critical phenomena and phase transitions into absorbing states." In: *Advances in Physics* 49.7 (2000), p. 815. DOI: 10.1080/00018730050198152.

[88] Heinz-Peter Breuer and Francesco Petruccione. *The Theory of Open Quantum Systems*. Oxford University Press, 2002, p. 625. ISBN: 0198520638.

[89] G. Lindblad. "On the generators of quantum dynamical semigroups." In: *Comm. Math. Phys* 48 (1976), p. 119.

[90] T. Kato. *Perturbation Theory of Linear Operators*. 2nd. Berlin: Springer, 1980.

[91] A.B. Bortz, M.H. Kalos, and J.L. Lebowitz. "A new algorithm for Monte Carlo simulation of Ising spin systems." In: *Journal of Computational Physics* 17.1 (1975), pp. 10 –18. ISSN: 0021-9991. DOI: http://dx.doi.org/10.1016/0021-9991(75)90060-1.

[92] M. B. Plenio and P. L. Knight. "The quantum-jump approach to dissipative dynamics in quantum optics." In: *Rev. Mod. Phys.* 70 (1998), pp. 101–144. DOI: 10.1103/RevModPhys.70.101.

[93] Andrew J. Daley. "Quantum trajectories and open many-body quantum systems." In: (2014). DOI: 10.1080/00018732.2014.933502. arXiv: 1405.6694.

[94] V. Volokitin, A. Liniov, I. Meyerov, M. Hartmann, M. Ivanchenko, P. Hänggi, and S. Denisov. "Towards quantum attractors: Sampling asymptotic states of modulated open systems with quantum trajectories." In: (2016). arXiv: 1612.03848.

[95] B. Everest. *Quantum Jump Monte Carlo Adaptive Algorithm*. https://github.com/everestbt/Quantum-Jump-Monte-Carlo-Adaptive-Algorithm/. 2017.

[96] Mikhail Lemeshko and Hendrik Weimer. "Dissipative binding of atoms by non-conservative forces." In: *Nature Communications* 4.2230 (2013). DOI: 10.1038/ncomms3230.

[97] Mikhail Lemeshko. "Manipulating scattering of ultracold atoms with light-induced dissipation." In: *Frontiers in Physics* 1.17 (2013). DOI: 10.3389/fphy.2013.00017.

[98] Roger L. DeKock. *Chemical Structure and Bonding*. University Science Books, 1989. ISBN: 093570261X.

[99] Wayne M. Itano, D. J. Heinzen, J. J. Bollinger, and D. J. Wineland. "Quantum Zeno effect." In: *Physical Review A* 41.2295 (1990). DOI: 10.1103/PhysRevA.41.2295.

[100] Saverio Pascazio and Mikio Namiki. "Dynamical quantum Zeno effect." In: *Physical Review A* 50.4582 (1994). ISSN: 1050-2947. DOI: 10.1103/PhysRevA.50.4582.

[101] Vera Frerichs and Axel Schenzle. "Quantum Zeno effect without collapse of the wave packet." In: *Physical Review A* 44.1962 (1991). ISSN: 1050-2947. DOI: 10.1103/PhysRevA.44.1962.

[102] P. Facchi, D. A. Lidar, and S. Pascazio. "Unification of dynamical decoupling and the quantum Zeno effect." In: *Physical Review A* 69 (2004). DOI: 10.1103/PhysRevA.69.032314.

[103] Congjun Wu, Doron Bergman, Leon Balents, and S. Das Sarma. "Flat Bands and Wigner Crystallization in the Honeycomb Optical Lattice." In: *Physical Review Letters* 99.070401 (2007). ISSN: 0031-9007. DOI: 10.1103/PhysRevLett.99.070401.

[104] Ryuji Takahashi and Shuichi Murakami. "Completely flat bands and fully localized states on surfaces of anisotropic diamond-lattice models." In: *Physical Review B* 88.235303 (2013). ISSN: 1098-0121. DOI: 10.1103/PhysRevB.88.235303.

[105] Yi-Fei Wang, Zheng-Cheng Gu, Chang-De Gong, and D. N. Sheng. "Fractional Quantum Hall Effect of Hard-Core Bosons in Topological Flat Bands." In: *Physical Review Letters* 107.146803 (2011). ISSN: 0031-9007. DOI: 10.1103/PhysRevLett.107.146803.

[106] B. Everest, M. R. Hush, and I. Lesanovsky. "Many-body out-of-equilibrium dynamics of hard-core lattice bosons with non-local loss." In: *Phys. Rev. B* 90.134306 (2014). DOI: 10.1103/PhysRevB.90.134306.

[107] Zeno. *Zeno's Paradoxes*. Ed. by W.C. Salmon. 2nd. Hackett Publishing Co. Inc.

[108] C.W. Gardiner. *Handbook of Stochastic Methods*. Berlin: Springer, 2004.

[109] Waseem S Bakr, Jonathon I Gillen, Amy Peng, Simon Fölling, and Markus Greiner. "A quantum gas microscope for detecting single atoms in a Hubbard-regime optical lattice." In: *Nature* 462 (2009), pp. 74–7. ISSN: 1476-4687. DOI: 10.1038/nature08482.

[110] Takeshi Fukuhara, Peter Schauß, Manuel Endres, Sebastian Hild, Marc Cheneau, Immanuel Bloch, and Christian Gross. "Microscopic observation of magnon bound states and their dynamics." In: *Nature* 502 (2013), pp. 76–9. ISSN: 1476-4687. DOI: 10.1038/nature12541.

[111] L. C. Struik. *Physical aging in amorphous polymers and other materials*. Elsevier (Amsterdam), 1978.

[112] S. Ciliberto. "Experimental analysis of aging." In: *Slow Relaxations and Nonequilibrium Dynamics in Condensed Matter*. Vol. 77. Springer, 2003, p. 555.

[113] K. Binder and W. Kob. *Glassy Materials and Disordered Solids: An Introduction to their Statistical Mechanics*. World Scientific, 2005.

[114] L. Peliti. *Statistical Mechanics in a Nutshell*. Princeton University Press, 2011.

[115] L. Berthier and M. D. Ediger. "Facets of glass physics." In: *Physics Today* 69.1 (2016), pp. 40–46. ISSN: 0031-9228. DOI: 10.1063/PT.3.3052.

[116] "Geometrical explanation and scaling of dynamical heterogeneities in glass forming systems." In: *Phys. Rev. Lett.* 89.035704 (2002). ISSN: 0031-9007. DOI: 10.1103/PhysRevLett.89.035704.

[117] W. Kob and H. C. Andersen. "Kinetic lattice-gas model of cage effects in high-density liquids and a test of mode-coupling theory of the ideal-glass transition." In: *Physical Review E* 48.6 (1993), pp. 4364–4377. ISSN: 1063-651X. DOI: 10.1103/PhysRevE.48.4364.

[118] V. Teboul. "A toy model mimicking cage effect, structural fluctuations, and kinetic constraints in supercooled liquids." In: *The Journal of chemical physics* 141.19 (2014), p. 194501. ISSN: 1089-7690. DOI: 10.1063/1.4901424.

[119] B. Everest, M. Marcuzzi, J. P. Garrahan, and I. Lesanovsky. "Emergent kinetic constraints, ergodicity breaking, and cooperative dynamics in noisy quantum systems." In: *Phys. Rev. E* 94.052108 (2016). DOI: 10.1103/PhysRevE.94.052108.

[120] A. S. Keys, L. O. Hedges, J. P. Garrahan, S. C. Glotzer, and D. Chandler. "Excitations Are Localized and Relaxation Is Hierarchical in Glass-Forming Liquids." In: *Physical Review X* 1.2 (2011), p. 021013. ISSN: 2160-3308. DOI: 10.1103/PhysRevX.1.021013.

[121] D. Poletti, P. Barmettler, A. Georges, and C. Kollath. "Emergence of Glasslike Dynamics for Dissipative and Strongly Interacting Bosons." In: *Phys. Rev. Lett.* 111.195301 (2013). DOI: 10.1103/PhysRevLett.111.195301.

[122] B. Everest, M. Marcuzzi, and I. Lesanovsky. "Atomic loss and gain as a resource for nonequilibrium phase transitions in optical lattices." In: *Phys. Rev. A* 93.023409 (Editor's Suggestion) (2016). DOI: 10.1103/PhysRevA.93.023409.

[123] M. M. Valado, C. Simonelli, M. D. Hoogerland, I. Lesanovsky, J. P. Garrahan, E. Arimondo, D. Ciampini, and O. Morsch. "Experimental observation of controllable kinetic constraints in a cold atomic gas." In: *Phys. Rev. A* 93.040701 (2016). DOI: 10.1103/PhysRevA.93.040701.

[124] A. Karabanov, D. Wisniewski, I. Lesanovsky, and W. Köckenberger. "Dynamic Nuclear Polarization as Kinetically Constrained Diffusion." In: *Phys. Rev. Lett.* 115.020404 (2015). DOI: 10.1103/PhysRevLett.115.020404.

[125] M. van Horssen, E. Levi, and J. P. Garrahan. "Dynamics of many-body localization in a translation-invariant quantum glass model." In: *Phys. Rev. B* 92.100305 (2015). DOI: 10.1103/PhysRevB.92.100305.

[126] James M Hickey, Sam Genway, and Juan P Garrahan. "Signatures of many-body localisation in a system without disorder and the relation to a glass transition." In: *Journal of Statistical Mechanics: Theory and Experiment* 2016.5 (2016), p. 054047.

[127] B. Everest, I. Lesanovsky, J. P. Garrahan, and E. Levi. "Role of interactions in a dissipative many-body localized system." In: *Phys. Rev. B* 95.024310 (2017). DOI: 10.1103/PhysRevB.95.024310.

[128] R. Löw, H. Weimer, J. Nipper, J. B. Balewski, B. Butscher, H. P. Büchler, and T. Pfau. "An experimental and theoretical guide to strongly interacting Rydberg gases." In: *Journal of Physics B: Atomic, Molecular and Optical Physics* 45.11 (2012), p. 113001.

[129] H. Labuhn, D. Barredo, S. Ravets, S. de Léséleuc, T. Macrì, T. Lahaye, and A. Browaeys. "A highly-tunable quantum simulator of spin systems using two-dimensional arrays of single Rydberg atoms." In: *ArXiv e-prints* (2015). arXiv: 1509.04543 [cond-mat.quant-gas].

[130] Saubhik Sarkar, Stephan Langer, Johannes Schachenmayer, and Andrew J. Daley. "Light scattering and dissipative dynamics of many fermionic atoms in an optical lattice." In: *Phys. Rev. A* 90.023618 (2014). DOI: 10.1103/PhysRevA.90.023618.

[131] H. Schempp et al. "Full Counting Statistics of Laser Excited Rydberg Aggregates in a One-Dimensional Geometry." In: *Phys. Rev. Lett.* 112.013002 (2014). DOI: 10.1103/PhysRevLett.112.013002.

[132] Z. Cai and T. Barthel. "Algebraic versus Exponential Decoherence in Dissipative Many-Particle Systems." In: *Phys. Rev. Lett.* 111.150403 (2013). DOI: 10.1103/PhysRevLett.111.150403.

[133] M. Marcuzzi, J. Schick, B. Olmos, and I. Lesanovsky. "Effective dynamics of strongly dissipative Rydberg gases." In: *J. Phys. A: Math. Theor.* 47.48 (2014), p. 482001. DOI: 10.1088/1751-8113/47/48/482001.

[134] P. Degenfeld-Schonburg and M. J. Hartmann. "Self-consistent projection operator theory for quantum many-body systems." In: *Phys. Rev. B* 89.245108 (2014). DOI: 10.1103/PhysRevB.89.245108.

[135] Jean-Sébastien Bernier, Dario Poletti, and Corinna Kollath. "Dissipative quantum dynamics of fermions in optical lattices: A slave-spin approach." In: *Phys. Rev. B* 90.205125 (2014). DOI: 10.1103/PhysRevB.90.205125.

[136] Bruno Sciolla, Dario Poletti, and Corinna Kollath. "Two-time correlations probing the dynamics of dissipative many-body quantum systems: aging and fast relaxation." In: *Phys. Rev. Lett.* 114.170401 (2015). DOI: 10.1103/PhysRevLett.114.170401.

[137] Y. S. Elmatad, R. L. Jack, D. Chandler, and J. P. Garrahan. "Finite-temperature critical point of a glass transition." In: *Proceedings of the National Academy of Sciences of the United States of America* 107.29 (2010), pp. 12793–8. ISSN: 1091-6490. DOI: 10.1073/pnas.1006306107.

[138] Omjyoti Dutta, Mariusz Gajda, Philipp Hauke, Maciej Lewenstein, Dirk-Sören Lühmann, Boris A Malomed, Tomasz Sowiński, and Jakub Zakrzewski. "Non-standard Hubbard models in optical lattices: a review." In: *Reports on Progress in Physics* 78.6 (2015), p. 066001.

[139] D. W. Schönleber, M. Gärttner, and J. Evers. "Coherent versus incoherent excitation dynamics in dissipative many-body Rydberg systems." In: *Physical Review A* 89.3 (2014), p. 033421. ISSN: 1050-2947. DOI: 10.1103/PhysRevA.89.033421.

[140] W. S. Bakr, A. Peng, M. E. Tai, R. Ma, J. Simon, J. I. Gillen, S. Fölling, L. Pollet, and M. Greiner. "Probing the Superfluid–to–Mott Insulator Transition at the Single-Atom Level." In: *Science* 329.5991 (2010), pp. 547–550. ISSN: 0036-8075. DOI: 10.1126/science.1192368.

[141] J. F. Sherson, C. Weitenberg, M. Endres, M. Cheneau, I. Bloch, and S. Kuhr. "Single-atom-resolved fluorescence imaging of an atomic Mott insulator." In: *Nat. Phys.* 467 (7311 2010), pp. 68–72. DOI: 10.1038/nature09378.

[142] T. E. Markland, J. A. Morrone, B. J. Berne, K. Miyazaki, E. Rabani, and D. R. Reichman. "Quantum fluctuations can promote or inhibit glass formation." In: *Nature Physics* 7.2 (2011), pp. 134–137.

[143] B. Olmos, I. Lesanovsky, and J. P. Garrahan. "Facilitated Spin Models of Dissipative Quantum Glasses." In: *Phys. Rev. Lett.* 109.020403 (2012). DOI: 10.1103/PhysRevLett.109.020403.

[144] Matteo Marcuzzi, Michael Buchhold, Sebastian Diehl, and Igor Lesanovsky. "Absorbing State Phase Transition with Competing Quantum and Classical Fluctuations." In: *Phys. Rev. Lett.* 116.245701 (2016). DOI: 10.1103/PhysRevLett.116.245701.

[145] M. Schreiber, S. S. Hodgman, P. Bordia, H. P. Lüschen, M. H. Fischer, R. Vosk, E. Altman, U. Schneider, and I. Bloch. "Observation of many-body localization of interacting fermions in a quasirandom optical lattice." In: *Science* 349.6250 (2015), pp. 842–845. ISSN: 0036-8075. DOI: 10.1126/science.aaa7432.

[146] P. W. Anderson. "Absence of Diffusion in Certain Random Lattices." In: *Phys. Rev.* 109 (5 1958), pp. 1492–1505. DOI: 10.1103/PhysRev.109.1492.

[147] Ferdinand Evers and Alexander D. Mirlin. "Anderson transitions." In: *Rev. Mod. Phys.* 80.1355 (2008). DOI: 10.1103/RevModPhys.80.1355.

[148] Boris L. Altshuler, Yuval Gefen, Alex Kamenev, and L. S. Levitov. "Quasiparticle Lifetime in a Finite System: A Nonperturbative Approach." In: *Phys. Rev. Lett.* 78.2803 (1997). DOI: 10.1103/PhysRevLett.78.2803.

[149] DM Basko, IL Aleiner, and BL Altshuler. "Metal–insulator transition in a weakly interacting many-electron system with localized single-particle states." In: *Ann. of Phys.* 321.5 (2006), pp. 1126–1205.

[150] I. Gornyi, A. Mirlin, and D. Polyakov. "Interacting Electrons in Disordered Wires: Anderson Localization and Low-T Transport." In: *Phys. Rev. Lett.* 95.206603 (2005). DOI: 10.1103/PhysRevLett.95.206603.

[151] Vadim Oganesyan and David A. Huse. "Localization of interacting fermions at high temperature." In: *Phys. Rev. B* 75.155111 (2007). DOI: 10.1103/PhysRevB.75.155111.

[152] Arijeet Pal and David A. Huse. "The many-body localization phase transition." In: *Phys. Rev. B* 82.174411 (2010).

[153] Wojciech De Roeck, Francois Huveneers, Markus Müller, and Mauro Schiulaz. "Absence of many-body mobility edges." In: *Phys. Rev. B* 93.014203 (2016). DOI: 10.1103/PhysRevB.93.014203.

[154] Marko Znidaric, Tomaz Prosen, and Peter Prelovsek. "Many-body localization in the Heisenberg XXZ magnet in a random field." In: *Phys. Rev. B* 77.064426 (2008).

[155] Jens H. Bardarson, Frank Pollmann, and Joel E. Moore. "Unbounded Growth of Entanglement in Models of Many-Body Localization." In: *Phys. Rev. Lett.* 109.017202 (2012). DOI: 10.1103/PhysRevLett.109.017202.

[156] Maksym Serbyn, Z. Papić, and Dmitry A. Abanin. "Universal Slow Growth of Entanglement in Interacting Strongly Disordered Systems." In: *Phys. Rev. Lett.* 110.260601 (2013). DOI: 10.1103/PhysRevLett.110.260601.

[157] David J. Luitz, Nicolas Laflorencie, and Fabien Alet. "Many-body localization edge in the random-field Heisenberg chain." In: *Phys. Rev. B* 91.081103 (2015).

[158] A. De Luca and A. Scardicchio. "Ergodicity breaking in a model showing many-body localization." In: *Europhysics Letters* 101.3 (2013), p. 37003.

[159] Pedro Ponte, Z. Papić, François Huveneers, and Dmitry A. Abanin. "Many-Body Localization in Periodically Driven Systems." In: *Phys. Rev. Lett.* 114.140401 (2015). DOI: 10.1103/PhysRevLett.114.140401.

[160] J. Smith, A. Lee, P. Richerme, B. Neyenhuis, P. W. Hess, P. Hauke, M. Heyl, D. A. Huse, and C. Monroe. "Many-body localization in a quantum simulator with programmable random disorder." In: *Nat. Phys.* (2016). ISSN: 1745-2473. DOI: 10.1038/nphys3783.

[161] Jae-yoon Choi, Sebastian Hild, Johannes Zeiher, Peter Schauß, Antonio Rubio-Abadal, Tarik Yefsah, Vedika Khemani, David A. Huse, Immanuel Bloch, and Christian Gross. "Exploring the many-body localization transition in two dimensions." In: *Science* 352.6293 (2016), pp. 1547–1552. ISSN: 0036-8075. DOI: 10.1126/science.aaf8834.

[162] Pranjal Bordia, Henrik P. Lüschen, Sean S. Hodgman, Michael Schreiber, Immanuel Bloch, and Ulrich Schneider. "Coupling Identical one-dimensional Many-Body Localized Systems." In: *Phys. Rev. Lett.* 116.140401 (2016). DOI: 10.1103/PhysRevLett.116.140401.

[163] Rahul Nandkishore, Sarang Gopalakrishnan, and David A. Huse. "Spectral features of a many-body-localized system weakly coupled to a bath." In: *Phys. Rev. B* 90.064203 (2014). DOI: 10.1103/PhysRevB.90.064203.

[164] Sonika Johri, Rahul Nandkishore, and R. N. Bhatt. "Many-Body Localization in Imperfectly Isolated Quantum Systems." In: *Phys. Rev. Lett.* 114.117401 (2015). DOI: 10.1103/PhysRevLett.114.117401.

[165] Emanuele Levi, Markus Heyl, Igor Lesanovsky, and Juan P. Garrahan. "Robustness of Many-Body Localization in the Presence of Dissipation." In: *Phys. Rev. Lett.* 116.237203 (2016). DOI: 10.1103/PhysRevLett.116.237203.

[166] Mark H Fischer, Mykola Maksymenko, and Ehud Altman. "Dynamics of a Many-Body-Localized System Coupled to a Bath." In: *Phys. Rev. Lett.* 116.160401 (2016). DOI: 10.1103/PhysRevLett.116.160401.

[167] M. V. Medvedyeva, T. Prosen, and M. Žnidarič. "Influence of dephasing on many-body localization." In: *Phys. Rev. B* 93.094205 (2016). DOI: 10.1103/PhysRevB.93.094205.

[168] Luca Cipelletti, S. Manley, R. C. Ball, and D. A. Weitz. "Universal Aging Features in the Restructuring of Fractal Colloidal Gels." In: *Phys. Rev. Lett.* 84.2275 (2000). DOI: 10.1103/PhysRevLett.84.2275.

[169] Luca Cipelletti, Laurence Ramos, S. Manley, E. Pitard, D. A. Weitz, Eugene E. Pashkovski, and Marie Johansson. "Universal non-diffusive slow dynamics in aging soft matter." In: *Faraday Discuss.* 123 (0 2003), pp. 237–251. DOI: 10.1039/B204495A.

[170] P. Falus, M. A. Borthwick, S. Narayanan, A. R. Sandy, and S. G. J. Mochrie. "Crossover from Stretched to Compressed Exponential Relaxations in a Polymer-Based Sponge Phase." In: *Phys. Rev. Lett.* 97.066102 (2006). DOI: 10.1103/PhysRevLett.97.066102.

[171] B. Ruta, Y. Chushkin, G. Monaco, L. Cipelletti, E. Pineda, P. Bruna, V. M. Giordano, and M. Gonzalez-Silveira. "Atomic-Scale Relaxation Dynamics and Aging in a Metallic Glass Probed by X-Ray Photon Correlation Spectroscopy." In: *Phys. Rev. Lett.* 109.165701 (2012). DOI: 10.1103/PhysRevLett.109.165701.

[172] Maksym Serbyn, Z. Papić, and Dmitry A. Abanin. "Criterion for Many-Body Localization-Delocalization Phase Transition." In: *Phys. Rev. X* 5.041047 (2015). DOI: 10.1103/PhysRevX.5.041047.

[173] H. Pichler, A. J. Daley, and P. Zoller. "Nonequilibrium dynamics of bosonic atoms in optical lattices: Decoherence of many-body states due to spontaneous emission." In: *Phys. Rev. A* 82.063605 (2010). DOI: 10.1103/PhysRevA.82.063605.

[174] Zi Cai and Thomas Barthel. "Algebraic versus Exponential Decoherence in Dissipative Many-Particle Systems." In: *Phys. Rev. Lett.* 111.150403 (2013). DOI: 10.1103/PhysRevLett.111.150403.

[175] Jean-Philippe Bouchaud. "Anomalous Relaxation in Complex Systems: From Stretched to Compressed Exponentials." In: *Anomalous Transport*. Wiley-VCH Verlag GmbH and Co. KGaA, 2008, pp. 327–345. ISBN: 9783527622979. DOI: 10.1002/9783527622979.ch11.

[176] Ranjini Bandyopadhyay, Dennis Liang, James L. Harden, and Robert L. Leheny. "Slow dynamics, aging, and glassy rheology in soft and living matter." In: (2006). DOI: 10.1016/j.ssc.2006.06.023. arXiv: 0606466 [cond-mat].

[177] AE Kolmogorov. "On the statistic theory of metal crystallization." In: *Izv Akad Nauk SSSR Ser Mat* 1 (1937), pp. 355–359.

[178] William A Johnson and Robert F Mehl. "Reaction kinetics in processes of nucleation and growth." In: *Trans. Aime* 135.8 (1939), pp. 396–415.

[179] Melvin Avrami. "Kinetics of phase change. I General theory." In: *J. Chem. Phys.* 7.12 (1939), pp. 1103–1112.

[180] Melvin Avrami. "Kinetics of phase change. II transformation-time relations for random distribution of nuclei." In: *J. Chem. Phys.* 8.2 (1940), pp. 212–224.

[181] Melvin Avrami. "Granulation, phase change, and microstructure kinetics of phase change. III." In: *J. Chem. Phys.* 9.2 (1941), pp. 177–184.

[182] Pranjal Bordia, Henrik Lüschen, Ulrich Schneider, Michael Knap, and Immanuel Bloch. "Periodically Driving a Many-Body Localized Quantum System." In: (2016). arXiv: 1607.07868.

[183] Henrik P. Lüschen, Pranjal Bordia, Sean S. Hodgman, Michael Schreiber, Saubhik Sarkar, Andrew J. Daley, Mark H. Fischer, Ehud Altman, Immanuel Bloch, and Ulrich Schneider. "Signatures of Many-Body Localization in a Controlled Open Quantum System." In: (2016). arXiv: 1610.01613.

[184] G. Ódor. "Universality classes in nonequilibrium lattice systems." In: *Rev. Mod. Phys.* 76 (3 2004), pp. 663–724. DOI: 10.1103/RevModPhys.76.663.

[185] H. Hinrichsen M. Henkel and S. Lübeck. *Non-Equilibrium Phase Transitions*. Vol. 1. Theoretical and Mathematical Physics. Springer, 2009.

[186] Kazumasa A. Takeuchi, Masafumi Kuroda, Hugues Chaté, and Masaki Sano. "Experimental realization of directed percolation criticality in turbulent liquid crystals." In: *Phys. Rev. E* 80.051116 (2009). DOI: 10.1103/PhysRevE.80.051116.

[187] Grégoire Lemoult, Liang Shi, Kerstin Avila, Shreyas V. Jalikop, Marc Avila, and Björn Hof. "Directed percolation phase transition to sustained turbulence in Couette flow." In: *Nature Physics* 12 (2016), pp. 254–258. DOI: 10.1038/nphys3675.

[188] R. M. W. van Bijnen, C. Ravensbergen, D. J. Bakker, G. J. Dijk, S. J. J. M. F. Kokkelmans, and E. J. D. Vredenbregt. "Patterned Rydberg excitation and ionization with a spatial light modulator." In: *New Journal of Physics* 17.2 (2015), p. 023045.

[189] F. Nogrette, H. Labuhn, S. Ravets, D. Barredo, L. Béguin, A. Vernier, T. Lahaye, and A. Browaeys. "Single-Atom Trapping in Holographic 2D Arrays of Microtraps with Arbitrary Geometries." In: *Phys. Rev. X* 4.021034 (2014). DOI: 10.1103/PhysRevX.4.021034.

[190] T. Wilk, A. Gaëtan, C. Evellin, J. Wolters, Y. Miroshnychenko, P. Grangier, and A. Browaeys. "Entanglement of Two Individual Neutral Atoms Using Rydberg Blockade." In: *Phys. Rev. Lett.* 104.010502 (2010). DOI: 10.1103/PhysRevLett.104.010502.

[191] D. Barredo, H. Labuhn, S. Ravets, T. Lahaye, A. Browaeys, and C. S. Adams. "Coherent Excitation Transfer in a Spin Chain of Three Rydberg Atoms." In: *Phys. Rev. Lett.* 114.113002 (2015). DOI: 10.1103/PhysRevLett.114.113002.

[192] N. Schlosser, G. Reymond, I. Protsenko, and P. Grangier. "Sub-poissonian loading of single atoms in a microscopic dipole trap." In: *Nature* 411.6841 (2001), pp. 1024–1027.

[193] N. Schlosser, G. Reymond, and P. Grangier. "Collisional Blockade in Microscopic Optical Dipole Traps." In: *Phys. Rev. Lett.* 89.023005 (2002). DOI: 10.1103/PhysRevLett.89.023005.

[194] M. D. Lukin, M. Fleischhauer, R. Cote, L. M. Duan, D. Jaksch, J. I. Cirac, and P. Zoller. "Dipole blockade and quantum information processing in mesoscopic atomic ensembles." In: *Physical Review Letters* 87.3 (2001), p. 037901.

[195] U. Raitzsch, R. Heidemann, H. Weimer, B. Butscher, P. Kollmann, R. Löw, H. P. Büchler, and T. Pfau. "Investigation of dephasing rates in an interacting Rydberg gas." In: *New J. Phys.* 11 (2009), p. 055014.

[196] C. Ates, T. Pohl, T. Pattard, and J. M. Rost. "Strong interaction effects on the atom counting statistics of ultracold Rydberg gases." In: *J. Phys. B* 39.11 (2006), p. L233. DOI: 10.1088/0953-4075/39/11/L02.

[197] K. P. Heeg, M. Gärttner, and J. Evers. "Hybrid model for Rydberg gases including exact two-body correlations." In: *Phys. Rev. A* 86.063421 (2012). DOI: 10.1103/PhysRevA.86.063421.

[198] S. Nakajima. "On Quantum Theory of Transport Phenomena: Steady Diffusion." In: *Progr. Theor. Phys.* 20.6 (1958), pp. 948–959. DOI: 10.1143/PTP.20.948.

[199] R. Zwanzig. "Ensemble Method in the Theory of Irreversibility." In: *J. Chem. Phys.* 33.5 (1960), pp. 1338–1341.

[200] I. Jensen and R. Dickman. "Nonequilibrium phase transitions in systems with infinitely many absorbing states." In: *Phys. Rev. E* 48 (3 1993), pp. 1710–1725. DOI: 10.1103/PhysRevE.48.1710.

[201] M. Kiffner, W. Li, and D. Jaksch. "Three-Body Bound States in Dipole-Dipole Interacting Rydberg Atoms." In: *Phys. Rev. Lett.* 111.233003 (2013).

[202] M. Kiffner, W. Li, and D. Jaksch. "Magnetic Monopoles and Synthetic Spin-Orbit Coupling in Rydberg Macrodimers." In: *Phys. Rev. Lett.* 110.170402 (2013). DOI: 10.1103/PhysRevLett.110.170402.

[203] D. Petrosyan and K. Mølmer. "Binding Potentials and Interaction Gates between Microwave-Dressed Rydberg Atoms." In: *Phys. Rev. Lett.* 113.123003 (2014). DOI: 10.1103/PhysRevLett.113.123003.

[204] S. Diehl, W. Yi, A. J. Daley, and P. Zoller. "Dissipation-Induced d-Wave Pairing of Fermionic Atoms in an Optical Lattice." In: *Physical Review Letters* 105.227001 (2010). DOI: 10.1103/PhysRevLett.105.227001.

[205] D. Barredo, S. Ravets, H. Labuhn, L. Béguin, A. Vernier, F. Nogrette, T. Lahaye, and A. Browaeys. "Demonstration of a Strong Rydberg Blockade in Three-Atom Systems with Anisotropic Interactions." In: *Phys. Rev. Lett.* 112.183002 (2014). DOI: 10.1103/PhysRevLett.112.183002.

[206] M. Buchhold, B. Everest, M. Marcuzzi, I. Lesanovsky, and S. Diehl. "Nonequilibrium effective field theory for absorbing state phase transitions in driven open quantum spin systems." In: *Phys. Rev. B* 95.014308 (Editor's Suggestion) (2017). DOI: 10.1103/PhysRevB.95.014308.

[207] R. Gutierrez, C. Simonelli, M. Archimi, F. Castellucci, E. Arimondo, D. Ciampini, M. Marcuzzi, I. Lesanovsky, and O. Morsch. "Experimental signatures of an absorbing-state phase transition in an open driven many-body quantum system." In: *ArXiv e-prints* (2016). arXiv: 1611.03288 [cond-mat.stat-mech].

Part I

APPENDIX

A

OPTICAL LATTICE AND SCALING OF TUNNELING AND DEPHASING

A key tool in cold atomic study is the use of optical lattices. The trapping of neutral atoms with laser light is imperative to the study of cold atoms as it allows for the systems to be contained and structured in ways that create interesting physical systems. A one-dimensional optical lattice is generated by overlapping two counter-propagating laser beams, the resulting interference pattern creates a standing wave of nodes and anti-nodes. The force then comes from the dipole force of the spatially varying AC-Stark shift due to the laser light applied. This causes either attraction or repulsion to the nodes and anti-nodes of the laser waveform and forms traps for either single or multiple atoms. This can be extended to easily create two-dimensional and three-dimensional lattices and through the use of advanced technologies highly complex lattice structures may be formed [189]. Through control of depth and other properties of the lattice the behaviour of the occupying atoms is influenced.

Here we briefly recall some basic results on tunnelling and dephasing amplitudes in cold-atomic systems held in optical lattices. A more detailed discussion can be found in Refs. [3, 130]. We consider a 1D lattice potential (setting $\hbar = 1$) of the form

$$V_0(x) = -\frac{\omega^2}{\Delta}(\cos^2(k_{lat}x) - 1) \tag{A.1}$$

where ω is the Rabi frequency and Δ is the detuning of the laser and $k_{lat} = \pi/a$ with a the lattice spacing. If we assume a deep lattice, i.e. $\frac{\hbar\omega^2}{\Delta} \gg E_r$, where $E_r = \hbar^2 k_{lat}^2/2m$, then the tunnelling rate scales as

$$\Omega \approx \frac{4}{\sqrt{\pi}}\left(\frac{\omega^2}{\Delta E_r}\right)^{3/4} E_r e^{-2\sqrt{\frac{\omega^2}{\Delta E_r}}}. \tag{A.2}$$

The dephasing rate due to the scattering of atoms in the lowest Bloch band of the lattice with photons has been instead calculated in Ref. [130] and reads

$$\gamma \approx \frac{\Gamma\omega^2 m}{2\Delta^2\sqrt{\pi}a}\left(\frac{\omega^2}{\Delta E_r}\right)^{3/4} E_r, \tag{A.3}$$

where Γ is the spontaneous decay rate of the excited state to the relaxed state. It is assumed that Γ is small in comparison to all other rates in the system. Taking the ratio of Eqs. (A.2) and (A.3),

$$\frac{\Omega}{\gamma} = \frac{8\Delta^2 a}{\Gamma\omega^2 m} e^{-2\sqrt{\frac{\omega^2}{\Delta E_r}}}, \tag{A.4}$$

it is seen that the physical parameters of the system can be easily tuned to adjust this ratio. Looking at the Rabi frequency, ω, which can be controlled by adjusting the power of the trapping laser, when this value is increased it will cause the ratio to reduce. The same follows for the other parameters in the system, which makes the limit $\gamma \gg \Omega$ accessible.